Materials Science & Engineering R 169 (2026) 101192

Contents lists available at ScienceDirect

Materials Science & Engineering R

journal homepage: www.elsevier.com/locate/mser

Accessing new dimensions in high-resolution materials exploration by cryo-electron microscopy

P. Koralli [a,1], F.L. Kyrilis [a,2], F. Hamdi [b,3], C.L. Chochos [a,4], P.L. Kastritis [a,b,c,*,5]

[a] Institute of Chemical Biology, National Hellenic Research Foundation, Athens 11635, Greece
[b] Department of Integrative Structural Biochemistry, Institute of Biochemistry and Biotechnology, Martin Luther University Halle-Wittenberg, Halle/Saale 06120, Germany
[c] Biozentrum and ZIK HALOmem, Martin Luther University Halle-Wittenberg, Halle/Saale 06120, Germany

ARTICLE INFO

Keywords:
Cryogenic electron microscopy
Materials science
Soft materials
Material characterization
Advanced imaging techniques

ABSTRACT

Cryo-electron microscopy (cryo-EM) is employed for structural analyses, visualizing high-resolution information across scales, *i.e.,* from tissues to small molecules. Developments allowing near-atomic resolution cryo-EM imaging of biological macromolecules were recognized by the 2017 Nobel Prize in Chemistry. In the materials science domain, despite specific applications, cryo-EM analysis presents discrete challenges related to sample preparation, imaging, and data interpretation, as function of the sample's innate physical chemistry. Here, we review recent progress in the field, focusing on overcoming intricacies in analysis of soft matter (*e.g.,* polymers, gels, colloids) and functional materials like metal-organic frameworks (MOFs), covalent organic frameworks (COFs), and hybrid perovskites. Sample preparation, including grid selection, surface treatments, and vitrification methods are compared, highlighting their effects on image quality and artifact reduction. Advanced cryo-EM methods, and their combination with scanning transmission electron microscopy (STEM) and low-dose energy loss spectroscopy (EELS) are also examined to evaluate their potential in describing complex molecular structures and their conformational heterogeneity. This review, overall, highlights the need for standardized, statistically empowered cryo-EM protocols inspired from biological applications, and integration of emerging technologies like machine learning and open data initiatives, to ultimately incorporate cryo-EM into materials research as a fundamental method.

1. Introduction

The properties of materials are fundamentally rooted in their constituents' structural arrangement and dynamic behavior. In the living world, functional entities exist across various length scales, from atoms to entire organisms, with highly complex properties emerging at the upper end of the nanoscale (Fig. 1). To address emerging challenges, new material properties are essential, which will necessitate the design of materials at the nanoscale and promote the development of novel multi-material nanocomposites. Their *direct* visualization at the atomic level is only amenable with electron microscopes.

Transmission electron microscopy (TEM) is a powerful tool to characterize materials, as it integrates imaging, diffraction, and spectroscopy techniques with ultra-high resolution [1]. High-resolution transmission electron microscopy (HRTEM) is commonly used for atomic-resolution imaging of crystal lattices and microstructures, while electron diffraction identifies crystal parameters [2]. Analytical spectroscopy techniques like energy dispersive X-ray spectroscopy (EDS) and electron energy loss spectroscopy (EELS) may provide valuable information about the composition, chemical bonds, valence states, and electronic structures, as well as their spatial distributions, especially when combined with scanning transmission electron microscopy

* Corresponding author at: Institute of Chemical Biology, National Hellenic Research Foundation, Athens 11635, Greece.
E-mail addresses: pkoralli@eie.gr (P. Koralli), fkyrilis@eie.gr (F.L. Kyrilis), farzad.hamdi@bct.uni-halle.de (F. Hamdi), chochos@eie.gr (C.L. Chochos), panagiotis.kastritis@bct.uni-halle.de (P.L. Kastritis).
[1] **Koralli:** 0000–0003-4965–0357
[2] **Kyrilis:** 0000–0002-4040–6289
[3] **Hamdi:** 0000–0002-2155–5000
[4] **Chochos:** 0000–0002-7783–157X
[5] **Kastritis:** 0000–0002-1463–8422

https://doi.org/10.1016/j.mser.2026.101192

Available online 6 February 2026

(STEM) [3]. The aforementioned electron microscopy techniques are mainly used under high vacuum conditions. Furthermore, the field of *in situ* TEM techniques is progressing, and currently allows real-time investigations of applied physical stimuli or chemically reactive environments [4]. Contrary to TEM techniques designed for room temperature use, cryogenic electron microscopy (cryo-EM) overcomes several limitations by preserving samples in a vitrified state [5]. While applications of cryo-EM started in the 1970s, the growth of the method accelerated in the mid-2000s following the advent of CMOS-based direct electron detectors (DED). This technological progress, characterized by reduced readout noise, higher frame rates underlined by massively parallel pixel architectures, improved radiation tolerance, and more efficient electron-sensitive pixel designs, profoundly transformed the imaging of extremely low-contrast specimens, such as the ones characterized by cryo-EM [6].

These detectors are low-noise single-electron counters capable of recording single-electron landing events with exceptional spatial resolution. Unlike other detectors, *e.g.*, optical fiber-coupled image sensors, the position of the electron landing on the sensor is not broadened. A combination of a high signal-to-noise ratio (SNR) [7] and the superior precision of detection position translates to the high detective quantum efficiency (DQE) of DEDs. The contribution of DEDs can be inscribed in several aspects; thus, their development and commercialization were the most significant hardware advances leading the "resolution revolution" [8]. DEDs record a high number of high-quality images. Currently, the number of images recorded during each microscopy session is incomparable to the era of traditional sheet film [9]. Due to the increase in DQE, the quality of the image is unprecedented, and the finest details of the sample can be recorded. Since the signal-to-noise ratio of the cameras is also very low, a minimal dose is required to record a certain amount of information. The high-speed data acquisition of advanced detectors and their enhanced SNR enabled the fractionation of the total electron dose of a single image exposure into multiple sub-frames. This allows for computational frame alignment post-acquisition to compensate for specimen motion, drift, and radiation damage [10]. Due to all these advantages, it is of no surprise that all biomolecular structures of resolution better than 2 Å utilized a DED (https://www.ebi.ac.uk/emdb/).

Another aspect of cryo-EM's success in molecular analysis is the parallel advances in the electron microscopes, which are much more stable than before. There are different stability aspects, *i.e.,* dampening the mechanical vibration, suppressing thermal fluctuation, cancelling electromagnetic stray fields, and stabilizing the microscope electronics. As a result, acquired images are sharper, with less drift, and a more reproducible imaging condition. Another improvement in cryo-EM is the level of microscope automation [11]. Many aspects of TEM functionalities are performed without human intervention in a modern, state-of-the-art microscope. This includes automation of microscope management and operation, such as cooling, loading, unloading, and control of mechanical components. In the end, such user-free functions

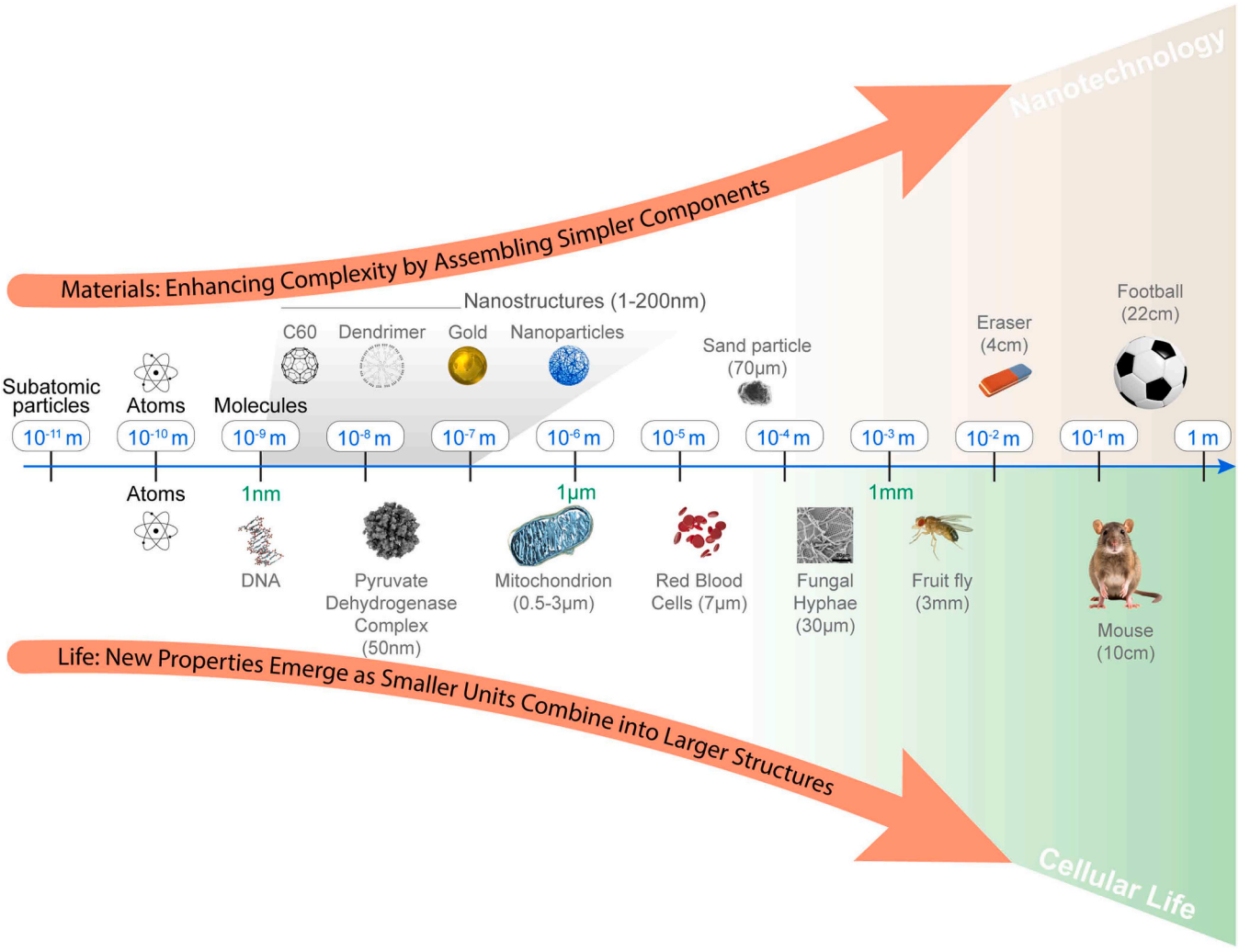

Fig. 1. Complexity as a function of length scale. Materials science accesses similar scales as biological systems, and therefore, must be amenable to technologically similar characterization procedures.

lead to less direct and in-person interaction between the operator and the microscope. As a result, microscopy became more accessible, easier, and more accurate. Most importantly, automation helps to acquire a high volume of data over the course of days, which not only reduces bias but also helps increase resolution via image processing techniques.

These advancements, mentioned above, have allowed for the resolution of three-dimensional (3D) protein structures at the atomic level, enhancing our knowledge of the fine structure of biomolecules and revolutionizing life sciences, especially in fields like drug design and disease mechanism research [12,13]. Thus, in recognition of their contributions, Jacques Dubochet, Joachim Frank, and Richard Henderson were awarded the 2017 Nobel Prize in Chemistry [14–18]. Recent examples of specific protein complexes, which are also of interest to materials scientists, have shown atomic resolution when the Coulomb potential map is reconstructed (Fig. 2) [19–21]

Even though cryo-EM is mainly employed in life sciences, nowadays, there is a great interest in its application in materials science as it offers a distinct approach to exploring the relationship among the structure and properties of materials under cryogenic temperatures, close to the boiling points of liquid nitrogen (~77 K) or liquid helium (~4 K) [22,23]. By operating at such ultralow temperatures, cryo-EM can efficiently mitigate the detrimental effects of beam radiation on the sample and decrease the dosage required for imaging [24]. This is especially advantageous for beam-sensitive materials such as battery materials and their interfaces [25–27], where, under cryogenic temperatures, their structure can be effectively preserved and imaged at the nano/atomic scale, yielding chemical components and structural information that correlate with their electrochemical performance [28]. Related to this, cryo-EM is also applied to study superconducting materials, which has been recently extensively reviewed elsewhere [29].

Moreover, cryo-EM is useful for examining the microstructure of soft matter, which is more susceptible to radiation damage compared to hard metals and ceramics [5]. Soft matter is a term used to describe a category of condensed matter that can incur dynamic changes due to its physical behavior occurring at an energy scale comparable with thermal energy (kT) [30]. This category is very heterogeneous and is described to comprise polymers [31,32], gels [31], colloids [31,32], emulsions [33], foams [33], surfactant assemblies [32], liquid crystals [32], and various biological materials [31,32], such as membranes, nucleic acids, and proteins. They are challenging to characterize due to emergent complex behaviors, following their characteristic softness [34]. These materials exhibit complex interactions with their surroundings due to diverse intra- and intermolecular dynamics [35]. To analyze soft matter, examination of the interaction potentials between nanosized objects, mostly in liquid environments, is particularly relevant.

Many accounts have recently emphasized the growing use of cryo-EM in materials science, especially in fields like battery materials, interfaces, quantum materials, and nanoscience [29,36–39]. This review focuses on cryo-EM in soft matter, examining different approaches and highlighting advancements in polymers, as well as in functional materials such as organic/inorganic systems (MOFs, COFs, hybrid perovskites). Finally, we discuss the challenges cryo-EM faces in visualizing soft matter assemblies at high resolution and outline emerging techniques for its future advancement, inspired by the rapid technical and methodological developments currently transforming biological research.

2. Advances in cryo-EM sample preparation: From grids to lamellae

Preparing specimens for cryo-EM requires skilled handling and precise techniques across several detailed steps, always considering potential effects on the vitreous state. Sample preparation consists of two main components: grid preparation and sample optimization. Grid preparation refers to procedures required to make a sample suitable for analysis employing a microscope under cryogenic conditions, including chemical or plasma treatment of the grid, sample deposition, and vitrification [40]. Sample optimization involves tailoring the specimen to

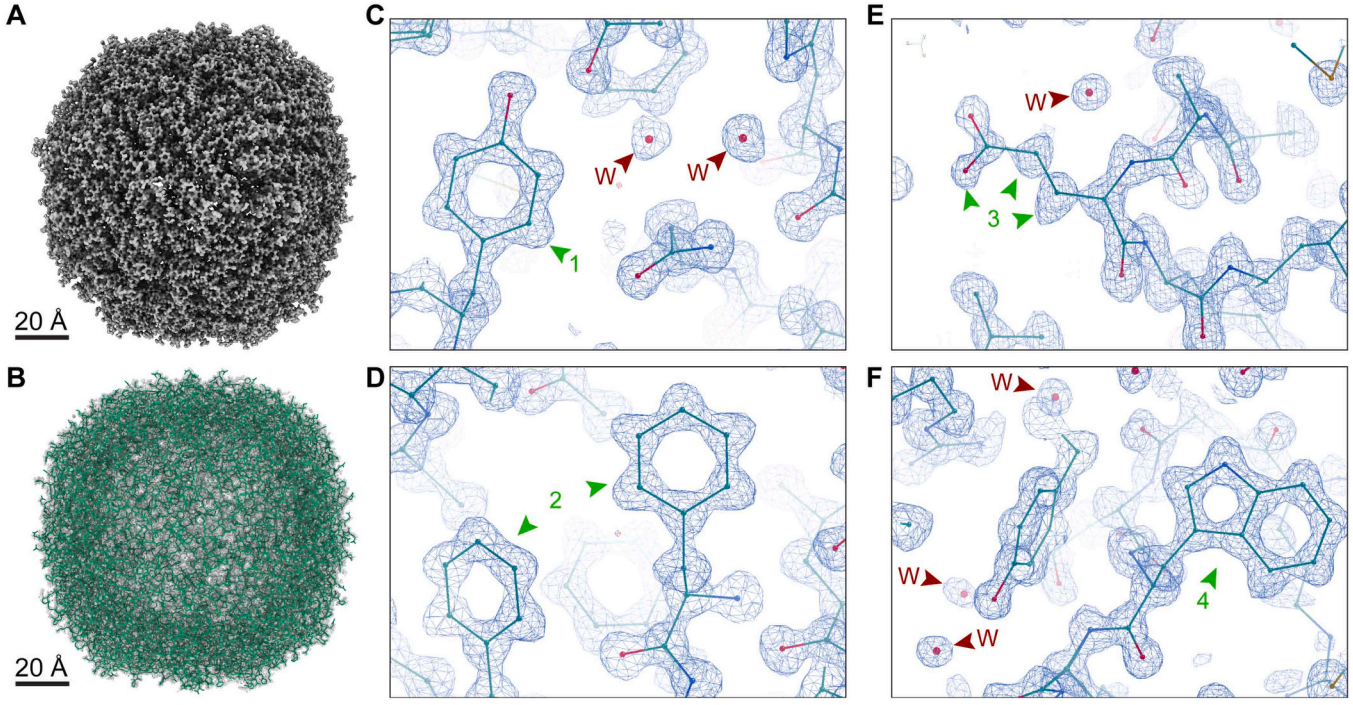

Fig. 2. Coulomb potential map of mouse heavy-chain apoferritin at 1.09 Å resolution (PDB ID: 8RQB) [19]. A. The cryo-EM map of the highest resolution apoferritin map reported to date (Scale bar: 20Å), B. Line representation of the model of mouse apoferritin, which is fitted in map (A) with high confidence (Scale bar: 20Å), C-F. Zoom in to selected regions of the map, where the true atomic resolution of the map is clearly illustrated with the aromatic rings of the amino acids side chains accurately fitted within the shown densities (green numbered arrows indicate examples of atomic resolution C.1: Tyr, D.2: Phe, E.3: Glu, F.4: Trp), as well as several waters (indicated with red arrows and the letter W) modelled within the given coulomb potential densities of the cryo-EM map.

achieve electron-transparent, structurally preserved regions and may include the production of thin sections (lamellae) using focused ion beam (FIB) milling. While FIB milling is a key sample preparation strategy in cryo-EM for materials, additional optimization approaches such as control of solvent or electrolyte composition, dispersion chemistry, and vitrification parameters are also commonly employed to preserve native solid–liquid interfaces, metastable phases, and reactive states in beam-sensitive materials systems [25,26,41,42]. These strategies differ fundamentally from biochemical approaches such as detergent screening or buffer optimization used in cryo-EM for biological samples [43], but they play an equally important role in determining specimen quality and fidelity in materials studies, particularly for functional and energy materials where interfacial chemistry and transient states are critical [44,45]. Moreover, to accurately examine the microstructural features such as composition, structure, and phase separation using a high-energy (80–300 keV) electron beam, the sample must be uniform, electron-transparent, and sufficiently thin to avoid multiple scattering events, typically requiring thicknesses in the range of tens to hundreds of nanometers [46–48]. Sample preparation is, therefore, crucial for achieving reliable results in cryo-EM, as it directly affects the quality of a specimen for imaging and analysis [49,50].

2.1. Design and selection of EM grids for optimal imaging

3 mm diameter circular grids are normally used to prepare samples for TEM, consisting of a metal mesh base covered by a support foil. In cryo-EM, the mesh is most commonly made of copper (Cu) or gold (Au), or molybdenum (Mo). Cu and Au are the most common materials of choice as they provide mechanical stability, facilitate electron conduction, and help regulate heat dissipation during imaging [51]. Gold has superior properties and also provides a chemically inert substrate for sensitive specimens, including reactive or corrosive specimens or living organisms sensitive to leached out metal ions [52]. Most common grid mesh sizes range from 100 to 400 bars per inch. For support films, perforated thin foils with various geometries, such as lacey films with irregular holes or holey foils featuring irregular or regular micrometer-scale perforations, are placed atop the mesh to support vitrified specimens. These support films can also be produced from various specimens based on the need. Carbon foils are the most widely used support films because they provide clear Thon rings for microscope alignment [53], whereas UltrAuFoil and HexAuFoil grids incorporate a gold mesh and gold foil to further enhance electrical conductivity and thermal dissipation, and reduce thermal mismatch drift [54]. Recent advances underscore that grid material has a substantial impact on sample behavior, as copper supports are prone to “cryo-crinkling” due to thermal-expansion mismatch with carbon films, while gold foils markedly reduce beam-induced motion and improve achievable resolution [55,56]. Alternative metals such as Mo or titanium (Ti) have been employed because their more closely matched thermal expansion coefficients help mitigate this problem [55]. Emerging titanium–nickel (Ti–Ni) alloy grids offer an alternative for challenging samples because their high stiffness, favorable thermal/electrical properties, and excellent chemical stability reduce charging artifacts, improve ice uniformity, and better withstand the mechanical stress of cryo-FIB milling and handling [57]. The grid-support film selection is not limited to the abovementioned combinations, which are just common selections in cryogenic electron microscopy of biological samples. The topic is well-elaborated in the electron microscopy of materials, and the materials, the geometry of the grid and the support films could be selected based on the specific properties of each sample and the analysis needs [58]. These needs could include chemical resistance and inertness, background x-ray, mechanical and thermal stability, and improved particle distribution for better visualization.

Some particles tend to adhere to the support film rather than dispersing into the foil holes, preventing effective EM analysis, and various modifications to sample carriers have been proposed to address this issue [59–62]. One common strategy is to deposit a continuous thin film -historically carbon, but increasingly graphene or graphene-oxide (GO)- to improve sample adhesion and promote dispersion, yielding successful results [59–61]. Graphene is atomically thin, highly conductive, and contributes minimal background, while functionalized GO sheets (or reduced GO, rGO) can be made hydrophilic to increase particle adsorption and reduce denaturation at the air-water interface. For example, rGO-coated grids have been shown to improve absorption of small proteins (*e.g.*, sub-100 kDa) and yield high-resolution reconstructions while avoiding air-water interface artifacts [63,64]. However, film must be kept thin to minimize background noise, and strong interactions between particles. Amorphous nickel–titanium (Ni–Ti) supports (*e.g.*, ANTcryo™) have emerged as a powerful alternative. These films combine very high electrical conductivity with minimal nonspecific protein binding, resulting in significantly reduced beam-induced motion and improved particle distribution, even compared to traditional carbon films [57]. Another approach includes chemical treatments to discourage particles from adhering to the foil and to guide them into the holes of the grid [62]. Grid support surfaces are frequently hydrophobic, hindering the effective dispersion of aqueous solutions. Low-energy plasma treatment is employed to modify surface characteristics of the grid and to increase hydrophilicity [50], and several protocols are applied for the grid’s treatment [65], and specifically for cryo-EM, plasma produced from residual air (glow discharge) is applied. Plasma treatment is also performed in specific cases using argon-oxygen mixtures; however, hydrogen may also be utilized to make plasma treatment gentler [40].

2.2. Contrast enhancement techniques of beam sensitive soft matter

In soft-matter and biological specimens, the TEM image contrast is intrinsically low because these materials consist almost entirely of light elements (H, C, N, O) with very small elastic-scattering factors [66–70]. As a result, the amplitude contrast that underpins conventional bright-field TEM is extremely weak, and neither diffraction contrast nor mass-thickness contrast [71] provides sufficient signal for reliable imaging. At the same time, such specimens tolerate only very low electron doses before undergoing radiolytic damage, which forces imaging to be performed in a dose-starved regime [51,72–75]. The combination of weak intrinsic scattering and strict dose limitations leads to images with inherently poor signal-to-noise ratios, far below those achievable for inorganic or metallic samples.

Because conventional near-focus imaging yields almost no visible contrast, cryo-TEM relies on phase contrast generated by deliberate underfocus [66,76]. Large defocus values enhance low-frequency contrast by converting phase shifts into detectable intensity modulations, but this comes at the cost of attenuating high spatial frequencies through the microscope’s envelope function [13]. Consequently, strong underfocus that is required to visualize soft matter also reduces achievable resolution and introduces oscillations in the contrast transfer function that complicate image interpretation [77]. Phase plates were developed to achieve near-focus phase contrast without resorting to large defocus [78–81], but in practice, they struggled with charging, contamination, and long-term stability, preventing widespread adoption [78,81–83]. Together, these factors explain why cryo-EM images of soft matter exhibit extremely low intrinsic contrast and why conventional diffraction or bright-field contrast mechanisms cannot be exploited for these specimens.

Currently, soft-matter samples are primarily investigated through drying, positive or negative staining, and/or cryo-fixation. Drying techniques, including freeze drying and critical point drying, are the most accessible and commonly used methods for investigating polymer self-assembly and vesicle formation [84]. A sample drop of 2–5 μL is deposited onto a carbon or polymer-coated grid and allowed to dry for a few minutes to several hours prior to imaging [85,86]. The technique derives from materials science and is appropriate for highly stable

materials [87,88]. Freeze drying, sublimation of surface water, and quick-freeze deep-etch are methods intended to preserve structural integrity; however, even with rapid vitrification, warming the sample to −80 °C to eliminate water can lead to recrystallization of vitrified water, which damages and alters the sample, particularly in colloidal suspensions [89–91]. Nevertheless, drying is highly inappropriate for hydrated soft materials, often resulting in significant artifacts, aggregation, deformation, or even complete restructuring [84,92]. Particularly for newly designed materials, discerning between artifact and genuine structure may necessitate comparing images of differently prepared samples, rendering dried samples dispensable. While some polymers may withstand drying, others, especially those reliant on water or solvents, such as amphiphilic block-copolymers, are unsuitable due to potential significant changes upon drying [92].

Positive staining presents a superior alternative, as it simultaneously fixes sample shape (in many cases), enhances contrast, and offers some protection against dehydration and radiation damage. Compared to negative staining, which includes lightly coating the sample with a fine-grained metal solution, positive heavy metal staining (iodine, ruthenium, and osmium tetroxide[93]) entails adding metals that adhere to specific sections of the sample [94]. However, staining exhibits certain drawbacks, mainly the concealing of internal features due to the stain-excluding surface, the limitation of the visible orientations due to sample support requirements, the imposition of a resolution limit dictated by stain grain size, and the inducement of significant dehydration in specimens [66] leading, frequently, to specimen flattening and/or shrinking [95]. In a similar fashion, cross-linking agents like aldehydes and peroxides offer advantages for stabilizing the specimen, but even if structures can be visualized, cannot reach atomic resolution due to non-specific interactions and probable structure deformation.

2.3. *Vitrification: Preserving native states through rapid freezing*

Cryo-fixation stands out as the premier preservation method in biological samples, such as proteins in aqueous solutions. Typically, a sample drop of a few microliters (3–4 μL) is applied to a hydrophilized grid and blotted. Concentration can greatly vary depending on the specimen's size and physicochemical properties, but it should generally fall within a range of a few μg to a few mg per ML. Up to now, blotting is the standard and most used technique to leave a thin solution layer in the grid holes [40]. More specifically, blotting is typically performed for a few seconds in an elevated humidity environment, where filter paper absorbs the excess fluid from the grid. The thickness of the created layer is adjusted through blot time, the properties of the filter paper, and the blot force [40]. At the end, the specimen is plunge-frozen into liquid ethane or ethane/propane. This rapid freezing generates a thin layer of vitreous ice, preventing ice crystal formation (that can lead to damage and obscure observation of the samples) [96]. The effectiveness of cryo-preservation is influenced by the thickness of the specimen, whilst there can be differences in the quality between the surface and the center of it, with thinner samples yielding optimal vitreous ice throughout, ensuring preservation [97].

Up to now vitrification instrumentation involves: (1) the manual plunger which refers mainly to a standard, guillotine-style manually operated blot-and-plunge device for the vitrification [98]; (2) a reliable alternative, less specialized though economical solution and portable manual cryogenic plunge freezer that allows for successful freezing of isolated specimen [99]; (3) the commercial and most commonly used *Leica EM Grid* and *Thermo Fisher Vitrobot*-grid plunge freezer units with one sided and double sided blotting option respectively; (4) the blot-free grid preparation approach of SPT Labtech named *chameleon*, that relies on automation and improves critical steps of the grid preparation process (*e.g.,* glow discharging, sample application etc.), while depositing the sample on top of the EM grid and promising more consistent and predictable ice thickness [100]; (5) the *VitroJet* that again refers to a blot free highly sophisticated instrument that deposits sample on the grid surface at sub-nanoliter volume scales reducing sample waste and sample is vitrified by jets of cryogen followed by submersion into a cryogen bath [101]; (6) and finally the amended microfluidic sample preparation method named *cryoWrite*, which entirely avoids paper blotting and allows the passivation of the air-water interface during the preparation process [102].

Cryo-EM of vitrified soft matter specimens, despite their inherent low contrast and reliance on phase contrast, provides unparalleled visualization of samples in their frozen-hydrated state and represents the foremost method for achieving high-resolution imaging. While vitrification of aqueous solutions is more effective for hydrophilic or amphiphilic samples, its utilization in hydrophobic-based samples can be performed in highly diluted aqueous solutions. To overcome this problem Wirix *et al.* utilized vitrified organic solvents to examine regioregular poly(3-hexyl thiophene) (rrP3HT) assemblies by cryo-ET, revealing a three-dimensional lamellar structure formed by the stacking of conjugated backbones with a spacing of 1.7 nm, indicating increased order within the bulk of the nanowires (Fig. 3) [103].

To avoid artifacts, it is essential to employ extra caution when using the plunge-freeze method to vitrify various organic solvents. Researchers have applied this technique to different organic solvents, including tetrahydrofuran, n-heptane, and toluene [104–107]. More specifically, Zhu *et al.* examined the formation of disk-cylinder and disk-sphere nanoparticles via a block copolymer blend solution construction, where they vitrified a fresh solution of poly(acrylic acid--*b*-methyl acrylate-*b*-styrene) triblock copolymer micelles in 1:2 by volume tetrahydrofuran to water, displaying a mixture of cylindrical and spherical micelles, along with a small amount of toroids[106]. Oostergetel and his colleagues studied solutions of the deblock copolymer polystyrene/poly-2-vinylpyridine in toluene [104], while others investigated the morphology of self-assembled micelles prepared from linear and cyclic poly(styrene-*b*-isoprene) block copolymers dispersed in n-heptane solvent [107]. Another example in blend components has been reported by Du *et al.*, where they pioneered the use of cryo-EM for examining the morphology of polymer micro-aggregates in rapidly frozen blend precursor solutions of polymer donor and polymerized small molecular acceptors (PSMAs) utilized for the fabrication of polymer solar cells [108]. By employing this technique, they imaged the preaggregation state of polymer blends in chloroform solutions, outlining the essential role that chemical structures of PSMA play on aggregation behavior in the blend solution and, by extension, the photovoltaic performance of the solar cells.

Furthermore, since many materials of interest are synthesized and used in organic solvents, a recent work by Zhang *et al.* reports the response of 23 different organic solvents to vitrification and electron exposure in cryo-TEM experiments [109]. This study revealed that 11 of the solvents can successfully be vitrified in liquid ethane, creating amorphous thin organic ice layers, and 10 of them can only be vitrified in liquid nitrogen, since they are fully dissolved in liquid ethane. Only chlorobenzene and n-decane failed to be vitrified, because they crystallized in liquid nitrogen. The 11 solvents that can be vitrified in liquid ethane are suggested for cryo-TEM experiments because they allow for better vitrification of materials contained within them. Nonetheless, these 11 organic solvents exhibit a range of physicochemical properties, making it challenging to attribute their low solubility in liquid ethane to a single characteristic. According to the electron tolerances of vitrified organic solvents, they are typically insufficient, significantly limiting the effectiveness of high-resolution cryo-TEM studies. However, it is proposed that the electron tolerance can be improved by adding water or radical scavengers [109].

Despite rapid advancements in cryo-EM, proper sample preparation remains a substantial bottleneck that must be customized and optimized for specific samples [110,111]. To minimize potential contamination and artifacts, various factors need to be considered, as mentioned previously [112]. Therefore, in addition to developing standard operating procedures for cryo-EM sample preparation, specialized protocols using

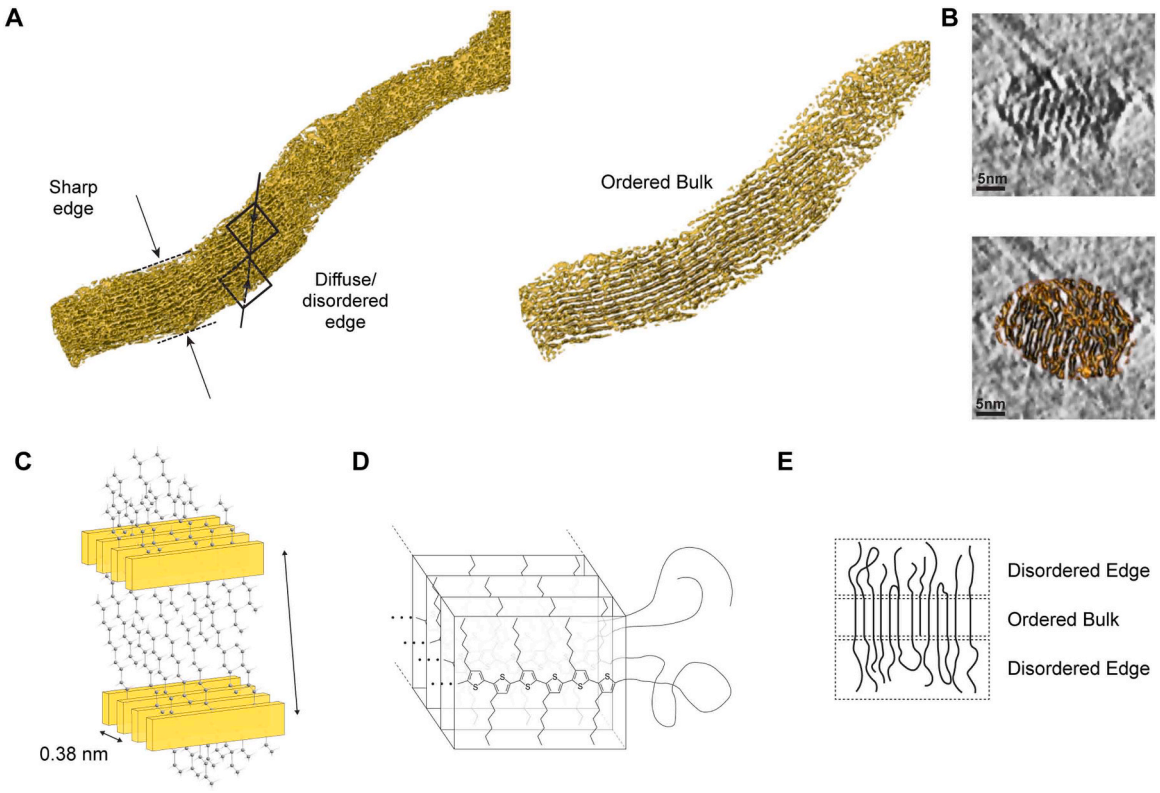

Fig. 3. Poly(3-hexylthiophene) assemblies in vitrified organic solvents visualized at nanometer scale resolution by cryo-EM. (A) A P3HT nanowire's isosurface produced via tomographic reconstruction. (B) Cross-sectional slice from the tomographic reconstruction of the wire, overlaid with the appropriate segment of the segmented structure. (C) Lamellar order model within the nanowire's core. (D) Model illustrating crystalline order in the bulk and disorder on the nanowire side. (E) Illustration displaying the ordered bulk and the disordered edges. Adapted with permission from ref. [103], Copyright 2014 American Chemical Society.

novel methods or equipment should be advanced, enhancing the efficiency as well as the quality of samples and broadening cryo-EM application to a wider range of materials.

2.4. *Techniques for lamella production from bulk specimen*

Transmission electron microscopy of soft matter is typically constrained by sample thickness, which optimally needs to be less than 300 nm, depending on acceleration voltage. If the sample exceeds this thickness, the image quality rapidly degrades, appearing mostly blurry or even black because insufficient electrons can penetrate to form an image. To address this, focused ion beam (FIB) milling can be used to locally thin thicker samples, producing *lamellae*, allowing precise targeting and extraction of specific areas and interfaces [113]. FIB/SEM, originally developed for the microelectronics industry to investigate failure mechanisms in circuit components, has since been adapted to produce high-quality TEM lamellae for a wide range of inorganic and organic semiconductors as thin films, as well as biological materials [114].

Nevertheless, specimens that are sensitive to ion or electron beams lack rigidity, contain water (such as polymers, lipids, and biological materials), or are temperature-dependent, as well as those reactive with gallium (*e.g.*, semiconductors), are unsuitable for FIB milling at room temperature due to potential alteration of the physical and chemical state of the sample through local heating, knock-on damage, radiolysis, and ion implantation [5,115]. Various techniques have been developed to moderate beam-induced damage during TEM lamella preparation. These include performing initial milling with a low-energy gallium ion (Ga^+) beam, followed by final milling with low-energy argon ions (Ar^+) and increasing the ion beam pitch (dwell overlap) [116–118]. Another promising approach, which is the preferred preparation technique for these types of materials, is cryo-freezing (mostly under high-pressure, but also, sometimes, using rapid freezing). Cryo-freezing leads to the development of cryo-compatible thinning methods, which reduce FIB-induced damage, making a substantial impact in fields such as energy research, polymers, and biological and biomimetic materials [113, 119]. An alternate method involves the generation of inductively coupled plasma from gases, such as nitrogen, oxygen, argon, or xenon. Under low beam current conditions, plasma sources exhibit probe sizes similar to gallium. However, under high beam current conditions, plasma species have lower probe sizes compared to gallium [120]. This suggests that plasma beams are suitable for milling large volumes under high currents while still being capable of the precise milling needed for thinner and more delicate lamella [121]. Grange and his group proposed a protocol for automated plasma focused ion beam (PFIB) milling lamellae of cryogenic cellular samples, demonstrating that a plasma FIB/SEM may be employed for *in situ* structural biology at near-atomic resolution levels [122]. This method also opens up possibilities for higher throughput in the field of material science, which is yet to be applied. Specifically, to attain the highest possible resolution, lamellae thickness is very important. For example, benchmarking of lamellae thickness, performed by the Gonen laboratory, indicated that optimal data for electron diffraction can be acquired at twice the mean electron free path, independent of TEM acceleration voltage. This corresponds to sample thicknesses of ~430, 540, and 640 nm for commonly used accelerating voltages of 120, 200, and 300 kV, respectively [123].

At the turn of the century, tomography on vitreous sections became feasible, using cryogenic ultramicrotomy to cut sections similarly to traditional plastic-embedded sections, eliminating the need for staining and fixation [124–127]. Nonetheless, this method faces limitations due to technical challenges and artifacts like knife marks, deformation, and preferential fracture in heterogeneous materials [128]. Recent advancements have led to the production of thinned areas within cryo-frozen specimens using FIB milling, which is more versatile and

precise than cryo-ultramicrotomy, producing samples with fewer artifacts and as close to their native state as possible. The process involves tilting the cryo-frozen sample and ablating excess material at a shallow angle to generate various geometries, such as wedges or thin lamellae, which can be imaged by cryo-TEM. This procedure is efficiently performed in dual-beam cryo-FIB-SEM microscopes, which integrate all necessary steps, including targeting, SEM imaging, sputter coating, platinum gas injection system (GIS) deposition, and milling, reducing the need for multiple transfers and handling that could damage the delicate samples. Unified holder designs between cryo-FIB-SEMs and transmission electron cryo-microscopes streamline the workflow [66]. Targeting during milling can be based on SEM imaging within the microscope or fluorescence images taken before loading the sample.

Brief SEM imaging minimizes radiation damage, and if more intense imaging is required, the sample can be sputter-coated with a conductive platinum layer to mitigate beam damage simultaneously [66]. Additionally, to prevent unwanted ion-beam erosion and minimize "curtaining" artifacts, the sample is coated with a thin metal layer, usually platinum, before milling [129,130]. This layer evens the milling speed and ensures a smooth lamella surface. After milling, a thin conductive layer (approximately 2 nm of platinum) is applied on top of the lamella to dissipate charge build-up and reduce beam-induced motion, enhancing beam tolerance for tomography [113].

An example of this technique, with applications in soft materials, comes from Wang and his group [131]. Recently, they showcased a straightforward and scalable electrochemical deposition technique for producing conductive organic-inorganic composite films with controlled size and thickness on a wafer-scale [131]. The derived quasi-layered composite film, dubbed as tungstate anion-linked polypyrrole (TALPy), demonstrates notable capacitive characteristics, and its internal composition was examined via cryo-FIB and cryo-EM. The exceptionally high milling rates with respect to silicon milled at room temperature and the excessive accelerating voltages caused the detachment of the thin film from the substrate. In this study, cryogenic temperatures were primarily employed to minimize beam damage. However, transfer was still necessary under cryogenic conditions to prevent the thin and flexible lamella from curling. As is revealed, the cryo-TEM sample suffers from ice contamination; notwithstanding, there was enough clean area available to investigate the underlying microstructure. The presence of dark spots within the grey matrix, as observed using cryo-TEM, strongly indicates the formation of tungstate aggregates.

Gels, matrices, and other complex soft materials, along with composite systems containing both hard and soft materials, present challenges in achieving a thin freezing layer, which often remains thick for TEM. Thus, cryo-EM is not frequently used to characterize them. The combination of cryo-FIB with high-pressure freezing could offer deeper structural insights into these materials. Similarly, the quite recent cryo-FIB lift-out technique demonstrates a preparation method that targets the extraction of material from high-pressure-frozen bulk multilayered specimens using a cryo-gripper tool [132]. Under this strategy [117], material is fended with the ion beam from both sides of a structure of interest, creating triangle-shaped trenches and leaving a vertical lamella in between. The lamella is subsequently almost severed from the bulk sample using the ion beam through a “J-cut” along the edges, retaining a little portion at the top to secure the lamella until it is mounted to the lift-out needle. Then, a cooled nanomanipulator needle is positioned near the lamella, and water vapor from the GIS is employed to bind the two, allowing the lamella to be entirely detached from the sample. The specimen is subsequently extracted from the bulk material, placed on a TEM half-grid utilizing water vapor, and thinned to electron transparency level. The frozen lamella is extracted from the cryo-FIB and preserved in liquid nitrogen until its transfer to the cryo-TEM.

Although the cryo-FIB lift-out technique is currently not widely used, it is expected to broaden the applications of cryo-FIB by allowing the extraction of a thin lamella from a larger sample through the selection of a specific region of interest [133,134]. Recently, Han and his group reported the ability of cryo-FIB to successfully extract thin specimens from highly sensitive bulk crystals and devices, such as metal-organic framework crystals and a hybrid halide perovskite single-crystal film solar cell [135]. This highlights the great potential of this technique to handle extremely sensitive materials and provide atomic-resolution imaging of local structures. Despite the advances of cryo-FIB in materials science, further analysis and reconstruction of the intrinsic structure are extremely limited as compared to biological specimens. Very few, if any, works have applied subtomogram averaging methods, even for specimens that are highly conformationally and chemically heterogeneous. We expect that such a transfer is feasible for several materials’ specimens in the future, drawing inspiration from “visual proteomics” [136].

3. Core capabilities and instrumental advances in cryo-EM

3.1. Electron beam damage phenomena and strategies for radiation-sensitive materials imaging in cryo-EM

Electron beam damage is the fundamental resolution-limiting factor in cryo-EM [137] and 3D electron diffraction (MicroED/3DED) [138] of soft matter. The process is governed by two stages: the initial physical interaction, followed by the cascading chemical degradation [139,140]. For low atomic number specimens (e.g., proteins, polymers, and organic frameworks), the dominant damage mechanism is radiolysis (ionization), which stems from inelastic scattering [24,58,115,141]. The incident high-energy electron transfers energy to the specimen, ejecting valence electrons and creating highly reactive free radicals, ultimately leading to the cleavage of chemical bonds (bond scission) and the irreversible loss of long-range structural order. While radiolysis (ionization) is generally the dominant damage mechanism in low-Z and organic/hybrid materials, elastic scattering/knock-on (atomic displacement) may also contribute [142]. Especially in heavy-element systems (e.g., halide or metal-containing hybrids perovskites), knock-on damage can become non-negligible, especially under imaging conditions with sufficient electron energy or after radiolysis-induced weakening of the lattice [58,115,142–149].

The specimen's resilience to this damage is quantified by the critical dose (D_c), which is the electron fluence (in $e^-/Å^2$) at which the high-resolution signal decays to 1/e (or 37 %) of its initial intensity [150–153]. The critical dose (D_c) is highly dependent on the specimen’s intrinsic chemical composition and structural stability. Beam-sensitive functional groups that lack efficient pathways to dissipate or delocalize deposited energy are the first to undergo radiolytic cleavage. In biological macromolecules, specific chemical moieties act as early “fuses”: carboxylate side chains (Asp, Glu) and disulfide bridges consistently exhibit some of the earliest site-specific damage under electron irradiation. The rapid degradation of these groups contributes to the characteristically low D_c values observed for proteins and other soft biological materials [51,154].

Organic polymers, particularly saturated aliphatic systems, are among the most beam-sensitive materials examined in TEM. Their susceptibility arises from the absence of electronic delocalization, which leaves the polymer backbone highly vulnerable to ionization-induced radiolysis. Comprehensive TEM damage reviews demonstrate that radiolysis is the dominant degradation pathway in organic and polymeric specimens, leading to rapid loss of mass, thinning, and morphological collapse under the electron beam [58,115,141,155]. Classic polymer microscopy studies likewise show that organic polymers experience severe radiation-induced degradation, with chain scission and mass loss as the primary signatures [156]. Direct irradiation experiments on aliphatic polyesters further confirm that main-chain scission is the principal reaction initiated by energetic electrons, resulting in substantial molecular-weight reduction and volatilization of degradation products [157,158]. Together, these findings establish that

aliphatic polymers undergo rapid backbone cleavage under electron irradiation, making them among the least dose-tolerant materials encountered in high-resolution electron microscopy.

Reticular frameworks such as MOFs and COFs exhibit pronounced beam sensitivity in electron microscopy due to the weakness of their characteristic bonding motifs, *i.e.,* metal-ligand coordination bonds in MOFs and covalent linker connections in COFs [159]. A comprehensive low-dose EM survey reports that for beam-sensitive frameworks (zeolites, MOFs, COFs), the critical dose for structural degradation can be as low as only a few to tens of electrons per $Å^2$, underscoring their extreme fragility under irradiation [160–163]. This behavior is exemplified in ZIF-8, where atomic-resolution imaging was achieved only by limiting the accumulated dose to ~4.1 $e^-·Å^{-2}$, beyond which the framework rapidly loses crystallinity [164]. COFs show similarly restricted dose budgets: COF-5 retains lattice fringes only up to ~26.5 $e^-·Å^{-2}$ [159], while other 2D COFs require even lower total exposures, typically 0.4–17 $e^-·Å^{-2}$, to avoid structural degradation [165]. Despite this general sensitivity, some MOFs exhibit substantially higher tolerance; in the MFM-300 series, experimentally measured critical electron fluences range from ~147 to ~1111 $e^-·Å^{-2}$, depending strongly on the metal identity [162]. These results demonstrate that while many COFs and MOFs fail at extremely low electron doses, their dose tolerance spans orders of magnitude, making per-material determination of D_c essential for reliable imaging.

As we mentioned earlier, cooling specimens to cryogenic temperatures is the primary method for reducing radiation damage in electron microscopy. While cryo-temperatures (typically ~100 K) do not prevent the first ionization event, they slow down the subsequent chemical damage by immobilizing the radiolytic products. At low temperature, free radicals produced by inelastic scattering remain trapped in the frozen matrix and cannot diffuse to react with surrounding molecules. This “cage effect”, originally described by James Franck and Eugene Rabinowitch, increases the probability of geminate recombination, which can restore some of the bonds broken by ionization. Recent simulations based on time-dependent density functional theory support the idea that, while the initial bond breaking is similar at room temperature and cryo-conditions, the fragments remain together under frozen water and fail to escape, consistent with a cage-based self-healing mechanism [51,58,72,115,139,140,166–169]. As a result, cryo-cooling significantly raises the critical dose tolerated by many organic and biological specimens. In practice, this benefit is also combined with dose fractionation: the total electron exposure is spread over many low-dose frames or “movie” frames. By collecting many such frames and aligning them computationally, high-resolution information can be extracted before radiation damage accumulates past the acceptable limit. As further discussed in the present work, dose fractionation also helps correct specimen drift and beam-induced motion arising from thermal changes or momentum transfer during electron irradiation. Together, these measures form the basis of modern low-dose imaging and cryo-EM movie acquisition [170–174].

Besides temperature, several other parameters strongly influence the rate and character of beam damage. The accelerating voltage is the most important parameter. It controls the balance between radiolysis and knock-on damage: lowering the voltage below the twice displacement energy threshold of a given atom suppresses knock-on events but generally increases the inelastic scattering cross section and thus radiolysis, which is often dominant [24]. That is why it is counterintuitively stated that the beam damage reduces with the increase of the accelerating voltage [115,175]. A careful investigation of the database on electron beam stopping power shows that the stopping power (i.e., the interaction between the beam and the sample) typically decreases with increasing electron energy up to 1–2 MeV [176]. Manufacturing TEMs of such energy level is obsolete, and these days the accelerating voltage of the commercial electron microscopes is limited to 300 kV.

It is also worth noting that although the total accumulated dose remains the dominant factor governing high-resolution signal loss in beam-sensitive materials [153], the dose rate can modulate the expression and kinetics of information loss in important ways. Across cryo-EM, soft organic materials, and insulating inorganic systems, dose-rate effects arise when the beam interacts with processes that unfold on comparable time scales, such as beam-induced motion, charging and charge-relaxation, radical diffusion and recombination, and local thermal transients [51,152,177–179]. Lower flux has been shown to reduce bubbling and motion in vitrified biological specimens, while some oxides and organics exhibit dose-rate thresholds or even non-monotonic behavior, reflecting complex coupling between radiolysis, charge buildup, and defect formation [177]. Importantly, recent ultrafast TEM and cryo-EM experiments demonstrate that delivering electrons in picosecond–nanosecond pulses does not measurably suppress radiolysis in soft or biological matter at room or cryogenic temperatures, indicating that the integrated fluence, rather than instantaneous current density, primarily determines damage [180]. In modern single-particle cryo-EM, dose-rate considerations are further shaped by detector physics: higher flux increases coincidence loss, reducing the effective information captured per unit specimen damage, making an optimal, moderate dose rate preferable in practice [181–183].

Sample thickness, local chemistry, and the surrounding environment also may play important roles in information conservation and beam damage mitigation. For example, thicker regions experience more multiple scattering, leading to higher energy deposition per unit area and faster loss of crystallinity at a given projected dose [24]. Encapsulation of beam-sensitive materials in thermally and electrically conductive layers, such as graphene, can reduce charging, spread heat, raise the effective critical dose, and scavenge radicals, as demonstrated for several low-dimensional inorganic systems [178,184–187]. Similarly, the addition of anti-oxidants can improve the radiation tolerance of the hydrated specimens [150].

Chemical bond properties and compositions of the specimen not only also affect the rate of beam damage but also the beam damage mitigation mechanisms. For example, conjugated π-polymers generally display greater beam resilience than many non-conjugated (aliphatic) polymers because their delocalized π-electron frameworks stabilize radiation-generated radicals and slow chain-scission cascades, while their higher crystallinity and tighter π–π packing can hinder radical diffusion and volatilization [153,188–190]. In contrast, saturated polymers, lacking extended electronic delocalization, undergo rapid radiolysis, producing mobile radicals that trigger chain scission, cross-linking, and mass loss at comparatively lower critical doses. As a result, π-conjugated systems often tolerate higher electron doses before structural collapse, particularly when aided by radical scavengers or conductive supports such as graphene. For organic thin films, the presence of oxygen and water significantly accelerates beam damage, whereas oxygen- and moisture-free preparation and imaging conditions yield higher critical doses and slower mass loss [153].

3.2. *Low-dose imaging in electron microscopy*

The dose management method in TEM is generally referred to as low-dose imaging. Low-dose imaging is the most important technique in the field of cryo-EM. In this technique, we try to minimize the dose needed to image the region of interest (ROI) by adjusting imaging conditions (like focusing, astigmatism correction, alignment operations) on a nearby region and taking the final image from the ROI. The microscope uses the stage or the image shift deflectors to navigate over the sample to illuminate the adjustment (focusing) or imaging (recording) area. Low-dose imaging can be done manually, but normally, they are integrated into the system as a set of pre-adjustable imaging conditions, *i.e.,* a set of magnification, condenser system arrangement, defocus, and deflectors. The user then finds the ROI in the low magnification and uses other preset imaging conditions to navigate around, adjust imaging conditions, and take an image in a sequence. A crucial part of such a system is

a responsive beam blanker. In the low-dose imaging technique, the beam is only open to take an image when the camera is active.

A major question about low-dose imaging is whether the focus remains accurate after navigating from the adjustment area to the ROI or not. The answer is no, but also it is not a vital issue; the reason is that cryo-EM normally uses phase contrast, which is developed by a certain amount of deviation from the focus. This intentional deviation from perfect focus captures phase differences and improves contrast by emphasizing imaginary planes beyond the specimen. This deviation is called defocus and leads to fluctuation in the imaging transfer function, suppressing some image information frequencies and developing contrasty outlines around the objects. The positive aspect is that we can calculate the defocus from the image using the well-established Contrast Transfer Function model [191], making some deviation from the adjusted situation acceptable and detectable in the image.

The evolution of low-dose imaging for cryo-TEM has greatly facilitated the examination of material systems that comprise organic components [39], allowing the visualization of soft nanoparticles, enabling the measurement of size and morphology for individual particles, and the assessment of sample polydispersity. The technique has been widely applied in the characterization of organic nanoparticles and hybrid assemblies. Modicano *et al.* investigated the size distribution of two different conjugated polymers that were encapsulated within the liquid midchain triglyceride (MCT) core of lipid nanocapsules (LNCs) in an attempt to form photostable probes for optical and photoacoustic bioimaging[192], while Jackman *et al.* formed drug-loaded poly(ethylene glycol)–poly(lactic acid) (PLA–PEG) block copolymer nanoparticles (AZDNPs) through a nanoemulsion technique, employing a modified oil-in-water emulsification solvent extraction method. This study focused on a detailed physicochemical characterization of the nanoparticles, examining their morphology and how these properties, especially nanoparticle polydispersity, affect biodistribution using cryo-EM [193]. Similar to this approach, cryo-EM was utilized to elucidate the architecture of oil-in-water nanoemulsions and their carriers of cannabidiol loaded conformation [194]. Using cryo-EM, Paxton *et al.* visualized how hybrid vesicles composed of 1, 2-dioleoyl-sn-glycero-3-phosphocholine (DOPC) lipids and poly (ethylene oxide-*b*-butadiene) (PEO-PBd) block copolymers adhere and fuse onto mesoporous silica nanoparticles [195]. The cryo-EM images showed that, despite increasing polymer content, conformal bilayer coatings can still form around the 3D silica cores; however, as the polymer fraction rises, vesicle adsorption on planar surfaces becomes increasingly heterogeneous—many intact adhered vesicles rather than smooth bilayers are observed. This structural insight from cryo-EM correlates with decreased lateral fluidity measured by other techniques and supports the conclusion that higher polymer loading disrupts fusion/film formation of hybrid vesicles [195]. De Mel *et al.* used cryo-EM to show that adding an n-alkyl-PEO polymer to phospholipid vesicles induces a transformation from unilamellar to multilamellar structures, with about a 9 % increase in vesicle size [196]. The images suggest that the polymer partially disrupts the lamellar organization of the bilayer, correlating with a ~30 % reduction in bending rigidity per bilayer measured by neutron spin echo (NSE) spectroscopy [196].

Another research group highlighted the significance of surface topography of PEGylated nanoparticles based on tuning the architecture of shape-persistent amphiphilic bottlebrush block copolymer (BBCP) building blocks to be utilized in biomedical applications [197]. More specifically, here, the authors used cryo-EM to image nanoparticles in their native hydrated state, to confirm their micellar core-shell structure, as well as to examine differences stemming from the changes in structural parameters of BBCP architecture, affecting the interactions of the NPs with proteins and cells. Additionally, cryo-EM was performed to visualize bolalipids aggregates [198], whilst a very recent study reported the successful visualization of individual polymer chains in the vitrified state without additives for contrast enhancement, owing to the significant mass contrast of the inorganic backbone [199]. Upon assembly with proteins, numerous protein copies bind at the level of a single polymer chain, resulting in structures resembling compact spherical complexes or rigid coils [199]. A systematic visualization of proteopolymersomes is also performed using low-dose protocols. Marušič *et al.* visualized the fusion of synthetic amphiphilic membranes and observed efficient membrane and content mixing [200]. Amphiphilic polymers and oppositely charged lipids can effectively undergo rapid fusion, while anionic lipids are not essential for the integration of membrane proteins in (proteo)polymersomes[201]. Both of above-mentioned works originate from the former study of the group that tested the functional integration of a proton pump in a polymer compartment [202], while other systems, such as giant unilamellar vesicles, can also be characterized using cryo-EM [203]. These applications underscore the versatility and necessity of low-dose techniques for preserving the native morphology of soft matter during imaging.

Understanding the physical and chemical properties of crystalline materials relies on crystallographic study. To determine the crystal structure of materials containing organic components, traditional methods use X-ray, neutron, or electron diffraction techniques in reciprocal space to identify the periodic structure of the crystal. However, these methods have limitations in terms of spatial resolution and cannot handle structures that are polycrystalline or locally disordered. In a recent study, Huang and his group reported the design and construction of free-standing two-dimensional woven polymer networks (2DWPNs) based on the woven polymerization of 1,4-bis(benzodioxaborole)benzene (BDBB) and 1,2-bis(4-pyridyl)ethylene (BPE) driven by dative B–N bonds [204]. The surface structural features of the 2D woven polymer nanosheets were observed with high spatial resolution and superstructure integrity at a molecular level by low-dose (0.5 e^- $pixel^{-1}$ s^{-1} or 3 e^- $Å^{-2}$ s^{-1}; e^-, electron) cryogenic TEM. Topological characteristics of the woven polymer networks can be distinctly observed with structural information transfer up to 2.2 Å (Fig. 4). This work demonstrates that combining low-dose and cryo-EM imaging techniques with a state-of-the-art electron direct detector and an ultrastable cryo-transfer holder can successfully image highly beam-sensitive materials, such as purely organic networks.

Li *et al.* introduced a novel cryo-EM technique to reveal atomic host-guest structures in MOFs [205], displaying that these structures can be maintained at low temperatures to achieve high-resolution imaging. When the sample ZIF-8 was exposed to an accumulated electron dose of 90 $e^-·Å^{-2}$ at cryogenic conditions, it only exhibited partial amorphization. On the contrary, when exposed to a dose of 50 $e^-·Å^{-2}$ at ambient temperature, its crystallinity was completely lost. Another research group investigated the mechanism of protein-MOF nucleation and growth using cryo-EM [206]. They showed that aggregation of amorphous particles plays a role in initiating the dissolution-recrystallization process. Tong *et al.* aimed to determine the atomic-level structure of biomacromolecule-MOFs and the inherent connection between their structure and activity. Interestingly, the optimal image quality is achieved with a total dose of 30 $e^-·Å^{-2}$, which is comparable to the dosage used for MOFs and COFs at ambient conditions [207]. This implies that although cryogenic conditions can significantly enhance stability, it may not be a universally efficient option for all materials in this category. In the case of COFs, recently Winter and his colleagues examined the influence of steric interactions within the pores of two-dimensional COFs on their network structures [208]. By introducing a linker design strategy that incorporates bulky functional groups, the researchers could impede *sql* net formation through steric interactions, resulting in a *kgm* structure which can lead to interesting optical and electronic properties [209]. In their study, cryo-EM was used for the structural characterization of the different COFs employing a low-dose strategy for imaging, with an average electron dose of 50 $e^-·Å^{-2}$ at a pixel size of 0.936 Å in electron counting mode, and a frame rate of 310/s [208].

Further advanced techniques in cryo-EM, including single particle analysis (SPA), electron tomography (ET), and subtomogram averaging, and electron diffraction for single particles and micro-crystals, have

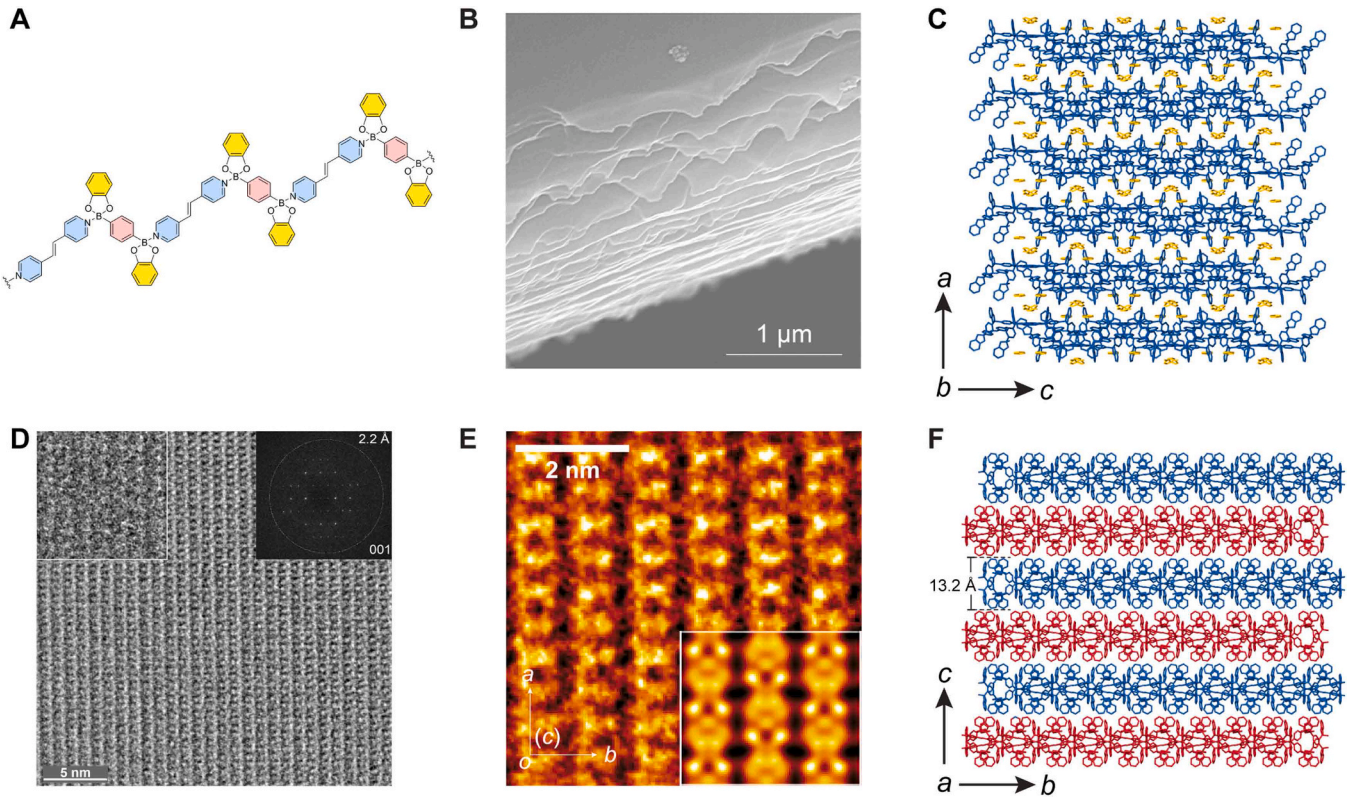

Fig. 4. Illustration and characterization of the crystalline 2DWPN-1. (A) Chemical structure of 2DWPN-1. (B) SEM image of the cross-section of a 2DWPN-1 crystal. (C) Perspective along the b-axis of the crystal arrangement in 2DWPN-1; PhMe molecules (yellow) are kept between layers, and H atoms have been excluded for enhanced clarity. (D) Cryogenic low-dose HRTEM image of crystalline 2DWPN-1 acquired along the [001] direction. The image underwent denoising, and the contrast inversion issues induced by the objective lens CTF were rectified. The insets display a raw image (upper left) and the fast Fourier transform pattern (upper right) of the HRTEM image, conveying structural information up to 2.2 Å. (E) A false-colour pattern averaged in the [010] direction, (F) Perspective along the a-axis of the crystal arrangement in 2DWPN-1; all solvent molecules and hydrogen atoms were excluded for clarity. Adapted from ref. [204] under a [CC BY 4.0] license.

substantially accelerated material characterization and are briefly reviewed below.

3.3. *High-Resolution structural determination via single particle analysis*

Single-particle cryo-EM creates 3D reconstructions by combining TEM images of isolated macromolecules, known as single particles, taken from different orientations. To achieve high-resolution 3D reconstructions, thousands of these images must be collected, aligned, and averaged [171]. The fundamental underlying concept is the "projection-slice theorem," which states that the Fourier transform of a 2D projection of a 3D object corresponds to a central slice of the 3D Fourier transform of that object [210]. This suggests that by acquiring sufficient 2D projections from various angles, where the particle has to ideally be in the center of the image, the entire Fourier space can be sampled and the object rebuilt using Fourier inversion.

The determination of the relative orientations of the 2D projections is extremely important for this process, typically accomplished in the past with an iterative algorithm known as "projection matching" [210,211]. The algorithm starts by creating an initial 3D reference structure, producing projections (reprojections) in different directions, and then determining the orientations of these projections by comparing them alongside the experimental single-particle images. After that, an updated 3D reference is generated using the experimental images, and the process is repeated until no more resolution gains are achieved. Currently, powerful maximum likelihood image processing algorithms have been developed, utilizing the Bayesian approach to data analysis [212]. These algorithms can handle the high volumes and complexity of data from the new detectors reliably and objectively, with marginal user intervention [213]. For this iterative process to succeed, the experimental data must be of high quality, with good angular coverage and no preferred particle orientations (orientation bias). Under these conditions, the algorithm usually converges to the correct structure even if the initial reference is a low-resolution representation [210] or random densities, especially when Bayesian inference is applied [211]. Nonetheless, if these conditions are not met, the algorithm might get stuck in a local minimum, leading to a model bias effect. This can be mitigated or identified by using an *ab initio*-derived model from the experimental data. Two common methods for generating such models are the random conical tilt method [214] and the "common lines" approach [215], but are rarely used presently, as single-particle analysis now includes enough particles for unbiased 3D reconstructions. Still, methods for generating references continue to grow, such as initial model generation with tomography and subtomogram averaging [216].

In the not-so-long distant past, the typical resolution achievable by cryo-EM SPA was relatively poor, often worse than 10 Å, leading to the method being dubbed "blob-ology." However, recent technological advancements in both hardware and software have dramatically improved this technique, allowing it to determine structures of complex macromolecules at near-atomic resolution. Traditionally associated with biological systems, cryo-EM SPA has only recently been applied to the structure determination of synthetic inorganic nanomaterials. A study successfully used cryo-EM SPA to analyze chemically and structurally homogeneous silica cages ("silicages") with a dodecahedral structure and sizes under 10 nm, achieving a resolution of around 2 nm [217] (Fig. 5). This resolution, of course, is much less detailed as compared to biomolecular structures resolved by cryo-EM nowadays. Although there were difficulties in achieving atomic resolution owing to the amorphous nature of the silica in these cages, this study demonstrated the potential of cryo-EM SPA for examining similar systems.

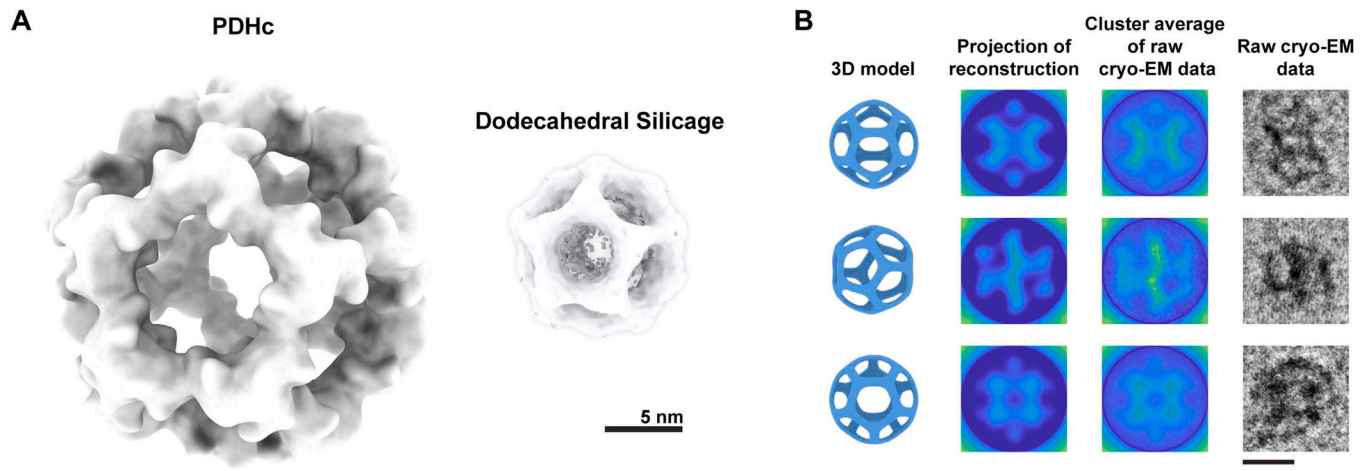

Fig. 5. Single-particle reconstruction of the dodecahedral silicage. (A) Comparison of the reconstructions of the pyruvate dehydrogenase complex (PDHc) core (left) and dodecahedral silicage (right). (B) A representative comparison of three distinct projections from the reconstruction and cryo-EM cluster averages alongside projections of a 3D dodecahedral cage model. Corresponding individual cryo-EM micrographs are presented, illustrating the distinction between the raw data and the reconstruction The scale bar in (B) denotes 10 nm. Adapted with permission from ref. [217].

In the case of polymeric materials, reconstructing single particles becomes more complex because polymers typically do not form uniform shapes, in contrast to biological samples, where each particle is near-identical. The underlying reasons are unclear, but biological samples have evolved in time and therefore have been optimized by natural selection for billions of years for a specific cellular function. The intrinsic structural flexibility of many polymers and polymer nanostructures renders multi-particle averaging challenging to reach atomic resolution, as also previously reported [46]. Consequently, most of their cryo-EM research is focused on examining high mass contrast systems (*e.g.,* supramolecular assemblies, polymer-based fibers, and micelles) rather than on visualizing individual chains of linear polymers [199]. Lee *et al.* have shown that observing the average distribution of a polymeric brush layer on a viral-polymer conjugate is feasible [218]. In this study, the authors investigated the immune shielding properties of three different polymers attached to virus-like particles (VLPs), which are protein structures resembling native viruses but are non-infectious, derived from the bacteriophage Qβ. Particles conjugated with poly(norbornene-(oligo(ethylene glycol) ester)) (PNB) showed the most effective shielding from antibody recognition. A cryo-EM reconstruction of the Qβ-PNB viral-polymer conjugate reveals a visual representation of the PNB brush layer (red) covering most of the viral capsid [218]. Recently, Xu *et al.* used metallo-supramolecular branched polymer (MSBP) in the preparation of cryo-samples for high-resolution SPA to enhance their quality [219]. This study addresses the common issue of air-water damage by suggesting the use of palladium-polyethylene glycol MSBP which seems to improve the distribution and orientation of proteins in vitreous ice, making them more suitable for SPA studies.

3.4. *Three-dimensional imaging with cryo-electron tomography*

Cryo-electron tomography shares similarities with SPA in deriving three-dimensional visualization of frozen-hydrated samples. However, cryo-ET achieves this by collecting a series of two-dimensional projections from a single specimen area, known as a tilt series. This is done by physically tilting the stage to various angles. The collected images are then computationally assembled into a three-dimensional reconstruction called a tomogram. Due to design constraints of the stage and sample holder, the tilting range is usually restricted to $\pm 70^{\circ}$, creating a wedge-shaped region of missing information in Fourier space, commonly referred to as “missing wedge”. This limitation leads to non-isotropic resolution, causing structural features to appear elongated in the beam direction [220,221]. To mitigate these effects, methods like dual-axis tomography -where tilt series are acquired around two orthogonal axes- can be employed, although they are not widely used due to technical challenges as well as discussions over their usefulness for downstream tomography analysis [222]. One of the most common 3D reconstruction techniques in cryo-ET is weighted back-projection, which back projects the 2D projections into 3D space while compensating for the uneven distribution of information in Fourier space [223]. Alternatively, iterative reconstruction algorithms, such as the simultaneous iterative reconstruction technique (SIRT) [224] and the algebraic reconstruction technique (ART) [225], minimize the discrepancies between experimental 2D projections and the reprojections of the 3D image. Currently, algorithms inspired by SPA analysis are also being employed in tomography reconstruction and subtomogram averaging, with software such as RELION [226], Warp [227], and M [228] spearheading the field.

Cryo-ET is particularly suitable for analyzing complex and pleomorphic structures since it does not require multiple copies of the structure of interest. In addition, angular and distance information across pleomorphic objects can be derived as the 3D information is encoded in the reconstructed tomogram. Due to the sensitivity of cryo-preserved soft matter samples to electron beams, tilt series acquisition must be conducted under low-dose conditions, distributing the total electron dose across the images. This generally results in a low signal-to-noise ratio in both 2D projections and the 3D reconstruction. Although several technical parameters, such as pixel size, angular range, and increment, influence the nominal resolution in cryo-ET, the low SNR is typically the limiting factor. Subtomogram averaging, mentioned above, is a technique used to enhance resolution in cryo-ET when (near-) identical copies of structures (such as macromolecular complexes or virus particles) are present in a tomogram. This involves selecting, aligning, and averaging subtomograms containing identical structures to improve the SNR and resolution while also reducing the impact of the missing wedge. Another limitation of cryo-ET is sample thickness; for samples thicker than about 500 nm, thinning methods are required.

For over ten years, electron tomography has been utilized to investigate the three-dimensional structures of soft material systems. Utilizing cryo-ET, Allen *et al.* produced the first three-dimensional reconstructions of the hydrophilic-hydrophobic microphase separation in hydrated Nafion nanostructure [229]. This understanding will be particularly useful, since Nafion is an extensively used membrane in proton exchange membrane electrolyzers and fuel cells, which are considered a promising solution for clean energy transportation, especially in a modernized low-duty vehicle fleet [229]. Understanding the

influence of the microstructure of the membrane on ion transport is central for the success of this specific application, as well as for assessing durability parameters of the material. Since precise manipulation of the internal and external shapes of polymer nanoparticles has garnered significant interest in nanosciences, Yuan and his group visualized and investigated in detail the internal and external shapes of a series of 1,2,4-triazolium-type poly(ionic liquid) nanoparticles [230]. The modification of altering the length of the alkyl tails linked to the imidazolium or triazolium cation was precisely visualized and examined using cryo-EM and cryo-ET, achieving sub-5 nm nanodomain spacing. Similarly, mixed poly(acrylic acid) (PAA)/polystyrene (PS) brush-grafted 67 nm silica nanoparticles in organic and aqueous solvents were investigated via cryo-ET, confirming the environmentally responsive nature of the specific nanoparticles [231]. In N,N-dimethylformamide (DMF) solvent, mixed PAA/PS brushes are seen to create laterally separated microdomains with a ripple length of 13.8 nm. Due to its lower grafting density compared to PAA, PS forms domains that are either cylindrical or truncated cone-shaped within the PAA matrix. In water, PAA chains form a more complete shell around the nanoparticle to enhance their interaction with the water, while PS chains collapse into the core of surface-tethered micelles near the silica core. Recently, Seneviratne and colleagues used a combination of small-angle X-ray scattering (SAXS) and cryo-ET, together with SPA, to resolve the nanoscale structure of hybrid vesicles consisting of phospholipids and block-copolymers [232]. They showed that as the polymer fraction increases, the membrane thickness grows dramatically (from ~52 Å for pure lipid to ~97 Å for pure polymer) and leads to two distinct structural states—one weakly and one strongly interdigitated—rather than a continuous transition. This bistability reveals that hybrid membranes, even when compositionally uniform, favor discrete architectures, offering key insight into how polymer–lipid composition governs bilayer organization [232].

3.5. Elemental contrast and nanoscale imaging in STEM

Scanning transmission electron microscopy is a well-established technique for characterizing materials at micro, nano, and atomic scales [233–235], demonstrating the ability to image dose-resistant specimens with optimal spatial resolutions exceeding 0.5 Å [236,237]. Furthermore, STEM imaging provides crucial structural information for understanding the relationship between material structures and their functionalities. Integrated differential phase contrast-STEM (iDPC--STEM) [238,239] is a specific imaging method within STEM that is effectively used to observe a variety of specimens [240–242], including metal hydrides, at subatomic resolutions, encompassing both heavy and light elements, including hydrogen [243]. Furthermore, iDPC-STEM has successfully imaged many crystalline and amorphous materials, such as beam-sensitive zeolites [244,245] and metal-organic frameworks [246], which can only be scanned with electron doses below 50 $e^-/Å^2$ to prevent structural damage [205]. By employing iDPC-STEM with a minimal exposure of 40 $e^-/Å^2$, a resolution of 1.8 Å was successfully achieved from a single micrograph of MOF materials of the Institute Lavoisier (MIL)-101 [247]. Recently, iDPC-STEM facilitated direct image interpretation to dose-sensitive low-contrast biological specimens without requiring defocusing and subsequent adjustment of the contrast-transfer function [248,249]. Additionally, cryo-STEM was utilized on single-particle specimens of ferritin loaded with Fe or Zn to accurately image and identify the metals within the protein cage [250].

4D-STEM employs convergent electron beams to scan a sample in two-dimensional real space, while a detector captures two-dimensional reciprocal-space data at each scan point. Unlike conventional STEM, which relies on detectors like bright-field, differential phase contrast, or high-angle annular dark-field and is constrained by scattering angles, 4D-STEM uses a direct electron detector to record the entire diffraction pattern. Subsequently, this extensive 4D dataset is examined utilizing "virtual" detectors and complicated algorithms (*e.g.*, HyperSpy, pyXem, LiberTEM, Pycroscopy, and py4DSTEM) [251] to extract specific information about the sample [37]. Previously, the distribution of crystallites in a polymer blend was mapped employing 4D-STEM [252]. A later study by Minor's group indicated that structure-property correlations in organic systems could potentially be observed by combining 4D-STEM with cryogenic temperatures, since the technique's flexibility and applicability to any semicrystalline or ordered organic material [253] enable measurement and comparison of phase morphology in these materials at an unprecedented spatial resolution [254]. They correlated the improved device performance achieved through processing and chemical additives with the distribution and orientation of nanocrystalline domains in the polymer by investigating two organic semiconductor thin film systems [254]. More precisely, they investigated the small molecule 7,7′-(4,4-bis(2-ethylhexyl)-4*H*-silolo[3,2-b:4,5-b′]dithiophene-2,6-diyl)bis(6-fluoro-4-(5′-hexyl[2,2′-bithiophen]-5-yl)benzo[*c*] [1,2,5]-thiadiazole), abbreviated as p-DTS $(FBTTh_2)_2$ processed with and without 1,8-diiodooctane solvent (DIO), revealing the impact of DIO on the morphology of the polymer. Moreover, they examined the microstructure of the poly[2,5-bis(3-tetradecylthiophen-2-yl)thieno[3,2-*b*]thiophene] (PBTTT) polymer under varying annealing conditions (as-cast and annealed in the liquid-crystal phase at 180 °C), demonstrating the efficacy of the 4D-STEM technique in elucidating the structure-property correlations pertinent to organic field-effect transistors. However, the focused electron probe caused damage, limiting the scanning step size to 10 nm with a 2 nm probe, even when samples were cooled to liquid nitrogen temperatures. By replacing the charge Charge-Coupled Device (CCD) detector used in these experiments with a DED capable of high dynamic range [174], it is possible to achieve improved spatial resolution and greater material stability. In such an attempt, employment of a fast direct electron detector to collect extensive, multi-dimensional diffraction datasets allowed for the mapping of intrinsic structural ordering in sensitive samples, such as semi-crystalline polymers [255]. This approach classified crystalline and amorphous phases in semi-crystalline polymers, thus quantifying diverse ordering length scales. Using low-temperature 4D-STEM enhances analysis of structure-function relationships and depicts the heterogeneous architecture of semi-crystalline polymers, crucial, *e.g.,* in energy-related applications. This capability is especially important in the energy sector, where intricate relationships between a material's microstructure and its macroscopic behavior are of economic value.

Cryogenic STEM has achieved notable advancements in organic mixed ionic-electronic conductors (OMIECs), an emerging class of soft, dynamic, and functional materials that exhibit both ionic and electronic conductivity. These materials hold significant promise as active components in thin-film electronic devices, which are utilized in a variety of applications, including energy storage and bioelectronics. Tsarfati *et al.* examined the microstructure of synthetically designed polymeric OMIEC thin films using two complementary electron microscopy techniques [256]: HRTEM and 4D-STEM, focusing on both their dried and hydrated states. Employing 4D-STEM, they acquired detailed microstructural data of the thin film of an ethylene glycol functionalized polythiophene based conjugated polymer, called p(g3T2) [257,258], over large fields of view in its dry state and successfully identified its three-characteristic crystalline spacings: lamellar stacking, backbone stacking, and π-π stacking, with dimensions ranging from ~3.4 Å to ~20 Å. Autocorrelation analysis of these planes revealed varying levels of polymer chain rigidity along the two packing directions. In the edge-on orientation (along the π-π stacking), the relative grain orientation can reach up to 35°, whereas in the face-on orientation (along the lamellar direction), it is limited to 10°. More recently, the same group published a study where they are investigating the structure of p(g3T2) across multiple length scales in both its dry and hydrated states, clarifying the microstructural changes occurring during film swelling in electrolyte and connecting the resultant mesoscale to the performance of the swollen material [259] (Fig. 6).

By applying the cryo-4D-STEM, the dry state was characterized as a

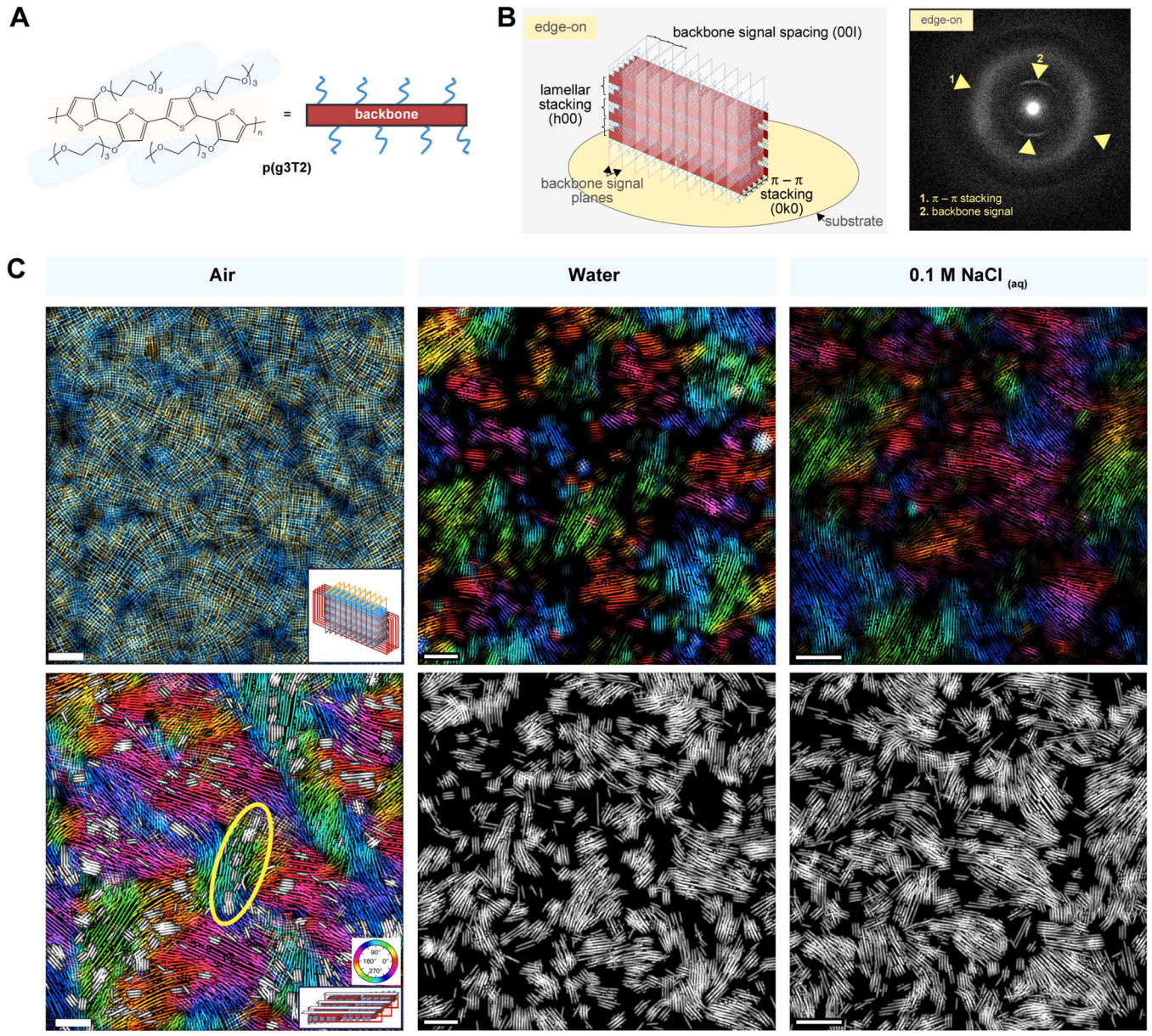

Fig. 6. Examination of the microstructure of a polymeric OMIEC thin film across multiple length scales using cryo 4D-STEM in both its dry and hydrated states (A) Chemical structure of p(g3T2) and its schematic. (B) Schematic of the typical crystalline structures in polythiophene-based polymers in edge-on orientation with respect to the substrate, where the characteristic crystallographic directions are indicated (left). Representative DPs from 4D-STEM scans of dry p(g3T2) films. A broad π–π stacking signal and an arc-shaped backbone signal, marked with yellow arrows 1 and 2, respectively, are shown (right). (C) Representative orientation maps of 4D-STEM scans of a dry p(g3T2) film, a water-hydrated p(g3T2) film, and a 0.1 M $NaCl_{(aq)}$-hydrated p(g3T2) film, respectively. Scale bars, 200 nm. On the upper line, 4D-STEM scans derived from the π–π stacking (edge-on maps) are depicted, whilst the maps at the bottom visualize the lamellar stacking (face-on maps). In the case of dry p(g3T2) film, the map at the bottom illustrates both the edge-on and face-on textures: the colored lines indicate the direction of polymer chains in the edge-on crystallites, and the white lines correspond to the direction of polymer chains in the face-on crystallites. Adapted with permission from ref. [259].

baseline for understanding the changes associated to swelling in the presence of the electrolyte. The hierarchical microstructure of the material was mapped at the mesoscale utilizing a comprehensive set of signals, allowing for visualization of heterogeneity, crystalline domains, and their orientation distribution, whilst correlations between the signals translated into unit-cell information and characteristics of the edge-on/face-on texture were identified. Additionally, they analyzed the hydrated state of the film in both water and aqueous electrolyte solutions, comparing the results with those from the dry state [259]. Such studies offer valuable insights into the microstructure of OMIECs, even in their hydrated operating state, which is essential for developing more efficient, low-cost organic-based functional devices.

A principal application of 4D-STEM is electron ptychography, which reveals the atomic structure of a specimen by reconstructing its transmission function from redundant convergent-beam electron diffraction patterns [260]. Ptychography is a lensless imaging technique initially suggested by Hoppe [261], where a sample is scanned using a properly configured probe in a 2D array [262]. This yields a collection of diffraction patterns recorded in the far field as a function of probe position, resulting in a 4D dataset. Utilizing this 4D dataset, quantitative phase data with elevated spatial resolution can often be extracted through several iterative phase retrieval algorithms [263,264]. However, despite the numerous advantages of 4D-STEM ptychography compared to traditional imaging methods, its application to materials that are highly sensitive to electron beams remains limited due to many practical challenges in both experimental setup and data analysis

[265–267]. The integration of rapid scanning methods, cryogenic sample preparation, and enhanced detector technologies effectively reduces potential sample damage while stabilizing the sample in its frozen-hydrated state. This synergy makes 4D-STEM an invaluable technique for obtaining high-resolution insights while preserving sample integrity. As a result, it becomes attractive particularly for studying beam-sensitive materials, including crystalline, semi-crystalline, amorphous, and mixed phases.

3.6. Atomic-level elemental mapping: Energy-Dispersive X-ray Spectroscopy and Electron Energy Loss Spectroscopy

A key factor in analyzing material processes is understanding both the structure and the atomic components, along with their spatial arrangements. EDS and EELS can be coupled with cryo-EM to provide a more comprehensive understanding of sensitive beam materials, such as soft matter, polymers, MOF, COF, and carbon nanostructures. Both EDS and EELS can be used to map the distribution of elements within a sample, which is useful for studying phase separation in polymer blends, identifying dopants in carbon nanostructures, and visualizing distributions of elements in soft matter, COF, and MOF assemblies. EDS may offer quantitative analysis of elemental composition, yielding insights into the stoichiometry of compounds and the concentration of elements in various regions of a sample. However, EDS typically requires relatively high electron doses and repeated exposures to obtain signals from the sample; limitations could be mitigated by cryo-EM. For materials that demonstrate inelastic electron scattering at low energies, EELS serves as a more dose-efficient alternative for elemental analysis, especially for detecting energy losses in low-energy regions [268]. Furthermore, EELS provides comprehensive insights into the chemical bonding environment of elements, facilitating the analysis of bond types, bond lengths, and electronic transitions. This information is crucial for understanding the properties of polymers and carbon nanostructures. Therefore, EDS and EELS offer complementary information about the sample.

Hondow and her team reported imaging and analysis of frozen hydrated suspensions using STEM-EDS-EELS under cryogenic conditions, which identified and separated CeO_2, Fe_2O_3, ZnO, and Ag nanoparticles in suspension [269]. The authors demonstrated that STEM allowed for larger electron fluxes (up to 2000 $e-/Å^2$) compared to conventional TEM (less than 100 $e-/Å^2$), without causing significant damage to the frozen vitreous ice. Another research group highlighted the importance of cryo-STEM-EDS for characterizing Pickering emulsions, which are liquid droplets stabilized by particles at the liquid/liquid interface, in their native state [270]. Very recently, Pfeil-Gardiner *et al.* presented a combination of EELS with single-particle image processing to visualize elemental mapping of cryo-preserved macromolecular complexes [271]. Reconstructed electron energy-loss (REEL) analysis facilitates a three-dimensional reconstruction of electron energy-loss spectroscopic data, enabling the accumulation of a high total electron dose across numerous copies of a complex. By analyzing two test samples, the authors demonstrate their ability to reliably locate abundant elements, highlighting the method's potential to probe the architecture of macromolecular complexes [271].

A key area utilizing high-resolution and elemental analysis via cryo-EM is for understanding the operational mechanisms in batteries. Despite batteries being primarily inorganic systems, several studies demonstrate the role of organic components, such as polymer electrolytes, in their performance. Highlighting cryo-EM applications in this context is, therefore, appropriate. Wu's group investigated the use of ion-dipole-reinforced poly-3-hydroxymethyl-3-methyloxetane as a novel solid-state electrolyte, presenting it as a significant alternative to conventional poly(ethylene oxide) in lithium metal batteries [272]. Cryo-TEM combined with EDS revealed the formation of a lithium fluoride (LiF)-rich interface, where lithium is deposited in a columnar shape rather than in protrusions or filaments, promoting uniformity and stability at the PHMP-Li interfaces [272]. Kourkoutis and her team utilized cryo-STEM and EELS to acquire high-resolution structural and chemical data regarding the dendrites and their corresponding solid-electrolyte interphase (SEI) layers [41]. He *et al.* examined the progressive growth of the SEI towards the interior of the Si anode using cryo-STEM-HAADF imaging and EDS tomography [273]. This study focuses on the observation of the evolution of the spatial correlation between the Si and the SEI layer, as the structural growth of Si occurs simultaneously with the formation of the SEI in the silicon nanowire. The findings highlight the role of vacancies created by the lithium (Li) ions during operation, rather than suggesting that the instability of the SEI is merely a response to the volume changes of the electrode [273]. Additionally, the same group published a similar study of SEI in rechargeable batteries [274]. More specifically, by combining cryo-STEM with EDS tomography, they showcased 2D EDS maps alongside corresponding 3D EDS tomograms. This demonstration highlighted the gradual mixing of the solid electrolyte interphase (SEI) layer with silicon, correlating structural and chemical changes during battery cycling [274].

3.7. Electron Diffraction techniques for crystalline and nanostructured samples

Electron diffraction (ED) is a powerful technique for structural determination at very high resolution, allowing deciphering molecular structures of complexes in their vitreous state that is not feasible with any other method [275,276]. Due to the de Broglie theory, the accelerated electrons in electron microscopes can behave like a wave and hence scatter upon passing through the matter. Like other wave-particle phenomena (*e.g.,* X-rays and neutrons), the scattered electrons can also form a diffraction pattern given that the scattering matter has an ordered structure. The diffraction pattern has substantially higher resolution information than images, but due to a lack of phase information, analysis comes with some difficulties. Several methods have been proposed to tackle this issue. The first method was based on retrieving phase information via very thin samples, i.e., 2D crystals, as first proposed by Klug and Berger and further developed by Henderson and Unwin [277]. This method is referred to as 2DED.

For thicker crystals, the abovementioned method does not readily work, and therefore, 3D electron diffraction (3DED) or microcrystal electron diffraction (MicroED) methods are applied. This is due to the increasingly complex image contrast formation mechanisms for thicker samples (in direct space). In return, some researchers tried to approach structure determination via other already established phasing methods, like direct phasing (for smaller molecules) and molecular replacement methods (in proteins) [278–285].

The most basic method, which involves tilting and recording the diffraction pattern, is called Electron Diffraction Tomography (EDT) [286,287]. In this approach, the sample rotates, and a diffraction pattern is recorded at each step. The resulting diffraction tilt series is handled using normal X-ray diffraction analysis packages. Electron diffraction, however, has some differences from other diffraction techniques like X-ray diffraction. One difference is wider scattering factors and wider interaction ranges. Electrons diffract by both the electron fields and the nuclei fields. This theoretically can give extra information about the atoms, *e.g.,* charge states, but it has not yet been deeply investigated [288]. The cross-section of the electron scattering event is also much bigger than other commonly available high-energy beams, *e.g.,* neutrons and X-rays. This is both an opportunity and a problem: It makes diffraction studies of much smaller crystals possible, but, on the other hand, promotes the dynamic diffraction mechanisms in slightly thicker samples. This makes structural analysis using kinematic models very difficult. Another dissimilarity between electron diffraction and other diffraction methods is the geometrical differences: Ewald Spheres are extremely big –like a flat plane– in ED. On the other hand, the electron reflection spots in the reciprocal space are elongated in the

through-the-thickness direction. This relaxes the Bragg condition but makes the reflection intensity read out inconsistent. To address this issue, several improvements are suggested: *i.e.,* continuous crystal rotation and concurrent recording of the diffraction pattern in certain periods (cRED) and undulating the beam over the sample (*i.e.,* Precession Electron Diffraction, PED).

Similar to the normal electron microscopy in direct space, ED can also be done with the low-dose method, *e.g.*, as described in our preprint [276]. In low-dose ED, the beam is adjusted in a region away from the crystal, and then the diffraction pattern is recorded on the crystal. This method is now gradually gaining a reputation for structural analysis of increasingly small crystals, which is one of ED's unique applications. As also mentioned previously, porous materials have attracted considerable interest in recent years, and detailed knowledge of their atomic structures is vital for understanding the structure-property relationship. On the one hand, most of these materials are soft and beam sensitive, and growing big enough crystals to make X-ray diffraction analysis is quite challenging [289]. 3DED or MicroED allows for the examination of such small crystals, providing valuable information about structures at the nanoscale [281–285]. Moreover, the electron beam undergoes deviation from the zone axis while collecting data, thereby reducing the impact of dynamical effects in thin samples, while the potential beam damage is mitigated if the measurement takes place in cryogenic conditions using low dose, allowing high-resolution structural analysis.

The incorporation of organic components decreases the structural stability of MOFs, thus, it is essential to focus on reducing the detrimental impact of radiation on MOF crystals. In 2011, an attempt to use 3DED for defining MOF structures (MFU-4l material) was achieved by applying automated diffraction tomography (ADT) in combination with electron precession [290]. Here, the reciprocal space is sampled by incrementally tilting a nanosized crystal across a whole tilt range permissible in TEM. Nanobeam electron diffraction was employed to generate a low-dose, small, semi-parallel electron beam and utilized scanning TEM to image and monitor the crystal, making this method suitable for beam-sensitive materials typically inaccessible by standard electron diffraction methods [291]. ADT can be used with PED to further improve intensity quality by incorporating the spacing between the tilts. This technique successfully resolved intricate nanoporous materials, like charoite [292]. In a recent study, a cooling sample holder and the rotation electron diffraction (RED) program were used to acquire MicroED datasets of Hf_{12}-BPDC and Zr_{12}-BPYDC nanoplates [293]. BPDC refers to biphenyldicarboxylate, and BPYDC refers to bipyridinedicarboxylate. This method significantly enhanced the tolerance of the MOF to the electron beam, thereby facilitating the accurate measurement of its structure. The MOFs with $P6_3/mmc$ space group are isostructural and consist of twelve-nucleus clusters (Hf_{12}/Zr_{12}) and organic ligands, whilst topological analysis reveals that the Hf_{12}/Zr_{12} metal nodes are 12-connected and form a hexagonal layer that is stacked in an ABAB pattern along the [001] direction.

Contrary to MOFs, COFs are mainly composed of organic molecules connected by robust covalent bonds that have higher bond energy, making them more structurally stable, withstanding even in acidic or basic environments. The process of creating COFs typically requires making compromises between the factors of "crystallinity" and "stability," meaning that even though COFs exhibit strong covalent bonds, they often suffer from low crystallinity, which restricts their performance and potential applications [281]. Therefore, the development of effective approaches for synthesizing COFs that are simultaneously stable and crystalline is a challenge in the field of porous material research. A successful application of 3DED to study COF structures was reported in 2013 and achieved using COF-320 [294]. Despite the poor quality of the diffraction data, along with a low resolution of up to 1.5 Å at 89 K, a total of 570 distinct reflections were recorded. Since then, several studies have been published in this field [159]. It is also reported that the atomic-level dynamics of submicrometer COF-300 single crystals by utilizing cryo-electron diffraction tomography (EDT) is feasible [295]. Here, *ab initio* structural analysis underlined the characterization of the contraction of the crystal upon H_2O adsorption and determined the positions of all non-hydrogen atoms of the framework, as well as the location of the guest molecules in the pores. Additionally, the COF-300 crystal expanded when an ionic liquid or polymer was included in the channels, which can confirm the conformational characteristics of the frameworks. In addition, Sun *et al.* recently reported for the first time that the hydrogen atoms of a COF, both on the framework and on the guest molecule, can be precisely located utilizing 3DED with continuous precession electron diffraction tomography (cPEDT) at cryogenic temperatures, providing new perspectives into the investigation of COFs [296].

4. Automation, AI tools, and the role of open data in cryo-EM workflows

Regardless of the microscopy method, statistical analysis is eventually required to improve the signal while reducing noise. Consequently, the field is progressing toward acquiring large datasets, which aims for systematicity and reproducibility, advancing EM into a true quantitative science. It is, therefore, appropriate to also briefly report on the recent advances in the computational handling of recorded cryo-EM data.

Traditionally, after acquiring raw images and spectra, and to reach near-atomic resolution for biological structures, data processing of those massive datasets is essential to extract representative and distinctive characteristics. Generally, this is a time-consuming process, primarily through traditional manual procedures, bearing the risk of introducing errors due to cognitive bias. Furthermore, multiple steps are being performed, like initial preprocessing to reduce noise and signal blurring, and then data processing that involves several algorithms, for segmentation, tracking, quantification, visualization, analytics, and modelling [297,298]. Recently, the extensive evolution of computer science and, particularly, computer vision, led to a continuous development of even more advanced computational methods and their incorporation into intuitive software tools, significantly improving the accuracy and convenience of analysis [299,300]. Specifically, for SPA, maximum-likelihood procedures based on Bayesian inference are employed to align, average, and classify the recorded frames, and reconstruct macromolecular complexes, enhancing the signal-to-noise ratios, thus resulting in improved reconstruction quality [301].

However, directly translating these SPA workflows from biomolecular systems to materials science introduces several fundamental limitations that must not be overlooked. Common SPA software used to date, such as RELION [161] and cryoSPARC [302], were originally developed with the assumption of extremely large numbers of near-identical particles. This redundancy allows accurate alignment and averaging of otherwise noisy 2D projections, often leading to high-resolution 3D reconstructions. In contrast, in materials science, samples tend to be polydisperse, polymorphic, or continuously heterogeneous, exhibiting broad size and shape distributions, coexisting crystal polymorphs, or smoothly varying structures. Under these conditions, averaging will either blur valid variations and fail to classify

successfully or force misclassification and bias the reconstruction [303]. Although modern heterogeneity-aware tools such as cryoSPARC's 3D-variability analysis [304] and deep-learning frameworks like CryoDRGN [305] can recover certain discrete and continuous forms of variability, they still require high particle counts, strong signal-to-noise, and, overall, narrow distributions. These requirements are often not met in materials datasets, where low particle yield, broad polydispersity, preferred orientation, and pronounced beam sensitivity limit the number and quality of usable particles.

In cryo-ET, the subtomogram averaging procedure aligns patterns with a reference and generates an average 3D map, reducing random noise and emphasizing shared structural characteristics [306].

In contrast to the extensively automated data processing methods utilized in biology [307], statistical analysis is necessary for obtaining trustworthy and representative results from cryo-EM images of materials. This procedure entails collecting data from random areas, extracting pertinent information from images, and quantifying the frequency to provide statistical outcomes [308]. Under this strategy, the use of AI-enabled approaches is highly desired. Machine learning (ML), a subset of artificial intelligence (AI), employs computer algorithms to autonomously learn from data and utilize this acquired knowledge for decision-making [309,310]. This technology has recently been applied to microscopy imaging and spectroscopy analysis, emerging as a next-generation deep learning (DL) that performs training without human supervision by using artificial neural networks. [311–313]. Also recently applied such entirely automated identification of macromolecules in heterogeneous specimens [314]. Both its physics-based foundations and its applications in structural biology were recognized with Nobel Prizes in 2024, in Physics and Chemistry, respectively.

Convolutional neural networks excel in image analysis tasks, demonstrating their capability to autonomously identify, segment, and analyze specific structures or attributes in TEM datasets. These algorithms can differentiate between original structural elements and random disturbances, resulting in effective noise reduction techniques that do not compromise the quality of the data. Furthermore, the use of ML in cryo-EM permits data analysis in real time and redefines data processing and automation in electron microscopy. The inherent adaptability, speed, and accuracy of ML algorithms enhance the accuracy of interpreting complicated microscopic structures, hence boosting cutting-edge microscopy techniques [227,315,316]. A recently published work introduced a novel method for accurately estimating the locations of oxygen atoms in water molecules surrounding protein structures [317]. This is achieved via the integration of two advanced deep learning models: a 3D U-net and a Multi-Layer Perceptron (MLP). This method offers fast inference runtimes, making it an excellent option for protein structure analysis and drug discovery applications.

ML, besides image analysis, has excellent opportunities for improving microscope operation, aiding and improving the entire cryo-EM workflow. Currently, image acquisition algorithms are supplemented with AI functions, however, it is envisioned that various operations (*e.g.*, preventing sample contamination, integrating cryo-ultramicrotomy and cryo-FIB techniques for sample preparation, and streamlining methods to ease the workflow) will integrate AI to minimize the risks and errors. The combination of AI with classical statistical approaches will increase automation of activities, enhance the efficiency of high-throughput sampling, improve accuracy, and uncover patterns that are not straightforward to identify using traditional methods.

Moreover, groundbreaking advances delivered by AI-driven algorithms during the last decade, transformed the perspective of structural prediction in the field of structural biology. In principle, AlphaFold [318] (developed at DeepMind, a subsidiary of Alphabet Inc.) and RoseTTAFold [319] (developed at the University of Washington in Seattle) relied for their training to depositories like UniProt and Protein Data Bank (PDB) [320], providing the necessary pool of data to predict protein structures with remarkable accuracy. In turn, the recent AlphaFold Protein Structure Database resource (https://alphafold.ebi.ac.uk/), in its initial release, enclosed a set of 365,000 predicted structures for unique UniProt entries, and currently includes 214 million models [321]. Finally, due recognition should also be extended to the recent advances in cryo-EM as well as the resulting open databases of Electron Microscopy Data Bank (EMDB) and EMPIAR for providing a storage collection of biomolecules' structural data and raw cryo-EM images, respectively. These data, in the future, will accelerate the accuracy of determining higher-order macromolecular structures (a challenge currently for AI-based structure prediction) by being utilized as accurate datasets.

With the trajectory defined, application of analogous principles could revolutionize the materials science field. Adoption of Open science and adherence to FAIR principles (Findable, Accessible, Interoperable, and Reusable) are critical to establish and develop a global repository of materials data. Similar to the aforementioned success seen in biological sciences, ML approaches could be applied in materials data to better understand and predict their properties. The increasing availability of such data to the materials science community must be centralized and already holds great potential to accelerate the pace of discovery in the field. Widespread availability of openly accessible datasets can serve as a catalyst for currently inconceivable discoveries and reshape research paradigms.

5. Challenges, innovations, and the future of cryo-EM for soft matter

Automated cryo-EM has revolutionized structural biology, but its applications are increasingly vital in materials science. While TEM with advanced analytical spectrometers remains a valuable tool for specific materials characterization, a single, automated cryo-EM equipped with advanced spectrometers such as EDS and EELS will provide significant advantages for a broad range of materials (polymers, nanoparticles, MOF, COF, carbon nanostructures) and biological applications. Its superior sample preservation, enhanced imaging of beam-sensitive materials, streamlined workflow, and optimized spectrometer performance will make it a powerful and efficient tool by pushing the boundaries of scientific knowledge, accelerating research in materials and biology scientific fields, and fostering technological innovation. Facilities and laboratories worldwide focused on cutting-edge materials and biological sample characterization, investing in a state-of-the-art automated cryo-EM with built-in advanced spectrometers, STEM options, along with a complete automated correlative workflow covering from the sample preparation up to data analysis (Fig. 7), should be a strategic priority and future policy. Currently, this type of cryo-EM is rare worldwide and of previous generation in terms of cameras, detectors, filters, etc., as well as the facilities containing complete automated correlative workflows.

Moreover, while cryo-EM has advanced materials science and holds promise for broader future applications as presented in this work, several challenges persist. Alongside the creation of standard operating procedures for sample preparation in cryo-EM, it is crucial to develop specialized protocols that incorporate innovative techniques or equipment. This progress is intended to improve both the efficiency and quality of samples, while also expanding the versatility of cryo-EM for various sample types as needed. Another major challenge is improving the spatial resolution of cryo-EM images, which requires, besides better samples, developing even more stable sample stages, faster cameras with

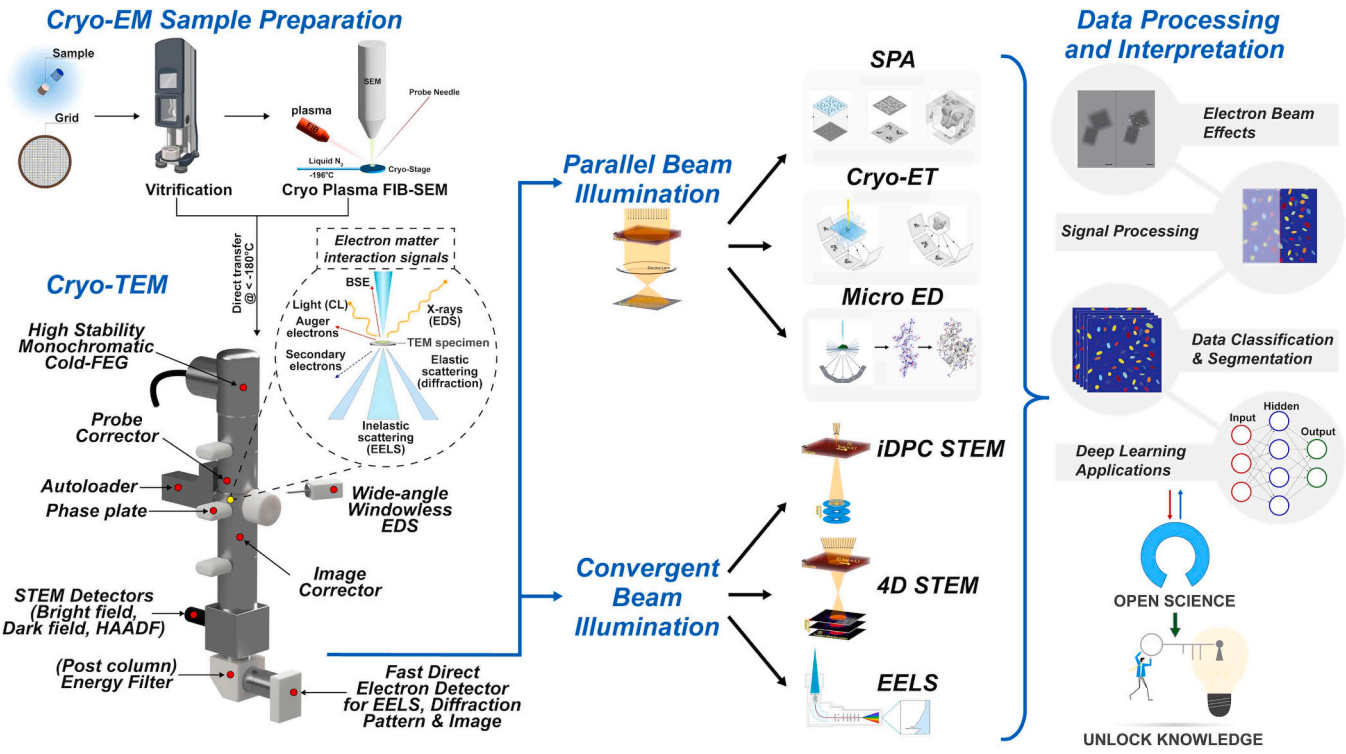

Fig. 7. Illustration of the cryo-electron microscopy facilities of the future containing the next generation of automated cryo-EM with advanced built-in spectrometers such as EDS, EELS, STEM, etc. Note that EELS is already adopted in cryo-EM workflows. While image correctors are hard to automate, ongoing developments gradually improve their integration. Probe correctors are currently rare, and advanced add-ons such as scanning modules and EDS remain less common. Finally, incorporating EDS with a cryo-stage poses technical hurdles but overcoming these could open opportunities for increased analytical capabilities in research and industrial settings.

larger detectors, more precise drift correction algorithms, and using lower-dose electron imaging techniques. It's also essential to assess cryo-EM's ability to analyze different materials and yield reliable results. To address this, correlative light and electron microscopy (CLEM) techniques can assist in the comprehensive micron-scale imaging for functional information and nanoscale analysis for precise structural and compositional details [322,323]. Additionally, incorporating probes like Raman or infrared (or even mass spectrometric capabilities) within the cryo-EM chamber could provide valuable information about amorphous or organic structures alongside crystalline materials.

ML and high-throughput calculations can facilitate automatic sampling and screening methods, enhancing the collection of realistic structural information. A notable example is the integration of cryo-EM with artificial intelligence, which has revolutionized structural biology research. AlphaFold [318], a Nobel-Prize-winning AI program, has accurately predicted many protein structures, rivalling experimental methods in modeling protein complexes. AI platforms like AlphaFold can decipher complex molecular structures with precision and efficiency, accelerating research. However, as mentioned before, such algorithms are based on open-source data produced by researchers for decades, in the form of > 240,000,000 Uniprot and > 220,000 protein data bank entries. Similar type of algorithms are needed in materials science, particularly for more complex macromolecular architectures such as polymers, supramolecular assemblies of nanoparticles, colloid nanoformulations and 2D-materials. While available data for small organic and inorganic compounds in the open databases such as Cambridge Crystallographic Data Centre (CCDC), Inorganic Crystal Structures Database (ICSD), Carolina Materials Database (CMD), Materials Project and Open Materials Database currently exist, similar open databases for polymers, nanoparticles, colloids and 2D-materials are totally missing.

In materials science, compared to traditional 2D projection TEM images, cryo-ET, which provides 3D structural information of the studied specimen, is underutilized but offers significant potential for material analysis. This is because the structural relationship of various regions of the material in 3D can be analyzed and, eventually, more accurately modeled using experimental data, *e.g.,* integrated with analysis utilizing Materials Studio (https://www.3ds.com/products/biovia/materials-studio) or the Schrödinger Suite (https://www.schrodinger.com/platform/), or future open-access options. The development of operando measurements or time-resolved cryo-EM is also essential for observing material evolution processes and capturing metastable intermediate states during rapid chemical reactions at low temperatures. The rapid advancements in AI technology have enabled various ML approaches to address pressing data analysis challenges in *in situ* TEM and 4D-STEM [324].

Currently, ML-enhanced data analytics primarily focuses on image processing to extract atomistic, morphological, and microstructural features. Additionally, there has been promising progress in automating electron diffraction and spectroscopy analyses. We anticipate that the deep synergy between *in situ* TEM, the development of open-access databases for materials science data, and ML-enhanced analytics will propel energy materials research forward [3]. Finally, establishing standardized workflows and protocols for cryo-EM across various

systems is crucial for promoting, not only industrial advancements, but also systematic comparisons across materials specimens, which may well fuel the next resolution revolution in cryo-EM, but now for soft matter.

Declaration of Competing Interest

The authors declare that they have no known competing financial interests or personal relationships that could have appeared to influence the work reported in this paper.

Acknowledgements

This work was supported by the Horizon Europe ERA Chair "hot4-cryo", project number 101086665 (to P.L.K.), the Federal Ministry for Education and Research (BMBF ZIK HALOmem, grant nos. 03Z22HN23, 03Z22HI2 and 03COV04 (to P.L.K.), the European Regional Development Funds (EFRE) for Saxony-Anhalt (grant no. ZS/2016/04/78115 and grant no. ZS/2024/05/187255 (to P.L.K.), the German Research Foundation (DFG, project numbers 391498659, RTG 2467 and 514901783, CRC 1664), the Martin Luther University Halle-Wittenberg and the National Hellenic Research Foundation. C.L.C. acknowledges the Hellenic Foundation for Research and Innovation (H.F.R.I.) under the "2nd Call for H.F.R.I. Research Projects to support Faculty Members & Researchers" (Project Number: 4694) and under the "Basic research Financing (Horizontal support of all Sciences)" call under the National Recovery and Resilience Plan "Greece 2.0" funded by the European Union –Next Generation EU (H.F.R.I. Project Number: 17007). We would like to thank all the Chochos and Kastritis lab members for fruitful discussions.

Data availability

No data was used for the research described in the article.

References

[1] J.C.H. Spence, The future of atomic resolution electron microscopy for materials science, Mater. Sci. Eng. R Rep. 26 (1999) 1–49, https://doi.org/10.1016/S0927-796X(99)00005-4.
[2] K.A. Taylor, R.M. Glaeser, Electron diffraction of frozen, hydrated protein crystals, Science 186 (1974) 1036–1037, https://doi.org/10.1126/science.186.4168.1036.
[3] H. Zheng, X. Lu, K. He, In situ transmission electron microscopy and artificial intelligence enabled data analytics for energy materials, J. Energy Chem. 68 (2022) 454–493, https://doi.org/10.1016/j.jechem.2021.12.001.
[4] M.L. Taheri, E.A. Stach, I. Arslan, P.A. Crozier, B.C. Kabius, T. LaGrange, A. M. Minor, S. Takeda, M. Tanase, J.B. Wagner, R. Sharma, Current status and future directions for in situ transmission electron microscopy, Ultramicroscopy 170 (2016) 86–95, https://doi.org/10.1016/j.ultramic.2016.08.007.
[5] J. Watt, D.L. Huber, P.L. Stewart, Soft matter and nanomaterials characterization by cryogenic transmission electron microscopy, MRS Bull. 44 (2019) 942–948, https://doi.org/10.1557/mrs.2019.285.
[6] A.R. Faruqi, G. McMullan, Direct imaging detectors for electron microscopy, Nucl. Instrum. Methods Phys. Res A 878 (2018) 180–190, https://doi.org/10.1016/j.nima.2017.07.037.
[7] G. McMullan, A.R. Faruqi, R. Henderson, Direct electron detectors, Methods Enzym. 579 (2016) 1–17, https://doi.org/10.1016/BS.MIE.2016.05.056.
[8] W. Kühlbrandt, The resolution revolution, Science 343 (2014) 1443–1444, https://doi.org/10.1126/science.1251652.
[9] D.B. Williams, C.B. Carter, Transmission Electron Microscopy, Springer US, Boston, MA, 2009, https://doi.org/10.1007/978-0-387-76501-3.
[10] A.F. Brilot, J.Z. Chen, A. Cheng, J. Pan, S.C. Harrison, C.S. Potter, B. Carragher, R. Henderson, N. Grigorieff, Beam-induced motion of vitrified specimen on holey carbon film, J. Struct. Biol. 177 (2012) 630–637, https://doi.org/10.1016/J.JSB.2012.02.003.
[11] D.N. Mastronarde, SerialEM: a program for automated tilt series acquisition on tecnai microscopes using prediction of specimen position, Microsc. Microanal. 9 (2003) 1182–1183, https://doi.org/10.1017/S1431927603445911.
[12] J. Frank, Single-particle imaging of macromolecules by cryo-electron microscopy, Annu Rev. Biophys. Biomol. Struct. 31 (2002) 303–319, https://doi.org/10.1146/annurev.biophys.31.082901.134202.
[13] Y. Cheng, Single-particle cryo-EM at crystallographic resolution, Cell 161 (2015) 450–457, https://doi.org/10.1016/j.cell.2015.03.049.
[14] R. Henderson, J.M. Baldwin, T.A. Ceska, F. Zemlin, E. Beckmann, K.H. Downing, Model for the structure of bacteriorhodopsin based on high-resolution electron cryo-microscopy, J. Mol. Biol. 213 (1990) 899–929, https://doi.org/10.1016/S0022-2836(05)80271-2.
[15] M. Adrian, J. Dubochet, J. Lepault, A.W. McDowall, Cryo-electron microscopy of viruses, Nature 308 (1984) 32–36, https://doi.org/10.1038/308032a0.
[16] J. Lepault, F.P. Booy, J. Dubochet, Electron microscopy of frozen biological suspensions, J. Microsc. 129 (1983) 89–102, https://doi.org/10.1111/j.1365-2818.1983.tb04163.x.
[17] J. Frank, A. Verschoor, M. Boublik, Computer averaging of electron micrographs of 40 S ribosomal subunits, Science 214 (1981) 1353–1355, https://doi.org/10.1126/science.7313694.
[18] M. van Heel, J. Frank, Use of multivariates statistics in analysing the images of biological macromolecules, Ultramicroscopy 6 (1981) 187–194, https://doi.org/10.1016/S0304-3991(81)80197-0.
[19] B. Küçükoğlu, I. Mohammed, R.C. Guerrero-Ferreira, S.M. Ribet, G. Varnavides, M.L. Leidl, K. Lau, S. Nazarov, A. Myasnikov, M. Kube, J. Radecke, C. Sachse, K. Müller-Caspary, C. Ophus, H. Stahlberg, Low-dose cryo-electron ptychography of proteins at sub-nanometer resolution, Nat. Commun. 15 (2024) 8062, https://doi.org/10.1038/s41467-024-52403-5.
[20] T. Nakane, A. Kotecha, A. Sente, G. McMullan, S. Masiulis, P.M.G.E. Brown, I. T. Grigoras, L. Malinauskaite, T. Malinauskas, J. Miehling, T. Uchański, L. Yu, D. Karia, E.V. Pechnikova, E. de Jong, J. Keizer, M. Bischoff, J. McCormack, P. Tiemeijer, S.W. Hardwick, D.Y. Chirgadze, G. Murshudov, A.R. Aricescu, S.H. W. Scheres, Single-particle cryo-EM at atomic resolution, Nature 587 (2020) 152–156, https://doi.org/10.1038/s41586-020-2829-0.
[21] K.M. Yip, N. Fischer, E. Paknia, A. Chari, H. Stark, Atomic-resolution protein structure determination by cryo-EM, Nature 587 (2020) 157–161, https://doi.org/10.1038/s41586-020-2833-4.
[22] D.W. McComb, J. Lengyel, C.B. Carter, Cryogenic transmission electron microscopy for materials research, MRS Bull. 44 (2019) 924–928, https://doi.org/10.1557/mrs.2019.283.
[23] K. Naydenova, A. Kamegawa, M.J. Peet, R. Henderson, Y. Fujiyoshi, C.J. Russo, On the reduction in the effects of radiation damage to two-dimensional crystals of organic and biological molecules at liquid-helium temperature, Ultramicroscopy 237 (2022) 113512, https://doi.org/10.1016/j.ultramic.2022.113512.
[24] R.F. Egerton, Control of radiation damage in the TEM, Ultramicroscopy 127 (2013) 100–108, https://doi.org/10.1016/j.ultramic.2012.07.006.
[25] S. Weng, Y. Li, X. Wang, Cryo-EM for battery materials and interfaces: Workflow, achievements, and perspectives, IScience 24 (2021) 103402, https://doi.org/10.1016/j.isci.2021.103402.
[26] X. Wang, Y. Li, Y.S. Meng, Cryogenic Electron Microscopy for Characterizing and Diagnosing Batteries, Joule 2 (2018) 2225–2234, https://doi.org/10.1016/j.joule.2018.10.005.
[27] E. Zhang, M. Mecklenburg, X. Yuan, C. Wang, B. Liu, Y. Li, Expanding the cryogenic electron microscopy toolbox to reveal diverse classes of battery solid electrolyte interphase, IScience 25 (2022) 105689, https://doi.org/10.1016/j.isci.2022.105689.
[28] Z. Ju, H. Yuan, O. Sheng, T. Liu, J. Nai, Y. Wang, Y. Liu, X. Tao, Cryo-Electron Microscopy for Unveiling the Sensitive Battery Materials, Small Sci. 1 (2021), https://doi.org/10.1002/smsc.202100055.
[29] Y. Zhu, Cryogenic Electron Microscopy on Strongly Correlated Quantum Materials, Acc. Chem. Res 54 (2021) 3518–3528, https://doi.org/10.1021/acs.accounts.1c00131.
[30] H. Wu, H. Friedrich, J.P. Patterson, N.A.J.M. Sommerdijk, N. de Jonge, Liquid-Phase Electron Microscopy for Soft Matter Science and Biology, Adv. Mater. 32 (2020), https://doi.org/10.1002/adma.202001582.
[31] R.A.L. Jones, Soft Condensed Matter, Oxford University Press Inc, New York, 2002.
[32] L.S. Hirst, Fundamentals of Soft Matter Science, CRC Press, 2019, https://doi.org/10.1201/9781315192383.
[33] S.R. Nagel, Experimental soft-matter science, Rev. Mod. Phys. 89 (2017) 025002, https://doi.org/10.1103/RevModPhys.89.025002.
[34] J. van der Gucht, Grand Challenges in Soft Matter Physics, Front Phys. 6 (2018), https://doi.org/10.3389/fphy.2018.00087.
[35] Y. Yan, J. Huang, B.Z. Tang, Kinetic trapping – a strategy for directing the self-assembly of unique functional nanostructures, Chem. Commun. 52 (2016) 11870–11884, https://doi.org/10.1039/C6CC03620A.
[36] Y. Li, W. Huang, Y. Li, W. Chiu, Y. Cui, Opportunities for Cryogenic Electron Microscopy in Materials Science and Nanoscience, ACS Nano 14 (2020) 9263–9276, https://doi.org/10.1021/acsnano.0c05020.
[37] X. Chen, Applications of Cryogenic Electron Microscopy in Characterizing Electrochemical Materials and Interfaces, Highlights Sci. Eng. Technol. 96 (2024) 14–20, https://doi.org/10.54097/7csg5b12.
[38] K. He, Cryogenic electron microscopy for emerging materials research: From quantum materials to energy applications, MRS Commun. 12 (2022) 471–482, https://doi.org/10.1557/s43579-022-00198-1.
[39] G. Wang, J.-H. Lin, Cryogenic transmission electron microscopy on beam-sensitive materials and quantum science, Chin. Phys. B 33 (2024) 086801, https://doi.org/10.1088/1674-1056/ad5af0.
[40] G. Weissenberger, R.J.M. Henderikx, P.J. Peters, Understanding the invisible hands of sample preparation for cryo-EM, Nat. Methods 18 (2021) 463–471, https://doi.org/10.1038/s41592-021-01130-6.
[41] M.J. Zachman, Z. Tu, S. Choudhury, L.A. Archer, L.F. Kourkoutis, Cryo-STEM mapping of solid–liquid interfaces and dendrites in lithium-metal batteries, Nature 560 (2018) 345–349, https://doi.org/10.1038/s41586-018-0397-3.

[42] M. Lee, Y. Jeon, S. Kim, I. Jung, S. Kang, S.-H. Jeong, J. Park, Unravelling complex mechanisms in materials processes with cryogenic electron microscopy, Chem. Sci. 16 (2025) 1017–1035, https://doi.org/10.1039/D4SC05188B.

[43] N. Liu, H.-W. Wang, Better Cryo-EM Specimen Preparation: How to Deal with the Air–Water Interface? J. Mol. Biol. 435 (2023) 167926 https://doi.org/10.1016/j.jmb.2022.167926.

[44] K. Liang, X. Yuan, X. Chen, B. Liu, J.T. Kim, J. Yu, D. Zhao, Y. Li, A Beginner's Guide to Cryo-EM for Battery Research, Nano Lett. 25 (2025) 7210–7223, https://doi.org/10.1021/acs.nanolett.5c00740.

[45] M.J. Zachman, Z. Tu, L.A. Archer, L.F. Kourkoutis, Nanoscale Elemental Mapping of Intact Solid–Liquid Interfaces and Reactive Materials in Energy Devices Enabled by Cryo-FIB/SEM, ACS Energy Lett. 5 (2020) 1224–1232, https://doi.org/10.1021/acsenergylett.0c00202.

[46] B. Kuei, M.P. Aplan, J.H. Litofsky, E.D. Gomez, New opportunities in transmission electron microscopy of polymers, Materials Science Engineering R Reports 139 (2020) 100516, https://doi.org/10.1016/j.mser.2019.100516.

[47] L. Sawyer, D. Grubb, G. Meyers. Polymer Microscopy, 3rd ed., Springer New York, New York, NY, 2008 https://doi.org/10.1007/978-0-387-72628-1.

[48] T. Uragami, Science and Technology of Separation Membranes, John Wiley & Sons Ltd, 2017.

[49] R.M. Glaeser, B.-G. Han, R. Csencsits, A. Killilea, A. Pulk, J.H.D. Cate, Factors that Influence the Formation and Stability of Thin, Cryo-EM Specimens, Biophys. J. 110 (2016) 749–755, https://doi.org/10.1016/j.bpj.2015.07.050.

[50] L.A. Passmore, C.J. Russo, Specimen Preparation for High-Resolution Cryo-EM, Methods Enzym. 579 (2016) 51–86, https://doi.org/10.1016/bs.mie.2016.04.011.

[51] M. Karuppasamy, F. Karimi Nejadasl, M. Vulovic, A.J. Koster, R.B.G. Ravelli, Radiation damage in single-particle cryo-electron microscopy: effects of dose and dose rate, J. Synchrotron Radiat. 18 (2011) 398–412, https://doi.org/10.1107/S090904951100820X.

[52] C.J. Russo, L.A. Passmore, Ultrastable gold substrates for electron cryomicroscopy, Science 346 (2014) 1377–1380, https://doi.org/10.1126/science.1259530.

[53] E. Ermantraut, K. Wohlfart, W. Tichelaar, Perforated support foils with pre-defined hole size, shape and arrangement, Ultramicroscopy 74 (1998) 75–81, https://doi.org/10.1016/S0304-3991(98)00025-4.

[54] C.J. Russo, L.A. Passmore, Ultrastable gold substrates: Properties of a support for high-resolution electron cryomicroscopy of biological specimens, J. Struct. Biol. 193 (2016) 33–44, https://doi.org/10.1016/j.jsb.2015.11.006.

[55] C.J. Russo, L.A. Passmore, Progress towards an optimal specimen support for electron cryomicroscopy, Curr. Opin. Struct. Biol. 37 (2016) 81–89, https://doi.org/10.1016/j.sbi.2015.12.007.

[56] G.G. Sgro, T.R.D. Costa, Cryo-EM Grid Preparation of Membrane Protein Samples for Single Particle Analysis, Front Mol. Biosci. 5 (2018), https://doi.org/10.3389/fmolb.2018.00074.

[57] X. Huang, L. Zhang, Z. Wen, H. Chen, S. Li, G. Ji, C. Yin, F. Sun, Amorphous nickel titanium alloy film: A new choice for cryo electron microscopy sample preparation, Prog. Biophys. Mol. Biol. 156 (2020) 3–13, https://doi.org/10.1016/j.pbiomolbio.2020.07.009.

[58] R.F. Egerton, Radiation damage to organic and inorganic specimens in the TEM, Micron 119 (2019) 72–87, https://doi.org/10.1016/j.micron.2019.01.005.

[59] E. Palovcak, F. Wang, S.Q. Zheng, Z. Yu, S. Li, M. Betegon, D. Bulkley, D.A. Agard, Y. Cheng, A simple and robust procedure for preparing graphene-oxide cryo-EM grids, J. Struct. Biol. 204 (2018) 80–84, https://doi.org/10.1016/j.jsb.2018.07.007.

[60] K. Naydenova, M.J. Peet, C.J. Russo, Multifunctional graphene supports for electron cryomicroscopy, Proc. Natl. Acad. Sci. 116 (2019) 11718–11724, https://doi.org/10.1073/pnas.1904766116.

[61] C.J. Russo, L.A. Passmore, Controlling protein adsorption on graphene for cryo-EM using low-energy hydrogen plasmas, Nat. Methods 11 (2014) 649–652, https://doi.org/10.1038/nmeth.2931.

[62] J.R. Meyerson, P. Rao, J. Kumar, S. Chittori, S. Banerjee, J. Pierson, M.L. Mayer, S. Subramaniam, Self-assembled monolayers improve protein distribution on holey carbon cryo-EM supports, Sci. Rep. 4 (2014) 7084, https://doi.org/10.1038/srep07084.

[63] C. Vénien-Bryan, C.A.H. Fernandes, Overview of Membrane Protein Sample Preparation for Single-Particle Cryo-Electron Microscopy Analysis, Int J. Mol. Sci. 24 (2023) 14785, https://doi.org/10.3390/ijms241914785.

[64] L. Nan, Z. Liming, X. Jie, W. Jia, H. Cuixia, L. Jun, Z. Xing, Z. Jincan, X. Kui, C. Hang, Y. Zi, G. Xin, W. Xinquan, P. Hailin, C. Yanan, W. Hong-Wei, Reduced graphene oxide membrane as supporting film for high-resolution cryo-EM, Biophys. Rep. 7 (2021) 227–238, https://doi.org/10.52601/bpr.2021.210007.

[65] A. Belkind, S. Gershmans, Plasma cleaning of surfaces, Vac. Technol. Coat. (2008) 46–57.

[66] L.E. Franken, K. Grünewald, E.J. Boekema, M.C.A. Stuart, A Technical Introduction to Transmission Electron Microscopy for Soft-Matter: Imaging, Possibilities, Choices, and Technical Developments, Small 16 (2020), https://doi.org/10.1002/smll.201906198.

[67] M. Carroni, H.R. Saibil, Cryo electron microscopy to determine the structure of macromolecular complexes, Methods 95 (2016) 78–85, https://doi.org/10.1016/j.ymeth.2015.11.023.

[68] H. Stahlberg, T. Walz, Molecular Electron Microscopy: State of the Art and Current Challenges, ACS Chem. Biol. 3 (2008) 268–281, https://doi.org/10.1021/cb800037d.

[69] E.V. Orlova, H.R. Saibil, Structural Analysis of Macromolecular Assemblies by Electron Microscopy, Chem. Rev. 111 (2011) 7710–7748, https://doi.org/10.1021/cr100353t.

[70] H. Okamoto, Y. Nagatani, Entanglement-assisted electron microscopy based on a flux qubit, Appl. Phys. Lett. 104 (2014), https://doi.org/10.1063/1.4865244.

[71] H. Kohl, R. Reimer, Scattering and Phase Contrast. Transmission Electron Microscopy, Springer, New York, NY, 2008.

[72] H. Xue, M. Zhang, J. Liu, J. Wang, G. Ren, Cryo-electron tomography related radiation-damage parameters for individual-molecule 3D structure determination, Front Chem. 10 (2022), https://doi.org/10.3389/fchem.2022.889203.

[73] R.M. Glaeser, R.J. Hall, Reaching the Information Limit in Cryo-EM of Biological Macromolecules: Experimental Aspects, Biophys. J. 100 (2011) 2331–2337, https://doi.org/10.1016/j.bpj.2011.04.018.

[74] E. D'Imprima, W. Kühlbrandt, Current limitations to high-resolution structure determination by single-particle cryoEM, Q Rev. Biophys. 54 (2021) e4, https://doi.org/10.1017/S0033583521000020.

[75] W. Kühlbrandt, Cryo-EM enters a new era, Elife 3 (2014), https://doi.org/10.7554/eLife.03678.

[76] R.J. Hall, E. Nogales, R.M. Glaeser, Accurate modeling of single-particle cryo-EM images quantitates the benefits expected from using Zernike phase contrast, J. Struct. Biol. 174 (2011) 468–475, https://doi.org/10.1016/j.jsb.2011.03.020.

[77] R.M. Glaeser, W.J.H. Hagen, B.-G. Han, R. Henderson, G. McMullan, C.J. Russo, Defocus-dependent Thon-ring fading, Ultramicroscopy 222 (2021) 113213, https://doi.org/10.1016/j.ultramic.2021.113213.

[78] R. Danev, B. Buijsse, M. Khoshouei, J.M. Plitzko, W. Baumeister, Volta potential phase plate for in-focus phase contrast transmission electron microscopy, Proc. Natl. Acad. Sci. USA 111 (2014) 15635–15640, https://doi.org/10.1073/pnas.1418377111.

[79] R. Danev, K. Nagayama, Transmission electron microscopy with Zernike phase plate, Ultramicroscopy 88 (2001) 243–252, https://doi.org/10.1016/S0304-3991(01)00088-2.

[80] K. Nagayama, R. Danev, Phase contrast electron microscopy: development of thin-film phase plates and biological applications, Philos. Trans. R. Soc. B Biol. Sci. 363 (2008) 2153–2162, https://doi.org/10.1098/rstb.2008.2268.

[81] M. Malac, S. Hettler, M. Hayashida, E. Kano, R.F. Egerton, M. Beleggia, Phase plates in the transmission electron microscope: operating principles and applications, Microscopy 70 (2021) 75–115, https://doi.org/10.1093/jmicro/dfaa070.

[82] R. Danev, R.M. Glaeser, K. Nagayama, Practical factors affecting the performance of a thin-film phase plate for transmission electron microscopy, Ultramicroscopy 109 (2009) 312–325, https://doi.org/10.1016/j.ultramic.2008.12.006.

[83] R. Pretzsch, M. Dries, S. Hettler, M. Spiecker, M. Obermair, D. Gerthsen, Investigation of hole-free phase plate performance in transmission electron microscopy under different operation conditions by experiments and simulations, Adv. Struct. Chem. Imaging 5 (2019) 5, https://doi.org/10.1186/s40679-019-0067-z.

[84] L.E. Franken, E.J. Boekema, M.C.A. Stuart, Transmission Electron Microscopy as a Tool for the Characterization of Soft Materials: Application and Interpretation, Adv. Sci. 4 (2017), https://doi.org/10.1002/advs.201600476.

[85] J.M. Petroski, Z.L. Wang, T.C. Green, M.A. El-Sayed, Kinetically Controlled Growth and Shape Formation Mechanism of Platinum Nanoparticles, J. Phys. Chem. B 102 (1998) 3316–3320, https://doi.org/10.1021/jp981030f.

[86] M. Hassellöv, J.W. Readman, J.F. Ranville, K. Tiede, Nanoparticle analysis and characterization methodologies in environmental risk assessment of engineered nanoparticles, Ecotoxicology 17 (2008) 344–361, https://doi.org/10.1007/s10646-008-0225-x.

[87] G. Bottari, A.J. Kumalaputri, K.K. Krawczyk, B.L. Feringa, H.J. Heeres, K. Barta, Copper–Zinc Alloy Nanopowder: A Robust Precious-Metal-Free Catalyst for the Conversion of 5-Hydroxymethylfurfural, ChemSusChem 8 (2015) 1323–1327, https://doi.org/10.1002/cssc.201403453.

[88] A.D. Ostrowski, E.M. Chan, D.J. Gargas, E.M. Katz, G. Han, P.J. Schuck, D. J. Milliron, B.E. Cohen, Controlled Synthesis and Single-Particle Imaging of Bright, Sub-10 nm Lanthanide-Doped Upconverting Nanocrystals, ACS Nano 6 (2012) 2686–2692, https://doi.org/10.1021/nn3000737.

[89] K.R. Miller, C.S. Prescott, T.L. Jacobs, N.L. Lassignal, Artifacts associated with quick-freezing and freeze-drying, J. Ultra Res 82 (1983) 123–133, https://doi.org/10.1016/S0022-5320(83)90047-3.

[90] L.G. Dowell, A.P. Rinfret, Low-Temperature Forms of Ice as Studied by X-Ray Diffraction, Nature 188 (1960) 1144–1148, https://doi.org/10.1038/1881144a0.

[91] J.A. Mc Millan, S.C. Los, Vitreous Ice: Irreversible Transformations During Warm-Up, Nature 206 (1965) 806–807, https://doi.org/10.1038/206806a0.

[92] A.C. Laan, A.G. Denkova, Cryogenic transmission electron microscopy: the technique of choice for the characterization of polymeric nanocarriers, EJNMMI Res 7 (2017), https://doi.org/10.1186/s13550-017-0290-3.

[93] L. Staniewicz, A.M. Donald, D.J. Stokes, The effect of osmium staining on lamellar spacing in thin polystyrene-polyisoprene diblock copolymer films, J. Phys. Conf. Ser. 241 (2010) 012077, https://doi.org/10.1088/1742-6596/241/1/012077.

[94] S. Brenner, R.W. Horne, A negative staining method for high resolution electron microscopy of viruses, Biochim Biophys. Acta 34 (1959) 103–110, https://doi.org/10.1016/0006-3002(59)90237-9.

[95] P. Serwer, Flattening and shrinkage of bacteriophage T7 after preparation for electron microscopy by negative staining, J. Ultra Res 58 (1977) 235–243, https://doi.org/10.1016/S0022-5320(77)90015-6.

[96] J. Dubochet, J. Lepault, R. Freeman, J.A. Berriman, J. -C. Homo, Electron microscopy of frozen water and aqueous solutions, J. Microsc. 128 (1982) 219–237, https://doi.org/10.1111/j.1365-2818.1982.tb04625.x.
[97] J. Dubochet, M. Adrian, J.-J. Chang, J.-C. Homo, J. Lepault, A.W. McDowall, P. Schultz, Cryo-electron microscopy of vitrified specimens, Q Rev. Biophys. 21 (1988) 129–228, https://doi.org/10.1017/S0033583500004297.
[98] H.P.M. Nguyen, K.L. McGuire, B.D. Cook, M.A. Herzik Jr., Manual Blot-and-Plunge Freezing of Biological Specimens for Single-Particle Cryogenic Electron Microscopy, J. Vis. Exp. (2022), https://doi.org/10.3791/62765.
[99] J.S. Depelteau, G. Koning, W. Yang, A. Briegel, An Economical, Portable Manual Cryogenic Plunge Freezer for the Preparation of Vitrified Biological Samples for Cryogenic Electron Microscopy, Microsc. Microanal. 26 (2020) 413–418, https://doi.org/10.1017/S1431927620001385.
[100] K.L. McGuire, B.D. Cook, S.M. Narehood, M.A. Herzik, Tuning ice thickness using the chameleon for high-quality cryoEM data collection, BioRxiv (2024), https://doi.org/10.1101/2024.05.01.592094.
[101] R.B.G. Ravelli, F.J.T. Nijpels, R.J.M. Henderikx, G. Weissenberger, S. Thewessem, A. Gijsbers, B.W.A.M.M. Beulen, C. López-Iglesias, P.J. Peters, Cryo-EM structures from sub-nl volumes using pin-printing and jet vitrification, Nat. Commun. 11 (2020) 2563, https://doi.org/10.1038/s41467-020-16392-5.
[102] L. Rima, M. Zimmermann, A. Fränkl, T. Clairfeuille, M. Lauer, A. Engel, H.-A. Engel, T. Braun, cryoWriter: a blotting free cryo-EM preparation system with a climate jet and cover-slip injector, Faraday Discuss. 240 (2022) 55–66, https://doi.org/10.1039/D2FD00066K.
[103] M.J.M. Wirix, P.H.H. Bomans, H. Friedrich, N.A.J.M. Sommerdijk, G. De With, Three-dimensional structure of P3HT assemblies in organic solvents revealed by cryo-TEM, Nano Lett. 14 (2014) 2033–2038, https://doi.org/10.1021/nl5001967.
[104] G.T. Oostergetel, F.J. Esselink, G. Hadziioannou, Cryo-Electron Microscopy of Block Copolymers in an Organic Solvent, Langmuir 11 (1995) 3721–3724. ⟨https://pubs.acs.org/sharingguidelines⟩.
[105] H. Cui, T.K. Hodgdon, E.W. Kaler, L. Abezgauz, D. Danino, M. Lubovsky, Y. Talmon, D.J. Pochan, Elucidating the assembled structure of amphiphiles in solution via cryogenic transmission electron microscopy, Soft Matter 3 (2007) 945–955, https://doi.org/10.1039/b704194b.
[106] J. Zhu, S. Zhang, K. Zhang, X. Wang, J.W. Mays, K.L. Wooley, D.J. Pochan, Disk-cylinder and disk-sphere nanoparticles via a block copolymer blend solution construction, Nat. Commun. 4 (2013) 2297, https://doi.org/10.1038/ncomms3297.
[107] J.-L. Putaux, E. Minatti, C. Lefebvre, R. Borsali, M. Schappacher, A. Deffieux, Vesicles made of PS-PI cyclic diblock copolymers: In situ freeze-drying cryo-TEM and dynamic light scattering experiments, Faraday Discuss. 128 (2005) 163, https://doi.org/10.1039/b403157a.
[108] J. Du, K. Hu, J. Zhang, L. Meng, J. Yue, I. Angunawela, H. Yan, S. Qin, X. Kong, Z. Zhang, B. Guan, H. Ade, Y. Li, Polymerized small molecular acceptor based all-polymer solar cells with an efficiency of 16.16% via tuning polymer blend morphology by molecular design, Nat. Commun. 12 (2021) 5264, https://doi.org/10.1038/s41467-021-25638-9.
[109] P. Zhang, H. Du, S. Cui, P. Zhou, Y. Xu, Response of organic solvents to vitrification and electron exposure in cryo-TEM experiments, Responsive Mater. 1 (2023), https://doi.org/10.1002/rpm.20230025.
[110] E.K. Richman, J.E. Hutchison, The nanomaterial characterization bottleneck, ACS Nano 3 (2009) 2441–2446, https://doi.org/10.1021/nn901112p.
[111] S.A. Arnold, S.A. Müller, C. Schmidli, A. Syntychaki, L. Rima, M. Chami, H. Stahlberg, K.N. Goldie, T. Braun, Miniaturizing EM Sample Preparation: Opportunities, Challenges, and "Visual Proteomics, Proteomics 18 (2018), https://doi.org/10.1002/pmic.201700176.
[112] D.P. Klebl, M.S.C. Gravett, D. Kontziampasis, D.J. Wright, R.S. Bon, D.C. F. Monteiro, M. Trebbin, F. Sobott, H.D. White, M.C. Darrow, R.F. Thompson, S. P. Muench, Need for Speed: Examining Protein Behavior during CryoEM Grid Preparation at Different Timescales, Structure 28 (2020) 1238–1248.e4, https://doi.org/10.1016/j.str.2020.07.018.
[113] D.M. Long, M.K. Singh, K.A. Small, J. Watt, Cryo-FIB for TEM investigation of soft matter and beam sensitive energy materials, Nanotechnology 33 (2022), https://doi.org/10.1088/1361-6528/ac92eb.
[114] L.A. Giannuzzi, J.L. Drown, S.R. Brown, R.B. Irwin, F.A. Stevie, Applications of the FIB lift-out technique for TEM specimen preparation, Microsc. Res Tech. 41 (1998) 285–290, https://doi.org/10.1002/(SICI)1097-0029(19980515)41:4<285::AID-JEMT1>3.0.CO;2-Q.
[115] R.F. Egerton, Mechanisms of radiation damage in beam-sensitive specimens, for TEM accelerating voltages between 10 and 300 kV, Microsc. Res Tech. 75 (2012) 1550–1556, https://doi.org/10.1002/jemt.22099.
[116] N.D. Bassim, B.T. De Gregorio, A.L.D. Kilcoyne, K. Scott, T. Chou, S. Wirick, G. Cody, R.M. Stroud, Minimizing damage during FIB sample preparation of soft materials, J. Microsc. 245 (2012) 288–301, https://doi.org/10.1111/j.1365-2818.2011.03570.x.
[117] M. Marko, C. Hsieh, R. Schalek, J. Frank, C. Mannella, Focused-ion-beam thinning of frozen-hydrated biological specimens for cryo-electron microscopy, Nat. Methods 4 (2007) 215–217, https://doi.org/10.1038/nmeth1014.
[118] X.L. Zhong, S.J. Haigh, X. Zhou, P.J. Withers, An in-situ method for protecting internal cracks/pores from ion beam damage and reducing curtaining for TEM sample preparation using FIB, Ultramicroscopy 219 (2020), https://doi.org/10.1016/j.ultramic.2020.113135.
[119] M.J. Zachman, E. Asenath-Smith, L.A. Estroff, L.F. Kourkoutis, Site-specific preparation of intact solid-liquid interfaces by label-free in situ localization and Cryo-focused ion beam lift-out, Microsc. Microanal. 22 (2016) 1338–1349, https://doi.org/10.1017/S1431927616011892.
[120] N.S. Smith, W.P. Skoczylas, S.M. Kellogg, D.E. Kinion, P.P. Tesch, O. Sutherland, A. Aanesland, R.W. Boswell, High brightness inductively coupled plasma source for high current focused ion beam applications, Journal Vacuum Science Technology B Microelectronics Nanometer Structures Processing Measurement Phenomena 24 (2006) 2902–2906, https://doi.org/10.1116/1.2366617.
[121] N. Bassim, K. Scott, L.A. Giannuzzi, Recent advances in focused ion beam technology and applications, MRS Bull. 39 (2014) 317–325, https://doi.org/10.1557/mrs.2014.52.
[122] C. Berger, M. Dumoux, T. Glen, N.B. y Yee, J.M. Mitchels, Z. Patáková, M. C. Darrow, J.H. Naismith, M. Grange, Plasma FIB milling for the determination of structures in situ, Nat. Commun. 14 (2023), https://doi.org/10.1038/s41467-023-36372-9.
[123] M.W. Martynowycz, M.T.B. Clabbers, J. Unge, J. Hattne, T. Gonen, Benchmarking the ideal sample thickness in cryo-EM, Proc. Natl. Acad. Sci. 118 (2021), https://doi.org/10.1073/pnas.2108884118.
[124] J. Bö, O. Lambert, A.S. Frangakis, L. Letellier, W. Baumeister, J.L. Rigaud, FhuA-mediated phage genome transfer into liposomes, A cryoElectron Tomogr. Study (2001) 1168–1175, https://doi.org/10.1016/S0960-9822(01)00349-9.
[125] C.-E. Hsieh, M. Marko, J. Frank, C.A. Mannella, Electron tomographic analysis of frozen-hydrated tissue sections, n.d. www.academicpress.com.
[126] A. Al-Amoudi, D.C. Díez, M.J. Betts, A.S. Frangakis, The molecular architecture of cadherins in native epidermal desmosomes, Nature 450 (2007) 832–837, https://doi.org/10.1038/nature05994.
[127] A. Al-Amoudi, L.P.O. Norlen, J. Dubochet, Cryo-electron microscopy of vitreous sections of native biological cells and tissues, J. Struct. Biol. 148 (2004) 131–135, https://doi.org/10.1016/j.jsb.2004.03.010.
[128] A. Al-Amoudi, D. Studer, J. Dubochet, Cutting artefacts and cutting process in vitreous sections for cryo-electron microscopy, J. Struct. Biol. 150 (2005) 109–121, https://doi.org/10.1016/j.jsb.2005.01.003.
[129] M.F. Hayles, D.J. Stokes, D. Phifer, K.C. Findlay, A technique for improved focused ion beam milling of cryo-prepared life science specimens, J. Microsc. 226 (2007) 263–269, https://doi.org/10.1111/j.1365-2818.2007.01775.x.
[130] D.J. Stokes, M.F. Hayles, Methodologies for the preparation of soft materials using cryoFIB SEM, Scanning Microsc. 7378 (2009) 70–81, https://doi.org/10.1117/12.821834.
[131] H. Liu, J. Liang, J. Watt, R.D. Tilley, R. Amal, D.-W. Wang, Wafer-scale quasi-layered tungstate-doped polypyrrole film with high volumetric capacitance, Nano Res 16 (2023) 4895–4900, https://doi.org/10.1007/s12274-021-3783-3.
[132] J. Mahamid, R. Schampers, H. Persoon, A.A. Hyman, W. Baumeister, J.M. Plitzko, A focused ion beam milling and lift-out approach for site-specific preparation of frozen-hydrated lamellas from multicellular organisms, J. Struct. Biol. 192 (2015) 262–269, https://doi.org/10.1016/j.jsb.2015.07.012.
[133] A.J. Smith, T. Laugks, S. Kleindiek, S. Albert, W.H.J. Wood, M.P. Johnson, B. D. Engel, W. Baumeister, J.M. Plitzko, M. Schaffer, Cryo-FIB Lift-out Sample Preparation Using a Novel Cryo-gripper Tool, Microsc. Microanal. 23 (2017) 844–845, https://doi.org/10.1017/S1431927617004883.
[134] C.D.J. Parmenter, M.W. Fay, C. Hartfield, H.M. Eltaher, Making the practically impossible "Merely difficult"—Cryogenic FIB lift-out for "Damage free" soft matter imaging, Microsc. Res Tech. 79 (2016) 298–303, https://doi.org/10.1002/jemt.22630.
[135] J. Zhou, N. Wei, D. Zhang, Y. Wang, J. Li, X. Zheng, J. Wang, A.Y. Alsalloum, L. Liu, O.M. Bakr, Y. Han, Cryogenic Focused Ion Beam Enables Atomic-Resolution Imaging of Local Structures in Highly Sensitive Bulk Crystals and Devices, J. Am. Chem. Soc. 144 (2022) 3182–3191, https://doi.org/10.1021/jacs.1c12794.
[136] A. Rigort, F.J.B. Bäuerlein, E. Villa, M. Eibauer, T. Laugks, W. Baumeister, J. M. Plitzko, Focused ion beam micromachining of eukaryotic cells for cryoelectron tomography, Proc. Natl. Acad. Sci. 109 (2012) 4449–4454, https://doi.org/10.1073/pnas.1201333109.
[137] H. Okamoto, T. Latychevskaia, H.-W. Fink, A quantum mechanical scheme to reduce radiation damage in electron microscopy, Appl. Phys. Lett. 88 (2006), https://doi.org/10.1063/1.2191096.
[138] D. Shi, R. Huang, Analysis and comparison of electron radiation damage assessments in Cryo-EM by single particle analysis and micro-crystal electron diffraction, Front Mol. Biosci. 9 (2022), https://doi.org/10.3389/fmolb.2022.988928.
[139] Y. Li, D.-D. Kang, J.-Y. Dai, L.-W. Wang, The cage effect of electron beam irradiation damage in cryo-electron microscopy, NPJ Comput. Mater. 10 (2024) 115, https://doi.org/10.1038/s41524-024-01299-2.
[140] L.A. Baker, J.L. Rubinstein, Radiation Damage in Electron Cryomicroscopy, Methods Enzym. 481 (2010) 371–388, https://doi.org/10.1016/S0076-6879(10)81015-8.
[141] R.F. Egerton, P. Li, M. Malac, Radiation damage in the TEM and SEM, Micron 35 (2004) 399–409, https://doi.org/10.1016/j.micron.2004.02.003.
[142] X. Xu, L. Xia, C. Zheng, Y. Liu, D. Yu, J. Li, S. Zhong, C. Li, H. Song, Y. Liu, T. Sun, Y. Li, Y. Han, J. Zhao, Q. Lin, X. Li, Y. Zhu, Unravelling nonclassical beam damage mechanisms in metal-organic frameworks by low-dose electron microscopy, Nat. Commun. 16 (2025) 261, https://doi.org/10.1038/s41467-024-55632-w.
[143] Z. Cai, Y. Wu, S. Chen, Energy-dependent knock-on damage of organic–inorganic hybrid perovskites under electron beam irradiation: First-principles insights, Appl. Phys. Lett. 119 (2021), https://doi.org/10.1063/5.0065849.
[144] C. Xiao, Z. Li, H. Guthrey, J. Moseley, Y. Yang, S. Wozny, H. Moutinho, B. To, J. J. Berry, B. Gorman, Y. Yan, K. Zhu, M. Al-Jassim, Mechanisms of Electron-Beam-Induced Damage in Perovskite Thin Films Revealed by Cathodoluminescence

Spectroscopy, J. Phys. Chem. C. 119 (2015) 26904–26911, https://doi.org/10.1021/acs.jpcc.5b09698.
[145] B. Yuan, Y. Yu, High-resolution transmission electron microscopy of beam-sensitive halide perovskites, Chem 8 (2022) 327–339, https://doi.org/10.1016/j.chempr.2022.01.006.
[146] N. Yi, S. Wang, Z. Duan, K. Wang, Q. Song, S. Xiao, Tailoring the Performances of Lead Halide Perovskite Devices with Electron-Beam Irradiation, Adv. Mater. 29 (2017), https://doi.org/10.1002/adma.201701636.
[147] Y. Zhou, H. Sternlicht, N.P. Padture, Transmission Electron Microscopy of Halide Perovskite Materials and Devices, Joule 3 (2019) 641–661, https://doi.org/10.1016/j.joule.2018.12.011.
[148] B. Jin, D. Zhao, F. Liang, L. Liu, D. Liu, P. Wang, M. Qiu, Electron-Beam Irradiation Induced Regulation of Surface Defects in Lead Halide Perovskite Thin Films, Research 2021 (2021), https://doi.org/10.34133/2021/9797058.
[149] A. Scheid, Y. Wang, M. Jung, T. Heil, D. Moia, J. Maier, P.A. van Aken, Electron Ptychographic Phase Imaging of Beam-sensitive All-inorganic Halide Perovskites Using Four-dimensional Scanning Transmission Electron Microscopy, Microsc. Microanal. 29 (2023) 869–878, https://doi.org/10.1093/micmic/ozad017.
[150] B. Kuei, E.D. Gomez, Pushing the limits of high-resolution polymer microscopy using antioxidants, Nat. Commun. 12 (2021) 153, https://doi.org/10.1038/s41467-020-20363-1.
[151] L.M. Valencia, M. de la Mata, M. Herrera, F.J. Delgado, J. Hernández-Saz, S. I. Molina, Induced damage during STEM-EELS analyses on acrylic-based materials for Stereolithography, Polym. Degrad. Stab. 203 (2022) 110044, https://doi.org/10.1016/j.polymdegradstab.2022.110044.
[152] Q. Chen, C. Dwyer, G. Sheng, C. Zhu, X. Li, C. Zheng, Y. Zhu, Imaging Beam-Sensitive Materials by Electron Microscopy, Adv. Mater. 32 (2020), https://doi.org/10.1002/adma.201907619.
[153] Z.J.W.A. Leijten, A.D.A. Keizer, G. de With, H. Friedrich, Quantitative Analysis of Electron Beam Damage in Organic Thin Films, J. Phys. Chem. C. 121 (2017) 10552–10561, https://doi.org/10.1021/acs.jpcc.7b01749.
[154] J. Hattne, D. Shi, C. Glynn, C.-T. Zee, M. Gallagher-Jones, M.W. Martynowycz, J. A. Rodriguez, T. Gonen, Analysis of Global and Site-Specific Radiation Damage in Cryo-EM, Structure 26 (2018) 759–766.e4, https://doi.org/10.1016/j.str.2018.03.021.
[155] A. Velazco, A. Béché, D. Jannis, J. Verbeeck, Reducing electron beam damage through alternative STEM scanning strategies, Part I: Experimental findings, Ultramicroscopy 232 (2022) 113398, https://doi.org/10.1016/j.ultramic.2021.113398.
[156] D.T. Grubb, Radiation damage and electron microscopy of organic polymers, J. Mater. Sci. 9 (1974) 1715–1736, https://doi.org/10.1007/BF00540772.
[157] J.S.C. Loo, C.P. Ooi, F.Y.C. Boey, Degradation of poly(lactide-co-glycolide) (PLGA) and poly(l-lactide) (PLLA) by electron beam radiation, Biomaterials 26 (2005) 1359–1367, https://doi.org/10.1016/j.biomaterials.2004.05.001.
[158] D. Krieg, M.T. Müller, R. Boldt, M. Rennert, M. Stommel, Additive Free Crosslinking of Poly-3-hydroxybutyrate via Electron Beam Irradiation at Elevated Temperatures, Polym. (Basel) 15 (2023) 4072, https://doi.org/10.3390/polym15204072.
[159] Z. Zhan, Y. Liu, W. Wang, G. Du, S. Cai, P. Wang, Atomic-level imaging of beam-sensitive COFs and MOFs by low-dose electron microscopy, Nanoscale Horiz. 9 (2024) 900–933, https://doi.org/10.1039/D3NH00494E.
[160] G. Li, S. Ning, H. Zhang, C.-H. Lee, D.A. Muller, Y. Han, Optimizing Electron Ptychography for Radiation-Sensitive Materials including Metal-Organic Frameworks, Microsc. Microanal. 31 (2025), https://doi.org/10.1093/mam/ozaf048.075.
[161] G. Li, M. Xu, W.-Q. Tang, Y. Liu, C. Chen, D. Zhang, L. Liu, S. Ning, H. Zhang, Z.-Y. Gu, Z. Lai, D.A. Muller, Y. Han, Atomically resolved imaging of radiation-sensitive metal-organic frameworks via electron ptychography, Nat. Commun. 16 (2025) 914, https://doi.org/10.1038/s41467-025-56215-z.
[162] E.-P. Tien, G. Cao, Y. Chen, N. Clark, E. Tillotson, D.-T. Ngo, J.H. Carter, S. P. Thompson, C.C. Tang, C.S. Allen, S. Yang, M. Schröder, S.J. Haigh, Electron beam and thermal stabilities of MFM-300(M) metal–organic frameworks, J. Mater. Chem. A Mater. 12 (2024) 24165–24174, https://doi.org/10.1039/D4TA03302G.
[163] Y. Liu, X. Liu, A. Su, C. Gong, S. Chen, L. Xia, C. Zhang, X. Tao, Y. Li, Y. Li, T. Sun, M. Bu, W. Shao, J. Zhao, X. Li, Y. Peng, P. Guo, Y. Han, Y. Zhu, Revolutionizing the structural design and determination of covalent–organic frameworks: principles, methods, and techniques, Chem. Soc. Rev. 53 (2024) 502–544, https://doi.org/10.1039/D3CS00287J.
[164] Y. Zhu, J. Ciston, B. Zheng, X. Miao, C. Czarnik, Y. Pan, R. Sougrat, Z. Lai, C.-E. Hsiung, K. Yao, I. Pinnau, M. Pan, Y. Han, Unravelling surface and interfacial structures of a metal–organic framework by transmission electron microscopy, Nat. Mater. 16 (2017) 532–536, https://doi.org/10.1038/nmat4852.
[165] I. Castano, A.M. Evans, R. dos Reis, V.P. Dravid, N.C. Gianneschi, W.R. Dichtel, Mapping Grains, Boundaries, and Defects in 2D Covalent Organic Framework Thin Films, Chem. Mater. 33 (2021) 1341–1352, https://doi.org/10.1021/acs.chemmater.0c04382.
[166] A. Meents, S. Gutmann, A. Wagner, C. Schulze-Briese, Origin and temperature dependence of radiation damage in biological samples at cryogenic temperatures, Proc. Natl. Acad. Sci. 107 (2010) 1094–1099, https://doi.org/10.1073/pnas.0905481107.
[167] S.B. Hayward, R.M. Glaeser, Use of Low Temperatures for Electron Diffraction and Imaging of Biological Macromolecular Arrays, in: W. Baumeister, W. Vogell (Eds.), Electron Microscopy at Molecular Dimensions. Proceedings in Life Sciences, Springer, Berlin, Heidelberg, 1980, pp. 226–233, https://doi.org/10.1007/978-3-642-67688-8_26.
[168] G.M. Parkinson, W. Jones, J.M. Thomas, Electron Microscopy at Liquid Helium Temperatures, in: W. Baumeister, W. Vogell (Eds.), Electron Microscopy at Molecular Dimensions. Proceedings in Life Sciences, Springer, Berlin, Heidelberg, 1980, pp. 208–225, https://doi.org/10.1007/978-3-642-67688-8_25.
[169] I. Dietrich, J. Dubochet, F. Fox, E. Knapek, R. Weyl, Reduction of Radiation Damage by Imaging with a Superconducting Lens System, in: W. Baumeister, W. Vogell (Eds.), Proceedings in Life Sciences, Electron Microscopy at Molecular Dimensions, Springer, Berlin, Heidelberg, 1980, pp. 234–244, https://doi.org/10.1007/978-3-642-67688-8_27.
[170] L. Kong, X. Zottig, J. Elferich, N. Grigorieff, Unbend Correct. Local beamInduc. Sample Motion cryoEM Images Using a 3D spline Model (2025), https://doi.org/10.7554/eLife.109119.1.
[171] Y. Cheng, N. Grigorieff, P.A. Penczek, T. Walz, A Primer to Single-Particle Cryo-Electron Microscopy, Cell 161 (2015) 438–449, https://doi.org/10.1016/j.cell.2015.03.050.
[172] A. Chari, H. Stark, Prospects and Limitations of High-Resolution Single-Particle Cryo-Electron Microscopy, Annu Rev. Biophys. 52 (2023) 391–411, https://doi.org/10.1146/annurev-biophys-111622-091300.
[173] H. Shigematsu, F.J. Sigworth, Noise models and cryo-EM drift correction with a direct-electron camera, Ultramicroscopy 131 (2013) 61–69, https://doi.org/10.1016/j.ultramic.2013.04.001.
[174] X. Li, P. Mooney, S. Zheng, C.R. Booth, M.B. Braunfeld, S. Gubbens, D.A. Agard, Y. Cheng, Electron counting and beam-induced motion correction enable near-atomic-resolution single-particle cryo-EM, Nat. Methods 10 (2013) 584–590, https://doi.org/10.1038/nmeth.2472.
[175] M. Hayashida, T. Kawasaki, Y. Kimura, Y. Takai, Estimation of suitable condition for observing copper–phthalocyanine crystalline film by transmission electron microscopy, Nucl. Instrum. Methods Phys. Res B 248 (2006) 273–278, https://doi.org/10.1016/j.nimb.2006.04.168.
[176] M.J. Berger, J.S. Coursey, M.A. Zucker, J. Chang, Stopping-Power & Range Tables for Electrons, Protons Helium Ions (1993).
[177] J.Z. Chen, C. Sachse, C. Xu, T. Mielke, C.M.T. Spahn, N. Grigorieff, A dose-rate effect in single-particle electron microscopy, J. Struct. Biol. 161 (2008) 92–100, https://doi.org/10.1016/j.jsb.2007.09.017.
[178] Y. Zhang, J.P. van Schayck, A. Pedrazo-Tardajos, N. Claes, W.E.M. Noteborn, P.-H. Lu, H. Duimel, R.E. Dunin-Borkowski, S. Bals, P.J. Peters, R.B.G. Ravelli, Charging of Vitreous Samples in Cryogenic Electron Microscopy Mitigated by Graphene, ACS Nano 17 (2023) 15836–15846, https://doi.org/10.1021/acsnano.3c03722.
[179] F. Karimi Nejadasl, M. Karuppasamy, E.R. Newman, J.E. McGeehan, R.B. G. Ravelli, Non-rigid image registration to reduce beam-induced blurring of cryo-electron microscopy images, J. Synchrotron Radiat. 20 (2013) 58–66, https://doi.org/10.1107/S0909049512044408.
[180] Y. Zhao, C. Qi, C. Zhu, Y. Zhu, Y. Zhang, T. Gu, H. Tian, W. Wang, S. Huang, H. Yang, J. Li, F. Sun, Radiation damage behavior of soft matter in ultrafast cryo-electron microscopy (cryo-UEM), Innov. Life 3 (2025) 100145, https://doi.org/10.59717/j.xinn-life.2025.100145.
[181] X. Li, S.Q. Zheng, K. Egami, D.A. Agard, Y. Cheng, Influence of electron dose rate on electron counting images recorded with the K2 camera, J. Struct. Biol. 184 (2013) 251–260, https://doi.org/10.1016/j.jsb.2013.08.005.
[182] P. Zambon, Modeling the impact of coincidence loss on count rate statistics and noise performance in counting detectors for imaging applications, Front Phys. 12 (2024), https://doi.org/10.3389/fphy.2024.1408430.
[183] R. Peng, X. Fu, J.H. Mendez, P.S. Randolph, B.E. Bammes, S.M. Stagg, Characterizing the resolution and throughput of the Apollo direct electron detector, J. Struct. Biol. X 7 (2023) 100080, https://doi.org/10.1016/j.yjsbx.2022.100080.
[184] R. Zan, Q.M. Ramasse, R. Jalil, T. Georgiou, U. Bangert, K.S. Novoselov, Control of Radiation Damage in MoS 2 by Graphene Encapsulation, ACS Nano 7 (2013) 10167–10174, https://doi.org/10.1021/nn4044035.
[185] S. Keskin, N. de Jonge, Reduced Radiation Damage in Transmission Electron Microscopy of Proteins in Graphene Liquid Cells, Nano Lett. 18 (2018) 7435–7440, https://doi.org/10.1021/acs.nanolett.8b02490.
[186] H. Cho, M.R. Jones, S.C. Nguyen, M.R. Hauwiller, A. Zettl, A.P. Alivisatos, The Use of Graphene and Its Derivatives for Liquid-Phase Transmission Electron Microscopy of Radiation-Sensitive Specimens, Nano Lett. 17 (2017) 414–420, https://doi.org/10.1021/acs.nanolett.6b04383.
[187] Z. Wang, J. Zhang, Graphene Liquid Cells for In Situ Transmission Electron Microscopy: Unveiling Nanomaterial Growth and Etching, Adv. Mater. (2025), https://doi.org/10.1002/adma.202518883.
[188] P. Singh, B.R. Venugopal, D.R. Nandini, Effect of Electron Beam Irradiation on Polymers, J. Mod. Mater. 5 (2018) 24–33, https://doi.org/10.21467/jmm.5.1.24-33.
[189] B. Kuei, C. Bator, E.D. Gomez, Imaging 0.36 nm Lattice Planes in Conjugated Polymers by Minimizing Beam Damage, Macromolecules 53 (2020) 8296–8302, https://doi.org/10.1021/acs.macromol.0c01082.
[190] B. Kuei, E.D. Gomez, Elucidating Mechanisms for Electron Beam Damage in Conjugated Polymers, Microsc. Microanal. 24 (2018) 1988–1989, https://doi.org/10.1017/S1431927618010425.
[191] H.P. Erickson, A. Klug, The Fourier Transform of an Electron Micrograph: Effects of Defocussing and Aberrations, and Implications for the Use of Underfocus Contrast Enhancement, Ber. Der Bunsenges. F. üR. Phys. Chem. 74 (1970) 1129–1137, https://doi.org/10.1002/bbpc.19700741109.
[192] P. Modicano, P.R. Neumann, M. Schüller, J. Holthof, F.L. Kyrilis, F. Hamdi, P. L. Kastritis, K. Mäder, L. Ann Dailey, Enhanced optical imaging properties of lipid

nanocapsules as vehicles for fluorescent conjugated polymers, Eur. J. Pharm. Biopharm. 154 (2020) 297–308, https://doi.org/10.1016/j.ejpb.2020.07.017.
[193] M.J. Jackman, W. Li, A. Smith, D. Workman, K.E. Treacher, A. Corrigan, F. Abdulrazzaq, S. Sonzini, Z. Nazir, M.J. Lawrence, N. Mahmoudi, D. Cant, J. Counsell, J. Cairns, D. Ferguson, E. Lenz, S. Baquain, C.M. Madla, S. van Pelt, J. Moss, A. Peter, S. Puri, M. Ashford, M. Mazza, Impact of the physical-chemical properties of poly(lactic acid)–poly(ethylene glycol) polymeric nanoparticles on biodistribution, J. Control. Release 365 (2024) 491–506, https://doi.org/10.1016/j.jconrel.2023.11.043.
[194] S. Demisli, E. Galani, M. Goulielmaki, F.L. Kyrilis, T. Ilić, F. Hamdi, M. Crevar, P. L. Kastritis, V. Pletsa, F. Nallet, S. Savić, A. Xenakis, V. Papadimitriou, Encapsulation of cannabidiol in oil-in-water nanoemulsions and nanoemulsion-filled hydrogels: A structure and biological assessment study, J. Colloid Interface Sci. 634 (2023) 300–313, https://doi.org/10.1016/j.jcis.2022.12.036.
[195] W.F. Paxton, P.T. McAninch, S.H.R. Shin, M.T. Brumbach, Adsorption and fusion of hybrid lipid/polymer vesicles onto 2D and 3D surfaces, Soft Matter 14 (2018) 8112–8118, https://doi.org/10.1039/C8SM00343B.
[196] J.U. De Mel, S. Gupta, L. Willner, J. Allgaier, L.R. Stingaciu, M. Bleuel, G. J. Schneider, Manipulating Phospholipid Vesicles at the Nanoscale: A Transformation from Unilamellar to Multilamellar by an n-Alkyl-poly(ethylene oxide), Langmuir 37 (2021) 2362–2375, https://doi.org/10.1021/acs.langmuir.0c03302.
[197] J. Grundler, K. Shin, H.-W. Suh, M. Zhong, W.M. Saltzman, Surface Topography of Polyethylene Glycol Shell Nanoparticles Formed from Bottlebrush Block Copolymers Controls Interactions with Proteins and Cells, ACS Nano 15 (2021) 16118–16129, https://doi.org/10.1021/acsnano.1c04835.
[198] F. Li, R.D. Harvey, P. Modicano, F. Hamdi, F. Kyrilis, S. Müller, K. Gruhle, P. Kastritis, S. Drescher, L.A. Dailey, Investigating bolalipids as solubilizing agents for poorly soluble drugs: Effects of alkyl chain length on solubilization and cytotoxicity, Colloids Surf. B Biointerfaces 212 (2022) 112369, https://doi.org/10.1016/j.colsurfb.2022.112369.
[199] R. Hlushko, E. Pozharski, V.M. Prabhu, A.K. Andrianov, Directly visualizing individual polyorganophosphazenes and their single-chain complexes with proteins, Commun. Mater. 5 (2024) 36, https://doi.org/10.1038/s43246-024-00476-6.
[200] N. Marušič, L. Otrin, J. Rauchhaus, Z. Zhao, F.L. Kyrilis, F. Hamdi, P.L. Kastritis, R. Dimova, I. Ivanov, K. Sundmacher, Increased efficiency of charge-mediated fusion in polymer/lipid hybrid membranes, Proc. Natl. Acad. Sci. 119 (2022), https://doi.org/10.1073/pnas.2122468119.
[201] L. Otrin, A. Witkowska, N. Marušič, Z. Zhao, R.B. Lira, F.L. Kyrilis, F. Hamdi, I. Ivanov, R. Lipowsky, P.L. Kastritis, R. Dimova, K. Sundmacher, R. Jahn, T. Vidaković-Koch, En route to dynamic life processes by SNARE-mediated fusion of polymer and hybrid membranes, Nat. Commun. 12 (2021) 4972, https://doi.org/10.1038/s41467-021-25294-z.
[202] N. Marušič, L. Otrin, Z. Zhao, R.B. Lira, F.L. Kyrilis, F. Hamdi, P.L. Kastritis, T. Vidaković-Koch, I. Ivanov, K. Sundmacher, R. Dimova, Constructing artificial respiratory chain in polymer compartments: Insights into the interplay between bo 3 oxidase and the membrane, Proc. Natl. Acad. Sci. 117 (2020) 15006–15017, https://doi.org/10.1073/pnas.1919306117.
[203] N. Otrin, L. Otrin, C. Bednarz, T.K. Träger, F. Hamdi, P.L. Kastritis, I. Ivanov, K. Sundmacher, Protein-rich rafts in hybrid polymer/lipid giant unilamellar vesicles, Biomacromolecules 25 (2024) 778–791, https://doi.org/10.1021/acs.biomac.3c00972.
[204] D. Xiao, Z. Jin, G. Sheng, L. Chen, X. Xiao, T. Shan, J. Wang, R. Navik, J. Xu, L. Zhou, Q.-H. Guo, G. Li, Y. Zhu, J.F. Stoddart, F. Huang, Single crystals of purely organic free-standing two-dimensional woven polymer networks, Nat. Chem. 16 (2024) 1906–1914, https://doi.org/10.1038/s41557-024-01580-3.
[205] Y. Li, K. Wang, W. Zhou, Y. Li, R. Vila, W. Huang, H. Wang, G. Chen, G.-H. Wu, Y. Tsao, H. Wang, R. Sinclair, W. Chiu, Y. Cui, Cryo-EM structures of atomic surfaces and host-guest chemistry in metal-organic frameworks, Matter 1 (2019) 428–438, https://doi.org/10.1016/j.matt.2019.06.001.
[206] A.F. Ogata, A.M. Rakowski, B.P. Carpenter, D.A. Fishman, J.G. Merham, P. J. Hurst, J.P. Patterson, Direct observation of amorphous precursor phases in the nucleation of protein–metal–organic frameworks, J. Am. Chem. Soc. 142 (2020) 1433–1442, https://doi.org/10.1021/jacs.9b11371.
[207] L. Tong, S. Huang, Y. Shen, S. Liu, X. Ma, F. Zhu, G. Chen, G. Ouyang, Atomically unveiling the structure-activity relationship of biomacromolecule-metal-organic frameworks symbiotic crystal, Nat. Commun. 13 (2022) 951, https://doi.org/10.1038/s41467-022-28615-y.
[208] A. Winter, F. Hamdi, A. Eichhöfer, K. Saalwächter, P.L. Kastritis, F. Haase, Enhancing structural control in covalent organic frameworks through steric interaction-driven linker design, Chem. Sci. 15 (2024) 14449–14457, https://doi.org/10.1039/D4SC03461A.
[209] J. Tu, W. Song, B. Chen, Y. Li, L. Chen, 2d Covalent Organic Frameworks with Kagome Lattice: Synthesis and Applications, Chem. A Eur. J. 29 (2023), https://doi.org/10.1002/chem.202302380.
[210] E. Nogales, S.H.W. Scheres, Cryo-EM: a unique tool for the visualization of macromolecular complexity, Mol. Cell 58 (2015) 677–689, https://doi.org/10.1016/j.molcel.2015.02.019.
[211] F.J. Sigworth, Principles of cryo-EM single-particle image processing, Microsc. (Oxf.) 65 (2016) 57–67, https://doi.org/10.1093/jmicro/dfv370.
[212] S.H.W. Scheres, A Bayesian View on Cryo-EM structure determination, J. Mol. Biol. 415 (2012) 406–418, https://doi.org/10.1016/j.jmb.2011.11.010.
[213] S.H.W. Scheres, RELION: implementation of a Bayesian approach to cryo-EM structure determination, J. Struct. Biol. 180 (2012) 519–530, https://doi.org/10.1016/J.JSB.2012.09.006.
[214] M. Radermacher, T. Wagenknecht, A. Verschoor, J. Frank, Three-dimensional reconstruction from a single-exposure, random conical tilt series applied to the 50S ribosomal subunit of Escherichia coli, J. Microsc. 146 (1987) 113–136, https://doi.org/10.1111/j.1365-2818.1987.tb01333.x.
[215] M. Van Heel, Angular reconstitution: a posteriori assignment of projection directions for 3D reconstruction, Ultramicroscopy 21 (1987) 111–123, https://doi.org/10.1016/0304-3991(87)90078-7.
[216] X. You, X. Zhang, J. Cheng, Y. Xiao, J. Ma, S. Sun, X. Zhang, H.-W. Wang, S.-F. Sui, In situ structure of the red algal phycobilisome–PSII–PSI–LHC megacomplex, Nature 616 (2023) 199–206, https://doi.org/10.1038/s41586-023-05831-0.
[217] K. Ma, Y. Gong, T. Aubert, M.Z. Turker, T. Kao, P.C. Doerschuk, U. Wiesner, Self-assembly of highly symmetrical, ultrasmall inorganic cages directed by surfactant micelles, Nature 558 (2018) 577–580, https://doi.org/10.1038/s41586-018-0221-0.
[218] P.W. Lee, S.A. Isarov, J.D. Wallat, S.K. Molugu, S. Shukla, J.E.P. Sun, J. Zhang, Y. Zheng, M. Lucius Dougherty, D. Konkolewicz, P.L. Stewart, N.F. Steinmetz, M. J.A. Hore, J.K. Pokorski, Polymer structure and conformation alter the antigenicity of virus-like particle-polymer conjugates, J. Am. Chem. Soc. 139 (2017) 3312–3315, https://doi.org/10.1021/jacs.6b11643.
[219] Y. Xu, Y. Qin, L. Wang, Y. Zhang, Y. Wang, S. Dang, Metallo-supramolecular branched polymer protects particles from air-water interface in single-particle cryo-electron microscopy, Commun. Biol. 7 (2024) 65, https://doi.org/10.1038/s42003-023-05752-8.
[220] P. Ercius, O. Alaidi, M.J. Rames, G. Ren, Electron tomography: a three-dimensional analytic tool for hard and soft materials research, Adv. Mater. 27 (2015) 5638–5663, https://doi.org/10.1002/adma.201501015.
[221] Z. Kochovski, G. Chen, J. Yuan, Y. Lu, 2020, Cryo-Electron microscopy for the study of self-assembled poly(ionic liquid) nanoparticles and protein supramolecular structures, (2020). https://doi.org/10.1007/s00396-020-04657-w/Published.
[222] D.N. Mastronarde, Dual-Axis Tomography: An Approach with Alignment Methods That Preserve Resolution, J. Struct. Biol. 120 (1997) 343–352, https://doi.org/10.1006/JSBI.1997.3919.
[223] P.F. Gilbert, The reconstruction of a three-dimensional structure from projections and its application to electron microscopy. II. Direct methods, Proc. R. Soc. Lond. B Biol. Sci. 182 (1972) 89–102, https://doi.org/10.1098/rspb.1972.0068.
[224] P. Gilbert, Iterative methods for the three-dimensional reconstruction of an object from projections, J. Theor. Biol. 36 (1972) 105–117, https://doi.org/10.1016/0022-5193(72)90180-4.
[225] R. Marabini, G.T. Herman, J.M. Carazo, 3D reconstruction in electron microscopy using ART with smooth spherically symmetric volume elements (blobs), Ultramicroscopy 72 (1998) 53–65, https://doi.org/10.1016/S0304-3991(97)00127-7.
[226] J. Zivanov, J. Otón, Z. Ke, A. von Kügelgen, E. Pyle, K. Qu, D. Morado, D. Castaño-Díez, G. Zanetti, T.A. Bharat, J.A. Briggs, S.H. Scheres, A Bayesian approach to single-particle electron cryo-tomography in RELION-4.0, Elife 11 (2022), https://doi.org/10.7554/eLife.83724.
[227] D. Tegunov, P. Cramer, Real-time cryo-electron microscopy data preprocessing with Warp, Nat. Methods 16 (2019) 1146–1152, https://doi.org/10.1038/s41592-019-0580-y.
[228] D. Tegunov, L. Xue, C. Dienemann, P. Cramer, J. Mahamid, Multi-particle cryo-EM refinement with M visualizes ribosome-antibiotic complex at 3.5 Å in cells, Nat. Methods 18 (2021) 186–193, https://doi.org/10.1038/s41592-020-01054-7.
[229] F.I. Allen, L.R. Comolli, A. Kusoglu, M.A. Modestino, A.M. Minor, A.Z. Weber, Morphology of hydrated as-cast Nafion revealed through cryo electron tomography, ACS Macro Lett. 4 (2015) 1–5, https://doi.org/10.1021/mz500606h.
[230] W. Zhang, Z. Kochovski, Y. Lu, B.V.K.J. Schmidt, M. Antonietti, J. Yuan, Internal Morphology-controllable self-assembly in poly(Ionic Liquid) nanoparticles, ACS Nano 10 (2016) 7731–7737, https://doi.org/10.1021/acsnano.6b03135.
[231] T.L. Fox, S. Tang, J.M. Horton, H.A. Holdaway, B. Zhao, L. Zhu, P.L. Stewart, In situ characterization of binary mixed polymer brush-grafted silica nanoparticles in aqueous and organic solvents by cryo-electron tomography, Langmuir 31 (2015) 8680–8688, https://doi.org/10.1021/acs.langmuir.5b01739.
[232] R. Seneviratne, G. Coates, Z. Xu, C.E. Cornell, R.F. Thompson, A. Sadeghpour, D. P. Maskell, L.J.C. Jeuken, M. Rappolt, P.A. Beales, High resolution membrane structures within hybrid lipid-polymer vesicles revealed by combining x-ray scattering and electron microscopy, Small 19 (2023), https://doi.org/10.1002/smll.202206267.
[233] L, H.K. Reimer, Transmission Electron Microscopy: Physics of Image Formation, Springer Science & Business Media, 2008.
[234] J.C.H. Spence, Experimental High-Resolution Electron Microscopy, Oxford Univ. Press, 1998.
[235] P.W. Hawkes, E. Kasper, Principles of Electron Optics. Wave Optics, 3rd ed., Elsevier, 1994 https://doi.org/10.1016/C2009-0-21257-8.
[236] Y. Jiang, Z. Chen, Y. Han, P. Deb, H. Gao, S. Xie, P. Purohit, M.W. Tate, J. Park, S. M. Gruner, V. Elser, D.A. Muller, Electron ptychography of 2D materials to deep sub-ångström resolution, Nature 559 (2018) 343–349, https://doi.org/10.1038/s41586-018-0298-5.
[237] R. Erni, M.D. Rossell, C. Kisielowski, U. Dahmen, Atomic-resolution imaging with a sub-50-pm electron probe, Phys. Rev. Lett. 102 (2009) 096101, https://doi.org/10.1103/PhysRevLett.102.096101.
[238] I. Lazić, E.G.T. Bosch, Analytical review of direct stem imaging techniques for thin samples, Adv. Imaging Electron Phys. 199 (2017) 75–184, https://doi.org/10.1016/bs.aiep.2017.01.006.

[239] I. Lazić, E.G.T. Bosch, S. Lazar, Phase contrast STEM for thin samples: Integrated differential phase contrast, Ultramicroscopy 160 (2016) 265–280, https://doi.org/10.1016/j.ultramic.2015.10.011.
[240] D. Song, X. Zhang, C. Lian, H. Liu, I. Alexandrou, I. Lazić, E.G.T. Bosch, D. Zhang, L. Wang, R. Yu, Z. Cheng, C. Song, X. Ma, W. Duan, Q. Xue, J. Zhu, Visualization of dopant oxygen atoms in a Bi 2 Sr 2 CaCu 2 O 8+ δ superconductor, Adv. Funct. Mater. 29 (2019), https://doi.org/10.1002/adfm.201903843.
[241] H. Nahor, Y. Kauffmann, S. Lazar, D. Shilo, W.D. Kaplan, Discerning interface atomistic structure by phase contrast in STEM: the equilibrated Ni-YSZ interface, Acta Mater. 154 (2018) 71–78, https://doi.org/10.1016/j.actamat.2018.05.011.
[242] N. Gauquelin, K.H.W. van den Bos, A. Béché, F.F. Krause, I. Lobato, S. Lazar, A. Rosenauer, S. Van Aert, J. Verbeeck, Determining oxygen relaxations at an interface: a comparative study between transmission electron microscopy techniques, Ultramicroscopy 181 (2017) 178–190, https://doi.org/10.1016/j.ultramic.2017.06.002.
[243] S. de Graaf, J. Momand, C. Mitterbauer, S. Lazar, B.J. Kooi, Resolving hydrogen atoms at metal-metal hydride interfaces, Sci. Adv. 6 (2020), https://doi.org/10.1126/sciadv.aay4312.
[244] L. Liu, N. Wang, C. Zhu, X. Liu, Y. Zhu, P. Guo, L. Alfilfil, X. Dong, D. Zhang, Y. Han, Direct Imaging of atomically dispersed molybdenum that enables location of aluminum in the framework of zeolite ZSM-5, Angew. Chem. Int. Ed. 59 (2020) 819–825, https://doi.org/10.1002/anie.201909834.
[245] B. Shen, X. Chen, D. Cai, H. Xiong, X. Liu, C. Meng, Y. Han, F. Wei, Atomic Spatial and Temporal Imaging of Local Structures and Light Elements inside Zeolite Frameworks, Adv. Mater. 32 (2020), https://doi.org/10.1002/adma.201906103.
[246] B. Shen, X. Chen, H. Wang, H. Xiong, E.G.T. Bosch, I. Lazić, D. Cai, W. Qian, S. Jin, X. Liu, Y. Han, F. Wei, A single-molecule van der Waals compass, Nature 592 (2021) 541–544, https://doi.org/10.1038/s41586-021-03429-y.
[247] B. Shen, X. Chen, K. Shen, H. Xiong, F. Wei, Imaging the node-linker coordination in the bulk and local structures of metal-organic frameworks, Nat. Commun. 11 (2020) 2692, https://doi.org/10.1038/s41467-020-16531-y.
[248] I. Lazić, M. Wirix, M.L. Leidl, F. de Haas, D. Mann, M. Beckers, E.V. Pechnikova, K. Müller-Caspary, R. Egoavil, E.G.T. Bosch, C. Sachse, Single-particle cryo-EM structures from iDPC–STEM at near-atomic resolution, Nat. Methods 19 (2022) 1126–1136, https://doi.org/10.1038/s41592-022-01586-0.
[249] X. Li, I. Lazić, X. Huang, M. Wirix, L. Wang, Y. Deng, T. Niu, D. Wu, L. Yu, F. Sun, Imaging biological samples by integrated differential phase contrast (iDPC) STEM technique, J. Struct. Biol. 214 (2022) 107837, https://doi.org/10.1016/j.jsb.2022.107837.
[250] N. Elad, G. Bellapadrona, L. Houben, I. Sagi, M. Elbaum, Detection of isolated protein-bound metal ions by single-particle cryo-STEM, Proc. Natl. Acad. Sci. 114 (2017) 11139–11144, https://doi.org/10.1073/pnas.1708609114.
[251] C. Ophus, Four-dimensional scanning transmission electron microscopy (4D-STEM): from scanning nanodiffraction to ptychography and beyond, Microsc. Microanal. 25 (2019) 563–582, https://doi.org/10.1017/S1431927619000497.
[252] O. Panova, X.C. Chen, K.C. Bustillo, C. Ophus, M.P. Bhatt, N. Balsara, A.M. Minor, Orientation mapping of semicrystalline polymers using scanning electron nanobeam diffraction, Micron 88 (2016) 30–36, https://doi.org/10.1016/j.micron.2016.05.008.
[253] E. Mohammadi, C. Zhao, Y. Meng, G. Qu, F. Zhang, X. Zhao, J. Mei, J.-M. Zuo, D. Shukla, Y. Diao, Dynamic-template-directed multiscale assembly for large-area coating of highly-aligned conjugated polymer thin films, Nat. Commun. 8 (2017) 16070, https://doi.org/10.1038/ncomms16070.
[254] O. Panova, C. Ophus, C.J. Takacs, K.C. Bustillo, L. Balhorn, A. Salleo, N. Balsara, A.M. Minor, Diffraction imaging of nanocrystalline structures in organic semiconductor molecular thin films, Nat. Mater. 18 (2019) 860–865, https://doi.org/10.1038/s41563-019-0387-3.
[255] B. Yang, Q. Zhang, H. Huang, H. Pan, W. Zhu, F. Meng, S. Lan, Y. Liu, B. Wei, Y. Liu, L. Yang, L. Gu, L.Q. Chen, C.W. Nan, Y.H. Lin, Engineering relaxors by entropy for high energy storage performance, Nat. Energy 8 (2023) 956–964, https://doi.org/10.1038/s41560-023-01300-0.
[256] Y. Tsarfati, K.C. Bustillo, L. Balhorn, T.J. Quill, J. Donohue, S.E. Zeltmann, B. Savitzky, C. Ophus, C.J. Takacs, I. McCulloch, A.M. Minor, A. Salleo, Microstructural study of organic mixed ionic-electronic conductor thin films using 4D-STEM and HRTEM, Microsc. Microanal. 28 (2022) 350–351, https://doi.org/10.1017/s143192762200215x.
[257] J. Gladisch, E. Stavrinidou, S. Ghosh, A. Giovannitti, M. Moser, I. Zozoulenko, I. McCulloch, M. Berggren, Reversible ELectronic Solid–gel Switching of A Conjugated Polymer, Adv. Sci. 7 (2020), https://doi.org/10.1002/advs.201901144.
[258] M. Moser, J. Gladisch, S. Ghosh, T.C. Hidalgo, J.F. Ponder, R. Sheelamanthula, Q. Thiburce, N. Gasparini, A. Wadsworth, A. Salleo, S. Inal, M. Berggren, I. Zozoulenko, E. Stavrinidou, I. McCulloch, Controlling electrochemically induced volume changes in conjugated polymers by chemical design: from theory to devices, Adv. Funct. Mater. 31 (2021), https://doi.org/10.1002/adfm.202100723.
[259] Y. Tsarfati, K.C. Bustillo, B.H. Savitzky, L. Balhorn, T.J. Quill, A. Marks, J. Donohue, S.E. Zeltmann, C.J. Takacs, A. Giovannitti, I. McCulloch, C. Ophus, A. M. Minor, A. Salleo, The hierarchical structure of organic mixed ionic–electronic conductors and its evolution in water, Nat. Mater. 24 (2025) 101–108, https://doi.org/10.1038/s41563-024-02016-6.
[260] R. Yu, H. Sha, J. Cui, W. Yang, Introduction to electron ptychography for materials scientists, Microstructures 4 (2024), https://doi.org/10.20517/microstructures.2024.46.
[261] W. Hoppe, Beugung im inhomogenen Primärstrahlwellenfeld. I. Prinzip einer Phasenmessung von Elektronenbeugungsinterferenzen, Acta Crystallogr. Sect. A 25 (1969) 495–501, https://doi.org/10.1107/S0567739469001045.
[262] X. Pei, L. Zhou, C. Huang, M. Boyce, J.S. Kim, E. Liberti, Y. Hu, T. Sasaki, P. D. Nellist, P. Zhang, D.I. Stuart, A.I. Kirkland, P. Wang, Cryogenic electron ptychographic single particle analysis with wide bandwidth information transfer, Nat. Commun. 14 (2023) 3027, https://doi.org/10.1038/s41467-023-38268-0.
[263] M.C. Cao, Z. Chen, Y. Jiang, Y. Han, Automatic parameter selection for electron ptychography via Bayesian optimization, Sci. Rep. 12 (2022) 12284, https://doi.org/10.1038/s41598-022-16041-5.
[264] A.M. Maiden, J.M. Rodenburg, An improved ptychographical phase retrieval algorithm for diffractive imaging, Ultramicroscopy 109 (2009) 1256–1262, https://doi.org/10.1016/j.ultramic.2009.05.012.
[265] G. Li, H. Zhang, Y. Han, 4D-STEM Ptychography for Electron-Beam-Sensitive Materials, ACS Cent. Sci. 8 (2022) 1579–1588, https://doi.org/10.1021/acscentsci.2c01137.
[266] X. Peng, P.M. Pelz, Q. Zhang, P. Chen, L. Cao, Y. Zhang, H.-G. Liao, H. Zheng, C. Wang, S.-G. Sun, M.C. Scott, Observation of formation and local structures of metal-organic layers via complementary electron microscopy techniques, Nat. Commun. 13 (2022) 5197, https://doi.org/10.1038/s41467-022-32330-z.
[267] B. Hao, Z. Ding, X. Tao, P.D. Nellist, H.E. Assender, Atomic-scale imaging of polyvinyl alcohol crystallinity using electron ptychography, Polymers 284 (2023) 126305, https://doi.org/10.1016/j.polymer.2023.126305.
[268] N. Dumaresq, N. Brodusch, S. Bessette, R. Gauvin, Elemental quantification using electron energy-loss spectroscopy with a low voltage scanning transmission electron microscope (STEM-EELS), Ultramicroscopy 262 (2024) 113977, https://doi.org/10.1016/j.ultramic.2024.113977.
[269] M. Ilett, R. Brydson, A. Brown, N. Hondow, Cryo-analytical STEM of frozen, aqueous dispersions of nanoparticles, Micron 120 (2019) 35–42, https://doi.org/10.1016/j.micron.2019.01.013.
[270] T. Roncal-Herrero, S. Micklethwaite, M. Ilett, J. Hitchcock, O. Cayre, N. Hondow, Analytical cryo electron microscopy for characterization of pickering emulsions, Microsc. Microanal. 25 (2019) 1706–1707, https://doi.org/10.1017/S1431927619009267.
[271] O. Pfeil-Gardiner, H.V.D. Rosa, D. Riedel, Y.S. Chen, D. Lörks, P. Kükelhan, M. Linck, H. Müller, F. Van Petegem, B.J. Murphy, Elemental mapping in single-particle reconstructions by reconstructed electron energy-loss analysis, Nat. Methods 21 (2024) 2299–2306, https://doi.org/10.1038/s41592-024-02482-5.
[272] K. Zhang, F. Wu, X. Wang, L. Zheng, X. Yang, H. Zhao, Y. Sun, W. Zhao, Y. Bai, C. Wu, An ion-dipole-reinforced polyether electrolyte with ion-solvation cages enabling high–voltage-tolerant and ion-conductive solid-state lithium metal batteries, Adv. Funct. Mater. 32 (2022), https://doi.org/10.1002/adfm.202107764.
[273] Y. He, L. Jiang, T. Chen, Y. Xu, H. Jia, R. Yi, D. Xue, M. Song, A. Genc, C. Bouchet-Marquis, L. Pullan, T. Tessner, J. Yoo, X. Li, J.-G. Zhang, S. Zhang, C. Wang, Progressive growth of the solid–electrolyte interphase towards the Si anode interior causes capacity fading, Nat. Nanotechnol. 16 (2021) 1113–1120, https://doi.org/10.1038/s41565-021-00947-8.
[274] Y. He, L. Jiang, Y. Xu, C. Wang, Cryo STEM EDS tomography probing of solid electrolyte interphase in rechargeable batteries, Microsc. Microanal. 29 (2023) 1718–1719, https://doi.org/10.1093/micmic/ozad067.888.
[275] A. Shaikhqasem, F. Hamdi, L. Machner, C. Parthier, C. Breithaupt, F.L. Kyrilis, S. M. Feller, P.L. Kastritis, M.T. Stubbs, Strategies for mitigating radiation damage and improving data completeness in 3D electron diffraction of protein crystals, Acta Cryst. (2026) 11–22, https://doi.org/10.1107/S2059798325011258.
[276] L. Machner, A. Shaikhqasem, T. Gruber, F. Hamdi, C. Breithaupt, J. Kniest, F. Wiebe, M. Lewitzky, C. Parthier, F.L. Kyrilis, J. Balbach, P.L. Kastritis, S. M. Feller, M.T. Stubbs, Mechanism of SHP2 activation by bis-Tyr-phosphorylated Gab1, Structure 34 (2026) 1–13, https://doi.org/10.1016/j.str.2025.11.018.
[277] P.N.T. Unwin, R. Henderson, Molecular structure determination by electron microscopy of unstained crystalline specimens, J. Mol. Biol. 94 (1975) 425–440, https://doi.org/10.1016/0022-2836(75)90212-0.
[278] J. Li, C. Lin, Y. Min, Y. Yuan, G. Li, S. Yang, P. Manuel, J. Lin, J. Sun, Discovery of complex metal oxide materials by rapid phase identification and structure determination, J. Am. Chem. Soc. 141 (2019) 4990–4996, https://doi.org/10.1021/jacs.9b00093.
[279] K. Fan, J. Li, Y. Xu, C. Fu, Y. Chen, C. Zhang, G. Zhang, J. Ma, T. Zhai, C. Wang, Single crystals of a highly conductive three-dimensional conjugated coordination polymer, J. Am. Chem. Soc. 145 (2023) 12682–12690, https://doi.org/10.1021/jacs.3c02378.
[280] H. Ning, Y. Zeng, S. Zuo, S.V. Kershaw, Y. Hou, Y. Li, X. Li, J. Zhang, Y. Yi, L. Jing, J. Li, M. Gao, Two-dimensional and subnanometer-thin quasi-copper-sulfide semiconductor formed upon copper–copper bonding, ACS Nano 15 (2021) 873–883, https://doi.org/10.1021/acsnano.0c07388.
[281] C. Ma, C. Lin, J. Li, MicroED as a powerful technique for the structure determination of complex porous materials, Chin. J. Struct. Chem. 43 (2024) 100209, https://doi.org/10.1016/j.cjsc.2023.100209.
[282] T. Gruene, E. Mugnaioli, 3D electron diffraction for chemical analysis: instrumentation developments and innovative applications, Chem. Rev. 121 (2021) 11823–11834, https://doi.org/10.1021/acs.chemrev.1c00207.
[283] P. Hogan-Lamarre, Y. Luo, R. Bücker, R.J.D. Miller, X. Zou, STEM SerialED: achieving high-resolution data for ab initio structure determination of beam-sensitive nanocrystalline materials, IUCrJ 11 (2024) 62–72, https://doi.org/10.1107/S2052252523009661.
[284] X. Zou, Discovery of Novel Nanoporous Materials Advanced by Electron Crystallography, in: K.; F.B.L.; R.L.; D.W.A. Wuthrich (Ed.), Chemistry Challenges

of the 21st Century, World Scientific Publishing Co. Pte. Ltd., 2024, pp. 167–173, https://doi.org/10.1142/9789811282324_0017.
[285] M. Gemmi, E. Mugnaioli, T.E. Gorelik, U. Kolb, L. Palatinus, P. Boullay, S. Hovmöller, J.P. Abrahams, 3D electron diffraction: the nanocrystallography revolution, ACS Cent. Sci. 5 (2019) 1315–1329, https://doi.org/10.1021/acscentsci.9b00394.
[286] U. Kolb, T. Gorelik, C. Kübel, M.T. Otten, D. Hubert, Towards automated diffraction tomography: Part I—Data acquisition, Ultramicroscopy 107 (2007) 507–513, https://doi.org/10.1016/j.ultramic.2006.10.007.
[287] U. Kolb, T. Gorelik, M.T. Otten, Towards automated diffraction tomography. Part II—Cell parameter determination, Ultramicroscopy 108 (2008) 763–772, https://doi.org/10.1016/j.ultramic.2007.12.002.
[288] M.A. Marques, M.D. Purdy, M. Yeager, CryoEM maps are full of potential, Curr. Opin. Struct. Biol. 58 (2019) 214–223, https://doi.org/10.1016/j.sbi.2019.04.006.
[289] J. Li, J. Sun, Application of X-ray diffraction and electron crystallography for solving complex structure problems, Acc. Chem. Res 50 (2017) 2737–2745, https://doi.org/10.1021/acs.accounts.7b00366.
[290] D. Denysenko, M. Grzywa, M. Tonigold, B. Streppel, I. Krkljus, M. Hirscher, E. Mugnaioli, U. Kolb, J. Hanss, D. Volkmer, Elucidating gating effects for hydrogen sorption in MFU-4-type triazolate-based metal–organic frameworks featuring different pore sizes, Chem. A Eur. J. 17 (2011) 1837–1848, https://doi.org/10.1002/chem.201001872.
[291] U. Kolb, T.E. Gorelik, E. Mugnaioli, A. Stewart, StructuraL Characterization of Organics Using Manual and Automated Electron Diffraction, Polym. Rev. 50 (2010) 385–409, https://doi.org/10.1080/15583724.2010.494238.
[292] I. Rozhdestvenskaya, E. Mugnaioli, M. Czank, W. Depmeier, U. Kolb, A. Reinholdt, T. Weirich, The structure of charoite, $(K,Sr,Ba,Mn)_{15-16}(Ca,Na)_{32}[(Si_{70}(O,OH)_{180})](OH,F)_{4.0}nH_2O$, solved by conventional and automated electron diffraction, Miner. Mag. 74 (2010) 159–177, https://doi.org/10.1180/minmag.2010.074.1.159.
[293] R. Dai, F. Peng, P. Ji, K. Lu, C. Wang, J. Sun, W. Lin, Electron crystallography reveals atomic structures of metal–organic nanoplates with $M_{12}(\mu_3\text{-}O)_8(\mu_3\text{-}OH)_8(\mu_2\text{-}OH)_6$ (M = Zr, Hf) secondary building units, Inorg. Chem. 56 (2017) 8128–8134, https://doi.org/10.1021/acs.inorgchem.7b00845.
[294] Y.-B. Zhang, J. Su, H. Furukawa, Y. Yun, F. Gándara, A. Duong, X. Zou, O. M. Yaghi, Single-crystal structure of a covalent organic framework, J. Am. Chem. Soc. 135 (2013) 16336–16339, https://doi.org/10.1021/ja409033p.
[295] T. Sun, L. Wei, Y. Chen, Y. Ma, Y.-B. Zhang, Atomic-level characterization of dynamics of a 3D covalent organic framework by cryo-electron diffraction tomography, J. Am. Chem. Soc. 141 (2019) 10962–10966, https://doi.org/10.1021/jacs.9b04895.
[296] W. Sun, P. Chen, M. Zhang, J. Ma, J. Sun, Locating hydrogen positions for COF-300 by Cryo-3D electron diffraction, Angew. Chem. Int. Ed. 62 (2023), https://doi.org/10.1002/anie.202305985.
[297] E. Meijering, A.E. Carpenter, H. Peng, F.A. Hamprecht, J.-C. Olivo-Marin, Imagining the future of bioimage analysis, Nat. Biotechnol. 34 (2016) 1250–1255, https://doi.org/10.1038/nbt.3722.
[298] P. Sarder, A. Nehorai, Deconvolution methods for 3-D fluorescence microscopy images, IEEE Signal Process Mag. 23 (2006) 32–45, https://doi.org/10.1109/MSP.2006.1628876.
[299] D. Kimanius, L. Dong, G. Sharov, T. Nakane, S.H.W. Scheres, New tools for automated cryo-EM single-particle analysis in RELION-4.0, Biochem. J. 478 (2021) 4169–4185, https://doi.org/10.1042/BCJ20210708.
[300] M. Olek, K. Cowtan, D. Webb, Y. Chaban, P. Zhang, IceBreaker: software for high-resolution single-particle cryo-EM with non-uniform ice, Structure 30 (2022) 522–531.e4, https://doi.org/10.1016/j.str.2022.01.005.
[301] F.J. Sigworth, P.C. Doerschuk, J.-M. Carazo, S.H.W. Scheres, An Introduction to Maximum-Likelihood Methods in Cryo-EM, Methods Enzym. 482 (2010) 263–294, https://doi.org/10.1016/S0076-6879(10)82011-7.
[302] A. Punjani, J.L. Rubinstein, D.J. Fleet, M.A. Brubaker, cryoSPARC: algorithms for rapid unsupervised cryo-EM structure determination, Nat. Methods 14 (2017) 290–296, https://doi.org/10.1038/nmeth.4169.
[303] D. Lyumkis, Challenges and opportunities in cryo-EM single-particle analysis, J. Biol. Chem. 294 (2019) 5181–5197, https://doi.org/10.1074/jbc.REV118.005602.
[304] A. Punjani, D.J. Fleet, 3D variability analysis: resolving continuous flexibility and discrete heterogeneity from single particle cryo-EM, J. Struct. Biol. 213 (2021) 107702, https://doi.org/10.1016/j.jsb.2021.107702.
[305] L.F. Kinman, B.M. Powell, E.D. Zhong, B. Berger, J.H. Davis, Uncovering structural ensembles from single-particle cryo-EM data using cryoDRGN, Nat. Protoc. 18 (2023) 319–339, https://doi.org/10.1038/s41596-022-00763-x.
[306] M. Chen, J.M. Bell, X. Shi, S.Y. Sun, Z. Wang, S.J. Ludtke, A complete data processing workflow for cryo-ET and subtomogram averaging, Nat. Methods 16 (2019) 1161–1168, https://doi.org/10.1038/s41592-019-0591-8.
[307] I. Skalidis, F.L. Kyrilis, C. Tüting, F. Hamdi, G. Chojnowski, P.L. Kastritis, Cryo-EM and artificial intelligence visualize endogenous protein community members, Structure 30 (2022) 575–589.e6, https://doi.org/10.1016/j.str.2022.01.001.
[308] W. Li, S. Weng, D. Su, X. Wang, Expanding the cryogenic electron microscopy from biology to materials science, Renewables 2 (2024) 73–87, https://doi.org/10.31635/renewables.024.202300046.
[309] Z. Ghahramani, Probabilistic machine learning and artificial intelligence, Nature 521 (2015) 452–459, https://doi.org/10.1038/nature14541.
[310] Y. LeCun, Y. Bengio, G. Hinton, Deep learning, Nature 521 (2015) 436–444, https://doi.org/10.1038/nature14539.
[311] M. Ge, F. Su, Z. Zhao, D. Su, Deep learning analysis on microscopic imaging in materials science, Mater. Today Nano 11 (2020) 100087, https://doi.org/10.1016/j.mtnano.2020.100087.
[312] S.R. Spurgeon, C. Ophus, L. Jones, A. Petford-Long, S.V. Kalinin, M.J. Olszta, R. E. Dunin-Borkowski, N. Salmon, K. Hattar, W.-C.D. Yang, R. Sharma, Y. Du, A. Chiaramonti, H. Zheng, E.C. Buck, L. Kovarik, R.L. Penn, D. Li, X. Zhang, M. Murayama, M.L. Taheri, Towards data-driven next-generation transmission electron microscopy, Nat. Mater. 20 (2021) 274–279, https://doi.org/10.1038/s41563-020-00833-z.
[313] E. Moebel, A. Martinez-Sanchez, L. Lamm, R.D. Righetto, W. Wietrzynski, S. Albert, D. Larivière, E. Fourmentin, S. Pfeffer, J. Ortiz, W. Baumeister, T. Peng, B.D. Engel, C. Kervrann, Deep learning improves macromolecule identification in 3D cellular cryo-electron tomograms, Nat. Methods 18 (2021) 1386–1394, https://doi.org/10.1038/s41592-021-01275-4.
[314] A. Zamanos, P. Koromilas, G. Bouritsas, P.L. Kastritis, Y. Panagakis, Towards Generalizable Particle Picking in Cryo-EM Images by Leveraging Masked AutoEncoders, in: ICML 2024 Workshop on Accessible and Efficient Foundation Models for Biological Discovery, Vienna, 2024.
[315] M. Schorb, I. Haberbosch, W.J.H. Hagen, Y. Schwab, D.N. Mastronarde, Software tools for automated transmission electron microscopy, Nat. Methods 16 (2019) 471–477, https://doi.org/10.1038/s41592-019-0396-9.
[316] F.L. Kyrilis, J. Belapure, P.L. Kastritis, Detecting protein communities in native cell extracts by machine learning: a structural biologist's perspective, Front Mol. Biosci. 8 (2021), https://doi.org/10.3389/fmolb.2021.660542.
[317] A. Zamanos, G. Ioannakis, I.Z. Emiris, HydraProt: a new deep learning tool for fast and accurate prediction of water molecule positions for protein structures, J. Chem. Inf. Model 64 (2024) 2594–2611, https://doi.org/10.1021/acs.jcim.3c01559.
[318] J. Jumper, R. Evans, A. Pritzel, T. Green, M. Figurnov, O. Ronneberger, K. Tunyasuvunakool, R. Bates, A. Žídek, A. Potapenko, A. Bridgland, C. Meyer, S. A.A. Kohl, A.J. Ballard, A. Cowie, B. Romera-Paredes, S. Nikolov, R. Jain, J. Adler, T. Back, S. Petersen, D. Reiman, E. Clancy, M. Zielinski, M. Steinegger, M. Pacholska, T. Berghammer, S. Bodenstein, D. Silver, O. Vinyals, A.W. Senior, K. Kavukcuoglu, P. Kohli, D. Hassabis, Highly accurate protein structure prediction with AlphaFold, Nature 596 (2021) 583–589, https://doi.org/10.1038/s41586-021-03819-2.
[319] M. Baek, F. DiMaio, I. Anishchenko, J. Dauparas, S. Ovchinnikov, G.R. Lee, J. Wang, Q. Cong, L.N. Kinch, R.D. Schaeffer, C. Millán, H. Park, C. Adams, C. R. Glassman, A. DeGiovanni, J.H. Pereira, A.V. Rodrigues, A.A. van Dijk, A. C. Ebrecht, D.J. Opperman, T. Sagmeister, C. Buhlheller, T. Pavkov-Keller, M. K. Rathinaswamy, U. Dalwadi, C.K. Yip, J.E. Burke, K.C. Garcia, N.V. Grishin, P. D. Adams, R.J. Read, D. Baker, Accurate prediction of protein structures and interactions using a three-track neural network, Science 373 (2021) 871–876, https://doi.org/10.1126/science.abj8754.
[320] wwPDB consortium, Protein Data Bank: the single global archive for 3D macromolecular structure data, Nucleic Acids Res 47 (2019) D520–D528, https://doi.org/10.1093/nar/gky949.
[321] S. Subramaniam, G.J. Kleywegt, A paradigm shift in structural biology, Nat. Methods 19 (2022) 20–23, https://doi.org/10.1038/s41592-021-01361-7.
[322] Y. Pan, C. Zhang, Z. Liu, C. Chen, Y. Li, Structural regulation with atomic-level precision: from single-atomic site to diatomic and atomic interface catalysis, Matter 2 (2020) 78–110, https://doi.org/10.1016/j.matt.2019.11.014.
[323] D.P. Hoffman, G. Shtengel, C.S. Xu, K.R. Campbell, M. Freeman, L. Wang, D. E. Milkie, H.A. Pasolli, N. Iyer, J.A. Bogovic, D.R. Stabley, A. Shirinifard, S. Pang, D. Peale, K. Schaefer, W. Pomp, C.L. Chang, J. Lippincott-Schwartz, T. Kirchhausen, D.J. Solecki, E. Betzig, H.F. Hess, Correlative three-dimensional super-resolution and block-face electron microscopy of whole vitreously frozen cells, Science 367 (2020), https://doi.org/10.1126/science.aaz5357.
[324] X. Li, O.E. Dyck, M.P. Oxley, A.R. Lupini, L. McInnes, J. Healy, S. Jesse, S. V. Kalinin, Manifold learning of four-dimensional scanning transmission electron microscopy, NPJ Comput. Mater. 5 (2019), https://doi.org/10.1038/s41524-018-0139-y.

Dr.-Ing. Panagiota Koralli is a mechanical engineer with a PhD in materials science from the National Technical University of Athens. Her research focuses on physical chemistry and analysis of nanomaterials, including thin films, nanocomposites, and nanoparticles. As a postdoctoral researcher, she has received research fellowships in the fields of materials science, nanotechnology & applications, conducting work at both the National Hellenic Research Foundation (NHRF) and the German Cancer Research Center (DKFZ). Since 2023, she is part of the Kastritis team at NHRF, contributing to the cryo-electron microscopy (cryo-EM) analysis of materials.

Dr. Fotis Kyrilis is a biologist and holds a PhD in structural biochemistry employing cryo-EM. As a Staff Scientist of the Kastritis Laboratory (2018–2022), he is expert in cryo-EM techniques and sample preparation methods, screening, and data acquisition with various electron microscopic methods. Since 2023, he is the junior group leader in the Kastritis team, responsible for smooth installation and operation of four cryo-electron microscopes in NHRF, Athens.

Dr. Farzad Hamdi is a staff scientist and the lead cryo-EM engineer of the department of Integrative Structural Biochemistry (ISB). Dr Hamdi has decades of experience in electron microscopy for both material and biological samples visualization, charactrization and study. He joined the Kastritis lab as a cryo-EM engineer in 2019, having previously worked as an assistant professor of electron microscopy at Sharif University in Tehran.

Dr. Christos Chochos is a senior researcher at the Institute of Chemical Biology (ICB) of the NHRF, holding a PhD in polymer science and technology. His research focuses on the design and synthesis of π-conjugated polymers and their self-assembly into nanoparticles for applications in organic electronics and nanomedicine. He has extensive expertise in structure-property relationship studies, with the goal to tailor polymeric systems for improved optoelectronic and biological performance.

Dr. Panagiotis Kastritis is professor for "Integrative Structural Biochemistry" at the Institute for Biochemistry & Biotechnology, University of Halle-Wittenberg (MLU), Halle, Germany. He has installed and heads the world-renowned cryo-EM laboratory in MLU from scratch. As the ERA Chair in NHRF, he also supervises the installation of the cryo-EM microscopes at the Foundation, leading the team that includes authors Dr. Koralli and Dr. Kyrilis. Kastritis is interested in analysis of the 3D structure of soft matter to understand chemical processes at unprecedented detail.